

# REPORT DOCUMENTATION PAGE

Form Approved  
OMB NO. 0704-0188

Public Reporting burden for this collection of information is estimated to average 1 hour per response, including the time for reviewing instructions, searching existing data sources, gathering and maintaining the data needed, and completing and reviewing the collection of information. Send comment regarding this burden estimates or any other aspect of this collection of information, including suggestions for reducing this burden, to Washington Headquarters Services, Directorate for information Operations and Reports, 1215 Jefferson Davis Highway, Suite 1204, Arlington, VA 22202-4302, and to the Office of Management and Budget, Paperwork Reduction Project (0704-0188,) Washington, DC 20503.

1. AGENCY USE ONLY ( Leave Blank)		2. REPORT DATE 11/30/02	3. REPORT TYPE AND DATES COVERED Final, Sept. 1, 1999 - Aug. 31, 2002	
4. TITLE AND SUBTITLE Experiments in Quantum Coherence and Computation with Single Cooper-pair Electronics			5. FUNDING NUMBERS DAAD19-99-1-0346	
6. AUTHOR(S) R.J. Schoelkopf				
7. PERFORMING ORGANIZATION NAME(S) AND ADDRESS(ES) Yale University, Dept. of Applied Physics PO Box 208284, New Haven, CT 06520-8284			8. PERFORMING ORGANIZATION REPORT NUMBER	
9. SPONSORING / MONITORING AGENCY NAME(S) AND ADDRESS(ES) U. S. Army Research Office P.O. Box 12211 Research Triangle Park, NC 27709-2211			10. SPONSORING / MONITORING AGENCY REPORT NUMBER 40320-PH-QC	
11. SUPPLEMENTARY NOTES The views, opinions and/or findings contained in this report are those of the author(s) and should not be construed as an official Department of the Army position, policy or decision, unless so designated by other documentation.				
12 a. DISTRIBUTION / AVAILABILITY STATEMENT  Approved for public release; distribution unlimited.			12 b. DISTRIBUTION CODE	
13. ABSTRACT (Maximum 200 words)  The aim of this project is to measure the coherence time of charge states in the single Cooper-pair box, which is a candidate system for realizing a solid-state, electronic qubit for quantum computation. Techniques for the control and measurement of these states are being developed and applied to demonstrate sufficient coherence to allow quantum computation. In the past year, we have observed coherent two-level system behavior for our Cooper-pair box qubits through microwave spectroscopy. We have obtained a worst case estimate of the decoherence time, under conditions of continuous measurement and maximal sensitivity to $1/f$ charge noise, of about 1 nanosecond. More interestingly, we have also been able to observe a very long (1 microsecond) inelastic lifetime for the qubit to decay into its ground state. This sets an interesting maximal limit on the coherence which could then be almost 1 million times longer than the single-bit operation time, and indicates that the dissipation in Al/AIOx/Al junctions can be very low. In addition, this long lifetime is present in the presence of the measurement by the RF-SET, and implies that high-fidelity single-shot measurements of the qubit state will be possible with this approach.				
14. SUBJECT TERMS			15. NUMBER OF PAGES 3	
			16. PRICE CODE	
17. SECURITY CLASSIFICATION OR REPORT <b>UNCLASSIFIED</b>	18. SECURITY CLASSIFICATION ON THIS PAGE <b>UNCLASSIFIED</b>	19. SECURITY CLASSIFICATION OF ABSTRACT <b>UNCLASSIFIED</b>	20. LIMITATION OF ABSTRACT  <b>UL</b>	

NSN 7540-01-280-5500

Standard Form 298 (Rev.2-89)  
Prescribed by ANSI Std. Z39-18  
298-102

## GENERAL INSTRUCTIONS FOR COMPLETING SF 298

The Report Documentation Page (RDP) is used for announcing and cataloging reports. It is important that this information be consistent with the rest of the report, particularly the cover and title page. Instructions for filling in each block of the form follow. It is important to ***stay within the lines*** to meet ***optical scanning requirements***.

**Block 1.** Agency Use Only (Leave blank)

**Block 2.** Report Date. Full publication date including day, month, and year, if available (e.g. 1 Jan 88). Must cite at least year.

**Block 3.** Type of Report and Dates Covered.

State whether report is interim, final, etc. If applicable enter inclusive report dates (e.g. 10 Jun 87 - 30 Jun 88).

**Block 4.** Title and Subtitle. A title is taken from the part of the report that provides the most meaningful and complete information. When a report is prepared in more than one volume, repeat the primary title, and volume number, and include subtitle for the specific volume. On classified documents enter the title classification in parentheses.

**Block 5.** Funding Numbers. To include contract and grant numbers; may include program element number(s) project number(s), task number(s), and work unit number(s). Use the following labels:

<b>C</b> - Contract	<b>PR</b> - Project
<b>G</b> - Grant	<b>TA</b> - Task
<b>PE</b> - Program Element	<b>WU</b> - Work Unit Accession No.

**Block 6.** Author(s). Name(s) of person(s) responsible for writing the report, performing the research, or credited with the content of the report. If editor or compiler, this should follow the name(s).

**Block 7.** Performing Organization Name(s) and Address(es). Self-explanatory.

**Block 8.** Performing Organization Report Number. Enter the unique alphanumeric report number(s) assigned by the organization performing the report.

**Block 9.** Sponsoring/Monitoring Agency Name(s) and Address(es). Self-explanatory.

**Block 10.** Sponsoring/Monitoring Agency Report Number. (if known)

**Block 11.** Supplementary Notes. Enter information not included elsewhere such as; prepared in cooperation with...; Trans. of...; To be published in.... When a report is revised, include a statement whether the new report supersedes or supplements the older report.

**Block 12a.** Distribution/Availability Statement.

Denotes public availability or limitations. Cite any availability to the public. Enter additional limitations or special markings in all capitals (e.g. NORFORN, REL, ITAR).

**DOD** - See DoDD 4230.25, "Distribution Statements on Technical Documents."

**DOE** - See authorities.

**NASA** - See Handbook NHB 2200.2.

**NTIS** - Leave blank.

**Block 12b.** Distribution Code.

**DOD** - Leave Blank

**DOE** - Enter DOE distribution categories from the Standard Distribution for unclassified Scientific and Technical Reports

**NASA** - Leave Blank.

**NTIS** - Leave Blank.

**Block 13.** Abstract. Include a brief (*Maximum 200 words*) factual summary of the most significant information contained in the report.

**Block 14.** Subject Terms. Keywords or phrases identifying major subject in the report.

**Block 15.** Number of Pages. Enter the total number of pages.

**Block 16.** Price Code. Enter appropriate price code (NTIS *only*).

**Block 17. - 19.** Security Classifications. Self-explanatory. Enter U.S. Security Regulations (i.e., UNCLASSIFIED). If form contains classified information, stamp classification on the top and bottom of the page.

**Block 20.** Limitation of Abstract. This block must be completed to assign a limitation to the abstract. Enter either UL (Unlimited) or SAR (same as report). An entry in this block is necessary if the abstract is to be limited. If blank, the abstract is assumed to be unlimited.

## REPORT DOCUMENTATION PAGE (SF298) (Continuation Sheet)

### Final Report (9/1/99-8/31/02):

Experiments in Quantum Coherence and Computation with Single Cooper-pair Electronics, R.J. Schoelkopf PI.

### Table of Contents

I. List of Figures	3
II. Summary of Achievements	3
III. Summary of Technical Approach	4
IV. Publications	5
V. Personnel and Budget Discussion	6
VI. Detailed Discussion of Technical Results	7
VII. Report of Inventions	11
VIII. Appendix: Copies of Major Publications	
A. "Amplifying Quantum Signals with the Single-Electron Transistor," M.H. Devoret and R.J. Schoelkopf, <i>Nature</i> 406, pp. 1039-1046 (2000).	12
B. "Measurement of the Excited State Lifetime of a Microelectronic Circuit," K.W. Lehnert <i>et al.</i> , to appear in <i>Physical Review Letters</i> , 2002.	20
C. "Qubits as Spectrometers of Quantum Noise," R.J. Schoelkopf <i>et al.</i> , 2002.	30

### List of Figures

- Figure 1: Circuit diagram of Cooper-pair box and RF-SET readout.
- Figure 2: Layout, image, and electromagnetic simulation of CPB/RF-SET chip.
- Figure 3: Spectroscopy of coherent states in Cooper-pair box.
- Figure 4: Extraction of ensemble-averaged decoherence time ( $T_2^*$ ) for box.
- Figure 5: Control of box Hamiltonian and determination of circuit parameters.
- Figure 6: Determination of inelastic lifetime ( $T_1$ ) of box.
- Figure 7: Observation of backaction due to SET measurement.

### Summary of Achievements

In the three years of this grant, we have made significant progress towards the goal realizing scalable quantum bits for information processing, using charge states in superconducting electronics. Specifically, we have made a single qubit, based on the single Cooper-pair box (CPB), which has a phase coherence quality factor greater than 100, and a very long inelastic lifetime corresponding to an intrinsic quality factor greater than 100,000. These results were obtained by performing the first ever charge measurements using a radio-frequency single-electron transistor (RF-SET), integrating it with the charge qubit, and performing both precision microwave spectroscopy and sub-microsecond resolved readouts of the qubit. Our results indicate that single-shot measurements of individual qubits with this technique will be possible. These results have been accepted for publication in *Physical Review Letters*. Moreover, we have studied the backaction of this type of charge measurement with an SET, both experimentally and theoretically, which is relevant to several other schemes for quantum computation that invoke similar measurement strategies. Significant effort was made in building fabrication expertise, experimental techniques, and apparatus. This project is continuing under a new three-year grant, during which we use these capabilities to further investigate the mechanisms and limits of decoherence in the CPB qubits, test the models of quantum measurement by the RF-SET, and investigate the entanglement of two CPB qubits using techniques analogous to cavity-QED in atomic physics.

- Developed fabrication process at Yale for Al-based SETs using electron-beam lithography.
- Began finite-element full-wave and electrostatic simulations of actual chip geometries.
- Revised chip designs for better control of electromagnetic coupling to gates.
- Measured equilibrium charge state of Cooper-pair box and observed  $2e$ -periodic Coulomb staircase.
- Performed CW spectroscopy of charge superpositions in box with microwave signal on gate.
- Tuned parameters of the CPB qubit using applied gate voltages and magnetic fields.
- Accurately determined all parameters of the qubit Hamiltonian by spectroscopy.
- Determined ensemble-averaged decoherence time ( $T_2^* \sim 1$  ns) from width of photon resonances.
- Observed dependence of CPB ground-state polarization on bias conditions of readout SET.
- Using time-gated RF-SET measurement, observed mixing of states by measurement backaction.
- Measured long inelastic lifetime of CPB excited state ( $T_1=1.3$   $\mu$ s), under conditions of continuous measurement.
- Separated effects of electric and magnetic noise on relaxation.
- Estimated that inelastic lifetime is sufficiently long to allow single-shot quantum state readouts using the RF-SET.
- A manuscript on the decoherence and lifetime measurements have been accepted by *Physical Review Letters*.

## Summary of Technical Approach

The goal of the project was to investigate the limits on coherence and control of quantum states in the “single Cooper-pair box,” which is a candidate system for performing quantum computation. These nanoelectronic devices utilize charging effects in small capacitance Josephson junctions, operated at millikelvin temperatures. Superpositions of two different charge states on these junctions serve as the qubit, which would form the basis of a future quantum computer. Experiments in Japan by Nakamura et al. have shown that some degree of coherent state control is possible, and they achieved coherent single-bit rotations (Rabi oscillations) between states. However, the decoherence processes and limits in these devices are not yet understood in detail, and these questions were the main focus of the current project.

Our approach was to utilize the RF-SET electrometer, whose high speed and good charge sensitivity allow a direct determination of the island charge of the Cooper-pair box. Since the fabrication used for the RF-SET is identical to that of the Cooper-pair box, the electrometer can be integrated on-chip (see Fig. 1) to probe the potential of the box capacitively. By fast control of the microwave signal that interrogates the RF-SET, the measurement can be turned off during the coherent state manipulations, and then the final state can be sampled on sub-microsecond timescales. In its quiescent state, the RF-SET adds only a small additional coupling to the electromagnetic environment. With the RF-SET charge measurements, we have shown that it will be possible to approach the ideal limit of a single-shot measurement on the state of a single qubit.

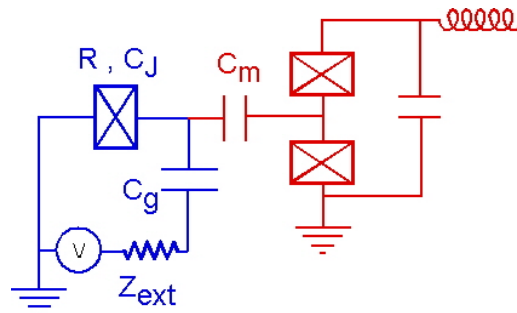


**Figure 1.** A circuit diagram of a Cooper-pair box qubit, capacitively coupled via  $C_m$  to an RF-SET electrometer, showing the L-C resonant tank circuit.

These devices are fabricated using a now-standard fabrication process, utilizing direct-write electron-beam lithography and a multiple angle evaporation of aluminum films. By oxidizing between depositions, it is possible to realize high-quality Al/AlO<sub>x</sub>/Al tunnel junctions with characteristic sizes down to about 50 nm. At the millikelvin temperatures of operation, the aluminum is a superconductor, with nearly all the conduction electrons bound up as Cooper-pairs. This allows one to realize a solid-state, microelectronic circuit which behaves as an effective spin  $\frac{1}{2}$  particle, and thus a candidate qubit. These qubits can have the parameters of their Hamiltonian tuned via the application of magnetic and electric fields, and their quantum states can be manipulated by fast signals on a capacitively-coupled gate lead that comes to room temperature. The samples for these experiments were fabricated by our collaborators in Prof. Per Delsing’s group at Chalmers University in Sweden, under a subcontract.

Several different types of measurements were performed using the same configuration of devices. First, continuous-wave spectroscopy of the box was performed, under the conditions of a continuous measurement by the RF-SET. From this data, we could extract the parameters of the box Hamiltonian, verify the coherent two-level physics of our circuit, and obtain a worst-case estimate of the decoherence time. The intrinsic high speed of the RF-SET then allowed a measurement of the dynamics on the sub-microsecond timescale. By measuring the decay time of an excited-state population, we could observe the inelastic relaxation rate, which was quite slow, and approached the limit expected by spontaneous emission. This was the first measurement of this timescale in superconducting charge qubits, and very encouraging for future developments. Other dynamical experiments were also performed, with somewhat less success. The signal-to-noise ratio of a single-shot measurement, based on our measured relaxation time, predicted a high-fidelity readout of individual states was possible. Our attempts to prove this, however, were limited by our inability, so far, to produce a pure excited state. Rabi and Ramsey experiments were also both inconclusive, because the parameters of the boxes measured so far were not optimal, requiring either very-high frequency or short duration pulses, which are difficult to realize. Future experiments in which the fabrication parameters of the qubit are controlled and improved can greatly ease these requirements, and are predicted to improve both the decoherence and relaxation times of the qubit. Because the backaction of our continuous SET measurement was clearly observable, we both observed its dependence on various biasing parameters of the setup, and also undertook theoretical investigations of the backaction of the SET. The initial steps on this resulted in an invited “insight review article” published in Nature in 2000 (see Appendix). These efforts are also continuing under the new grant period, including an expanded theoretical collaboration with Prof. Steve Girvin at Yale.

## Publications

### Peer-reviewed journals:

"Amplifying Quantum Signals with the Single-Electron Transistor,"  
M.H. Devoret and R.J. Schoelkopf, *Nature* 406, pp. 1039-1046 (2000).

### Conference proceedings:

"Observing Single Electron Tunneling Events in a Superconducting Single Electron Transistor,"  
K.W. Lehnert, P. Wahlgren, Per Delsing, and R.J. Schoelkopf, *Proceedings of the XXXVIth Rencontres de Moriond, Les Arcs France, 2001*, eds. T. Martin, G. Montambaux, J.T. Tanh Van, (EDP Sciences, France) pp. 117-120.

"Qubits as Spectrometers of Quantum Noise,"  
R.J. Schoelkopf, A.A. Clerk, S.M. Girvin, K.W. Lehnert, and M.H. Devoret, to appear in *Proceedings of NATO-ARW Workshop on Quantum Noise in Mesoscopic Physics, Delft 2002*, ed. Y. Nazarov (Kluwer Scientific). Also appears on cond-mat archive: cond-mat/0210247.

### Conference presentations:

"Measuring Quantum Coherence in the Single Cooper-Pair Box," K.W. Lehnert  
invited talk at APS March Meeting, 2002  
contributed talk at Applied Superconductivity Conference, 2002  
Condensed-Matter Seminars at Physics Departments at Michigan State University, Purdue University, Massachusetts Institute of Technology, University of Pennsylvania, Brown University, JILA/Univ. of Colorado, University of Minnesota, Cornell University, Harvard University; Spring 2002.

"Measuring Quantum Coherence in the Single Cooper-Pair Box," R.J. Schoelkopf  
Physics Colloquium, Yale University, 11/01, Solid-State Seminar, SUNY Stonybrook, 12/01.

"Fast Electrometry of Coherent Macroscopic States in the Cooper-pair Box," R.J. Schoelkopf  
invited presentation at ITP Workshop on Nanoscience, Santa Barbara, CA, Aug., 2001.

"Probing the Dynamics of Single-Charge Circuits with Fast Electrometry," R.J. Schoelkopf  
invited presentations at: Applied Superconductivity Conference 2000, Virginia Beach, Sept. 2000;  
International Workshop on Mesoscopic Electronics, Ascona, Switzerland, Oct. 2000;  
XXXVIth Rencontres de Moriond, Savoie, France, Jan 2001.

### Submitted manuscripts:

"Measurement of the Excited State Lifetime of a Microelectronic Circuit,"  
K.W. Lehnert, K. Bladh, L.F. Spietz, D. Gunnarson, D.I. Schuster, Per Delsing, and R.J. Schoelkopf,  
to appear in *Physical Review Letters*, 2002.

"Quantum Fluctuations in the Single-Electron Box,"  
K.W. Lehnert, K. Bladh, D. Gunnarson, Per Delsing, and R.J. Schoelkopf,  
submitted to *Phys. Rev. Letters*, 2002.

"Measuring the Backaction of an SET on the Single-Electron Box,"  
B.A. Turek, K.W. Lehnert, K. Bladh, D. Gunnarson, Per Delsing, and R.J. Schoelkopf,  
In preparation for *Phys. Rev. Letters*, 2002.

### Technical reports:

"Amplifying Quantum Signals with the Single-Electron Transistor,"  
M.H. Devoret and R.J. Schoelkopf, *Nature* 406, pp. 1039-1046 (2000).

"Measurement of the Excited State Lifetime of a Microelectronic Circuit,"  
K.W. Lehnert, K. Bladh, L.F. Spietz, D. Gunnarson, D.I. Schuster, Per Delsing, and R.J. Schoelkopf,  
to appear in *Physical Review Letters*, 2002.

"Qubits as Spectrometers of Quantum Noise,"  
R.J. Schoelkopf, A.A. Clerk, S.M. Girvin, K.W. Lehnert, and M.H. Devoret, to appear in *Proceedings of NATO-ARW Workshop on Quantum Noise in Mesoscopic Physics, Delft 2002*, ed. Y. Nazarov (Kluwer Scientific). Also appears on cond-mat archive: cond-mat/0210247.

## Personnel and Budget Discussion

Several postdoctoral fellows and students were supported in part or in full by this grant, though no student theses have yet been written. The main researcher supported by this grant was a postdoctoral fellow, Dr. Konrad Lehnert, who performed many of the experiments which are reported here. Dr. Lehnert leaves the project this December, to begin a new position as Associate Fellow of the Joint Institute for Laboratory Astrophysics (JILA) and Adjoint Professor of Physics at The University of Colorado. A second postdoc, Dr. Ryan Held, was funded for a short period of time from this grant, concentrating on fabrication and electromagnetic simulation of qubit chips. The students funded include Lafe Spietz, Ben Turek, and David Schuster. Mr. Turek and Mr. Schuster now have their tuition and stipend provided by supplementary SUSPENSE grants for graduate support, but their equipment and supplies continue to be drawn from this grant. A subcontract to Chalmers University in Goteborg, Sweden allowed our collaborators there to fabricate the initial devices with SETs and Cooper-pair boxes that were used in these experiments. A small amount of salary was provided for Prof Michel Devoret, during a year-long sabbatical visit to our lab in 1999-2000. This led to a major publication in Nature, as well as Prof Devoret's eventual move to the US to join the Yale Applied Physics department. Some funds were also used for summer salary for the PI.

Especially during the one to two years of this project, there was a major effort in building apparatuses and infrastructure, and therefore significant expenses in supplies and equipment. A dilution refrigerator was purchased with PI's university setup funds, but supplies for the wiring and filtering of the refrigerator for the qubit experiments were supplied by this grant, as well as some specialty equipment such as cryogenic RF amplifiers. Because of the overlap with the renewal grant covering this project, funds from the last year of this grant were rebudgeted and applied towards the purchase of a second dilution refrigerator, which will double our experimental capability when it becomes operation in mid-2003. Other major equipment purchases included a 40 GHz network analyzer, a superconducting magnet and associated low-loss dewar, microwave components for cabling and pulse generation, the fast data-acquisition cards, finite-element analysis software packages for microwave and electrostatic circuit simulation, and RF synthesizers with fast pulse capability for generating the carrier for the RF-SET readouts.

## Detailed Discussion of Technical Results

Following the general approach described in the summary above, during this funding period we developed the capability for performing single-charge measurements, using the high-speed version of the single electron transistor (RF-SET) as a high-performance electrometer. During this project, we performed the first ever charge measurements with an RF-SET, and have improved the techniques, control software, and calibration procedures so that both very high speed (submicrosecond) and truly high-precision (level of a millielectron of charge) charge measurements are now routine. Several manuscripts employing these results to study the single Cooper-pair and single electron box are now in press or in preparation, and this work will continue.

Several generations of chip layouts were fabricated and modeled, and two different designs have been measured at cryogenic temperatures. An atomic force microscope image of the type of chip used for the coherence measurements, showing the Cooper-pair box (with a small SQUID loop to allow in-situ tuning of the Josephson energy) and the integrated RF-SET readout electrometer, is presented in Figure 2. Two samples of slightly different designs were studied, for which the electrometers had a charge noise of approximately  $4 \times 10^{-5}$  electrons/rt(Hz) at high frequencies.

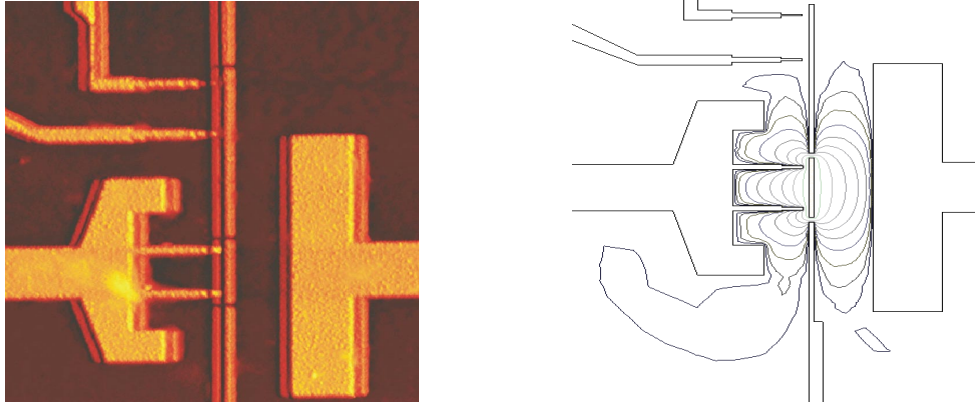


**Figure 2.** Atomic force microscope image (left) of single Cooper-pair qubit (bottom) and RF-SET measuring electrometer (top), fabricated in Al/AlO<sub>x</sub>/Al tunnel junctions using direct-write electron-beam lithography. The CPB has two junctions formed into a superconducting loop, which allows a tuning of the effective Josephson energy,  $E_J$ , with a magnetic field. Right image is results of a 3-d finite element simulation of the electromagnetics of this structure, used to find the full capacitance matrix for the circuit.

In our first measurements on the CPB qubit, a simple scheme was used in which the electrometer continuously measures the time-averaged charge on the box, and acquisition times per point are longer than the dynamical timescales in the box. This is therefore an ensemble measurement, with many realizations of the single pseudo-spin acquired sequentially in time. Nonetheless, this mode allows a rapid characterization of the CPB spectrum. By studying the average charge as a function of temperature, several important parameters of the system, including the gate capacitance, the measurement capacitance that couples the box to the electrometer, and the total box capacitance or charging energy  $E_C$ , were determined.

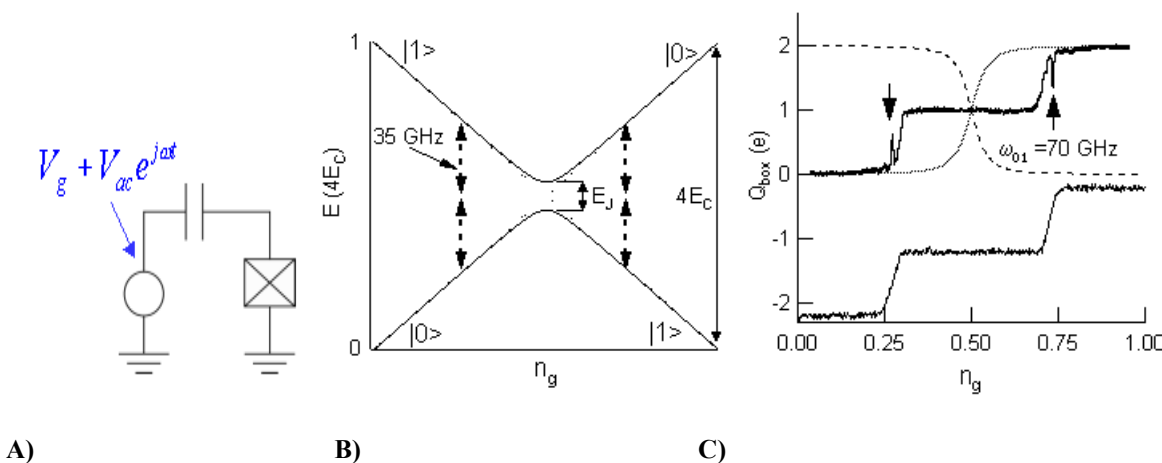


**Figure 3:** CW spectroscopy of Cooper-pair box, as observed in a continuous measurement with the RF-SET. **A)** A high-frequency (35 GHz) microwave signal, plus a dc gate voltage, are applied to the CPB. **B)** Diagram of energy levels vs. dc gate voltage. At two points, on either side of the degeneracy point, the energy level splitting is resonant with the microwave drive, and transitions between ground and excited states are driven. On the left hand side, the drive causes transitions from the charge 0 to charge 1 state, while the opposite is true on the right-hand side, thus an absorption peak and dip, respectively. **C)** Average charge on the CPB as a function of normalized gate voltage. Lower curve is without microwaves, the dotted and dashed curves show the expected ground and

excited state charge signal, solid upper curve shows the resonant absorption features caused by the coupling of ground and excited states. The actual peaks observed correspond to two-photon transitions, where the box's energy splitting is  $\sim 70$  GHz.

With this setup, the signal-to-noise in the determination of the charge state of the box is very high. In fact, when performing CW spectroscopy of the charge states in the CPB, the photon resonance peaks can even be seen in realtime on an oscilloscope. In this measurement, a CW microwave excitation is applied to the gate of the box, and resonant absorption peaks (see Fig. 3) are observed where the energy splitting between the ground and excited states matches the applied photon frequency. By studying the photon peak height and width as a function of the microwave power applied, we can extract (see Fig. 4) the ensemble averaged decoherence time,  $T_2^*$ , using standard results for the driven two-level system. The measured coherence time of about 1 nanosecond is similar to that observed without echo methods by Nakamura, and probably limited by the low-frequency  $1/f$  offset charge noise of the device. However, our initial use of a continuous measurement means that additional dephasing due to the SET electrometer may be present. A determination of the dominant dephasing mechanism, and a separation of the measurement effects, are now underway and will be extended in future work. We have even observed that the SET is able to drive transitions ("state mixing") between states in the box, which limits the investigations to large energy splittings, away from the degeneracy point in gate voltage. Using time-gated measurements with the RF-SET, we have measured this mixing time due to the SET is about 10 microseconds.

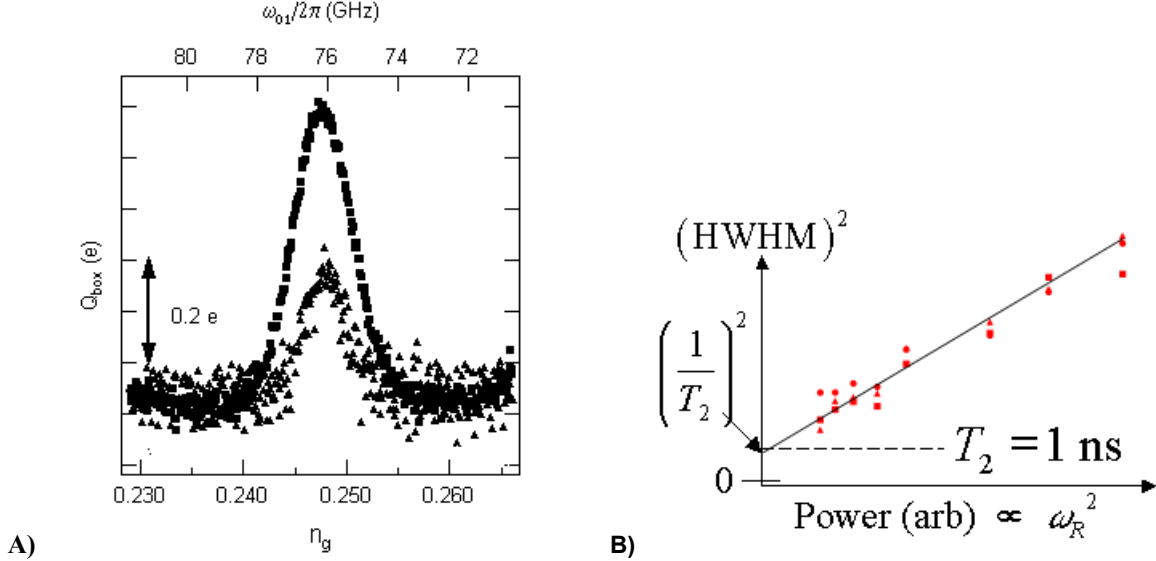


**Figure 4:** **A)** Expanded view of a photon peak from Figure 3. **B)** The power dependence of the linewidth of the photon peaks in Figure 3. The square of the observed photon peak width is plotted against the microwave power, or Rabi frequency squared. The linear behavior allows the extraction of a  $T_2^*$  value for the CPB of  $\sim 1$  nanosecond.

One of the first tasks that we needed to perform with this system is to determine the parameters of our box and electrometer circuit, and to verify that the Hamiltonian of our circuit matches that of a driven two-level or qubit. The expected Hamiltonian of the Cooper-pair box circuit is

$$\mathbf{H} = -2E_C(1 - 2n_g)\boldsymbol{\sigma}_z - \frac{E_J}{2}\boldsymbol{\sigma}_x \quad (\text{Equation.1}),$$

where  $\boldsymbol{\sigma}_x$  and  $\boldsymbol{\sigma}_z$  are Pauli spin matrices and  $n_g$  is total polarization charge applied to the gate electrode,  $n_g = C_g V_g / 2e - n_{off}$ , in units of a Cooper-pair's charge. The offset charge  $n_{off}$  accounts for the uncontrolled potential from charges nearby the box island. The charging energy,  $E_C = e^2 / 2C_\Sigma$ , is the electrostatic energy required to add one electron to the island and the Josephson energy,  $E_J^{max} = \hbar\pi\Delta / 4e^2 R_J$ , is the effective tunneling matrix element for Cooper-pairs across a junction with resistance  $R_J$  in a superconductor with BCS gap  $\Delta$ . The junction is in fact a composite of two junctions shorted together to form a loop with  $1(\mu\text{m})^2$  area (Fig. 2). The effective Josephson energy  $E_J$  of the pair of junctions is tuned by introducing magnetic flux  $\Phi$  into this loop, as  $E_J = E_J^{max} \cos(\pi\Phi / \Phi_0)$ , where  $\Phi_0$  is the quantum of flux ( $h/2e$ ).

This Hamiltonian was verified by performing the CW spectroscopy with continuous measurement (as described above), by applying a continuous microwave stimulus to the gate of the Cooper-pair box, and tuning the parameters of the TLS to find the resonance condition. In Fig. 3B we show the ground-state and excited-state energies of the Hamiltonian of Eq. 1 as a function of the reduced gate voltage,  $n_g$ . Figure 3B shows that as  $n_g$  is tuned through  $1/2$ , the charge of the ground and excited states exchange,

with the ground state acquiring a charge of one Cooper pair and the excited state attaining zero charge. Also plotted is an ensemble-averaged measurement of the charge on the box as a function of  $n_g$ . It is apparent that the box does not remain in its ground state over a range in  $0.3 < n_g < 0.7$ . This behavior is caused by backaction generated by currents flowing through the RF-SET. We proceed by studying the box in the range of  $n_g$  where it does remain in its ground state. When a 38 GHz microwave signal is applied to the gate, we observe clear evidence that the box is a coherent two-level system. Resonant peaks appear (Fig. 3C) in  $Q_{box}$  that are sharp and symmetrically spaced about  $n_g = 0.5$ . The two features, a peak for  $n_g < 0.5$  and a dip for  $n_g > 0.5$ , both correspond to the change in  $Q_{box}$  when the box spends some time in the excited state. Because  $Q_{box}$  is an average of thousands of repeated measurements, the peak height indicates the probability of finding the box in its excited state.

The resonant peaks permit a spectroscopic determination of the parameters in the box's Hamiltonian. By plotting the locations of the resonances as a function of  $n_g$  and  $\Phi$ , we find good agreement between this spectroscopy and the difference  $E_{01} = \hbar\omega_{01}$  between ground-state and excited-state energy expected from Eq. 1. An independent measurement of  $E_C$ , observing the thermal smearing of the Coulomb staircase in the normal state, demonstrates that these peaks occur when the irradiating frequency  $\omega$  is half  $\omega_{01}$ , indicating that these peaks correspond to a 2-photon transition. We find a single value for  $E_C$  and for  $E_J^{\max}$  that account for the location of the resonant peaks at applied frequencies between 32 and 38 GHz giving resonant peaks for  $\omega_{01}$  between 64 and 76 GHz (Fig. 5A). At lower frequencies, the 2-photon peaks would appear at an  $n_g$  for which the box does not stay in the ground state while being measured and are therefore not visible (For lower frequencies, we have observed the 3-photon peaks whose location in  $n_g$  is consistent with our interpretation). We are able to extract the parameters of the Hamiltonian,  $4E_C/h = 149.1 \pm 0.4$  GHz and  $E_J^{\max}/h = 13.04 \pm 0.2$  GHz. The uncertainties arise from the systematic deviation from linearity of the function generator, which created the ramp voltage for  $V_g$ . Because these measurements were made at a temperature  $T = 0.015$  K, they are in the limit  $k_B T \ll E_J^{\max} \ll 4E_C$ .

Consistent with the behavior of a TLS, the peaks disappear for  $\Phi = \Phi_0/2$  when  $E_J$  approaches 0, which demonstrates that  $E_J$  provides the coupling between the charge states (Fig. 5B). This can be understood geometrically from the fact that an oscillating gate voltage with amplitude  $V_g^{ac} = 2en_g^{ac}/C_g$  adds a term to the Hamiltonian in Eq. 1  $n_g^{ac} \cos(\omega t)\sigma_z$ , which is collinear with ground state of the quasi-spin described by Eq. 1 when  $E_J = 0$ . The microwave excitation therefore applies no torque which could excite the quasi-spin from its ground state.

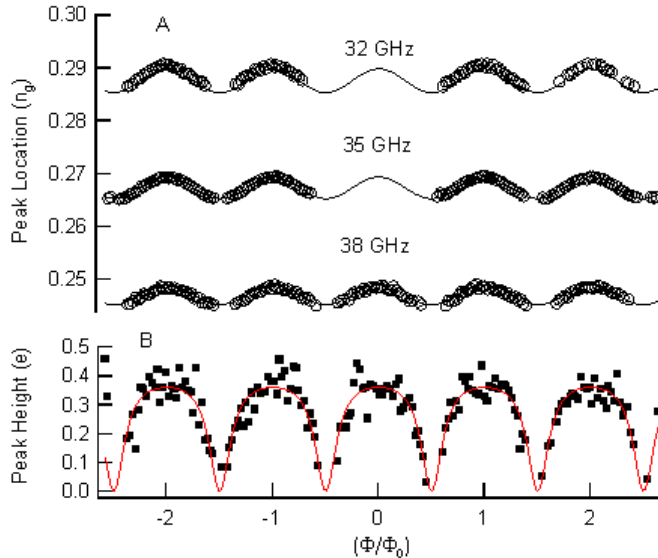


**Figure 5 A.)** The symbols (open circles) represent the locations of resonant peaks as a function the two control parameters of the Hamiltonian,  $n_g$  and  $\Phi$ , for three frequencies,  $\omega = 32$  (top), 35, and 38 (bottom) GHz. The three lines are a fit to the data, using Eq. 1 to find  $n_g$  given  $\omega_{01}$  and  $\Phi$  for  $\omega_{01} = 64, 70$  and  $76$  GHz. **B.)** The size, in electrons, of a 38 GHz resonant peak as a function of  $\Phi$  (squares). Note that the peaks disappear when  $E_J$  approaches zero.

In order to measure the excited-state lifetime  $T_1$ , we excite the box and then measure the time required to relax back to the ground state. A 38 GHz signal is continuously applied to the gate and the box gate is tuned to  $n_g = 0.248$  and  $E_J = E_J^{\text{max}}$  so that the microwaves resonantly couple the ground and excited state through a 2-photon transition. Abruptly,  $n_g$  is then shifted to  $n_g = 0.171$  in 30 ns, slowly enough to be adiabatic but much faster than  $T_1$ . The microwave excitation no longer resonantly couples the ground and excited state, and the probability of being in the excited state decays in a time  $T_1$ . By averaging many of the transient responses to this stimulus, we find  $T_1 = 1.3 \mu\text{s}$  (Fig. 6). The lifetime is a quantity which is insensitive to slow drifts in  $n_{\text{off}}$  and demonstrates that the intrinsic quality factor of the TLS,  $Q_1 = T_1 \omega_{01} = 5 \times 10^5$ .

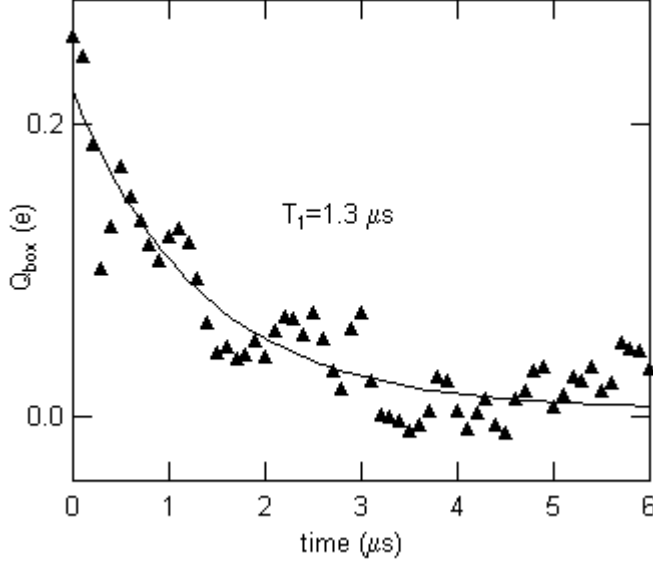


**Figure 6:** The average charge on the box is plotted (triangles) as a function of time  $t$ , relative to  $t = 0$ , when  $n_g$  is shifted from  $n_g = 0.248$  to  $0.171$  in 30 ns. With 38 GHz microwaves applied, the shift in gate brings the box out of resonance with the microwave excitation. The decay in the charge on the box represents the decay of the probability of the box being in its excited state after the shift in  $n_g$ . An exponential fit to the data implies  $T_1 = 1.3 \mu\text{s}$  (line).

We can compare this long lifetime, with the spontaneous emission rate induced by the quantum fluctuations of a generic electromagnetic environment. Calculating the spontaneous emission rate using Fermi's golden rule gives

$$\frac{1}{T_1} = \left( \frac{C_g^T}{C_\Sigma} \right)^2 \left( \frac{e}{\hbar} \right)^2 \sin^2(\theta) S_V(\omega_{01}) \quad (2)$$

where  $S_V(\omega) = 2\hbar\omega(\text{Re}(Z_0))$  is the voltage spectral density (per Hz) of the quantum fluctuations of an environment with an impedance  $Z_0$  at frequency  $\omega$  and  $\sin\theta = E_J / \hbar\omega_{01}$ . The quantity  $C_g^T$  is the total capacitance of the box to nearby metal traces, including intentional coupling to the gate lead and other unintended capacitive coupling (Fig. 1). We calculate  $T_1$  for a  $Z_0 = 50 \Omega$  environment to be between 1 and 4  $\mu\text{s}$ , extracting  $C_g^T = 60 \text{ aF}$  with about 50% uncertainty from an electrostatic simulation of the chip layout. We do not claim to have demonstrated that the lifetime is limited by spontaneous emission; however, if there are additional relaxation processes, either due to the nearby electrometer or fluctuations of some microscopic degree of freedom in the box, their influence is at most comparable to that of spontaneous emission into a  $50 \Omega$  environment. This very long lifetime emphasizes the importance of understanding and reducing the excess dephasing.

Our measurement of the excited state lifetime of box is remarkable for two reasons. First, it shows that a quantum-coherent microelectronic circuit can have a lifetime that approaches the limit set by spontaneous emission of a photon into the electromagnetic environment. Furthermore, it is achieved while the two-level system is continuously measured. This means that the coherence time in the Cooper-pair box can be long lived, if the sources of inhomogeneous decoherence can be reduced. M. Devoret and coworkers (formerly at Saclay, and now at Yale) have indeed observed dephasing times close to the inelastic lifetime limit in a similar system, by

operating at the charge degeneracy point,  $n_g = 0.5$ . Furthermore, given the observed electrometer sensitivity of  $4 \times 10^{-5} e/\sqrt{\text{Hz}}$ , the excited-state lifetime is long enough that a single measurement can discriminate between the box in its excited state and the box in its ground state with 99% confidence. Both of these are vital to implementing a quantum computer. In future work we intend to operate these CPB qubits at a charge-noise insensitive point in gate bias ( $n_g=0.5$ ), and also to perform single-shot readouts of the quantum state, both of which are required before proceeding to studies of entanglement in superconducting qubits and implementation of quantum logic gates.

One attractive feature of the RF-SET measurements we perform is that the operating point of the SET, and its backaction effects on the CPB, can be widely varied. In fact, we have already observed a dependence of the average charge state of the CPB, i.e. the degree of polarization of our psuedo-spin, on this operating point (see Fig 9). We find that higher bias, and higher drain-source current, lead to an increase in “mixing”, or driven transitions between states in the CPB. We could further observe the evolution of the quantum state of the CPB as a function of time after turning on the measurement, which allowed us to determine a “mixing time” for the states of about 10  $\mu\text{s}$ . By repeating and refining these types of measurements, and by tuning the Josephson energy and energy level splitting of the box, we can use the CPB two-level system as a spectrum analyzer to measure the full noise spectrum produced by the SET. Another interesting possibility is to observe the dephasing effects of the measurement on the width of photon resonances, i.e. the actual dephasing.

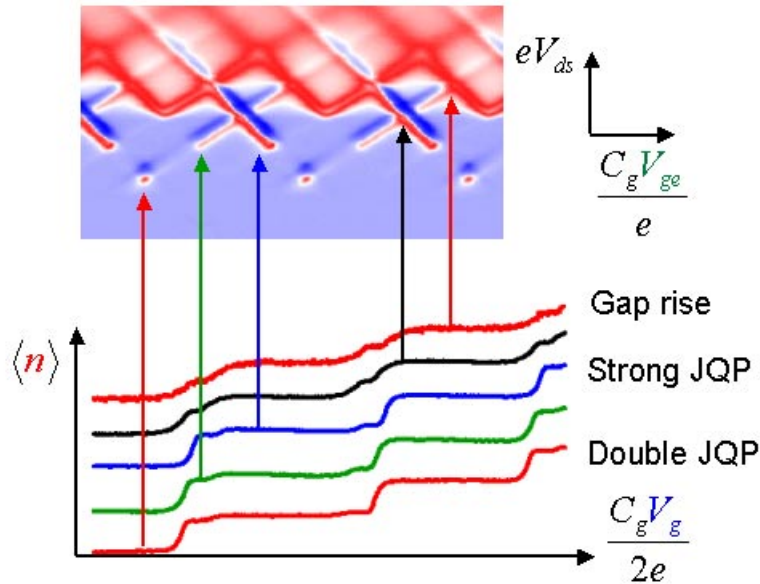


**Figure 7:** Dependence of CPB states on bias conditions of the SET electrometer. The top panel shows the conductance through the measuring SET as a function of the voltage on the SET drain source ( $V_{ds}$ , vertical axis) and gate ( $V_{ge}$ , horizontal axis) voltage. The arrows indicate several operating points which have been investigated. Bottom panel shows the average charge on the CPB as a function of box gate voltage that is observed for each operating point.

The RF-SET is an appealing measurement device not only because of its tunability, but because the measurement process itself can be understood quantum mechanically. Most theoretical treatments of this problem, however, have focused on the simpler case of a normal SET. In this limit, it is expected that the SET can be nearly quantum limited, i.e. the dephasing introduced by the measurement approaches that required by the uncertainty principle. However, the actual measuring SET is superconducting, leading to more complicated dynamics and operating possibilities (e.g. the complicated charging diamonds of Fig. 7). In our first samples, we found that the least invasive continuous measurement was obtained at low drain-source bias on the SET, using a resonant Cooper-pair/quasiparticle tunneling feature (or “double JQP”). We are further exploring these types of features in the superconducting SET, and have begun to compare with theoretical models developed in collaboration with Steve Girvin’s group at Yale. We will explore the various parameters of the SET such as resistance, capacitance, and coupling to the CPB, and how to optimize these for both continuous and pulsed quantum measurements in future.

### Report of Inventions

No inventions, patentable or otherwise, to report.

### Appendix: Copies of Major Publications

Three publications, as described above, are appended to this electronic file.

# Amplifying quantum signals with the single-electron transistor

Michel H. Devoret\*† & Robert J. Schoelkopf\*

\*Department of Applied Physics, Yale University, New Haven, Connecticut 06520, USA

†Service de Physique de l'Etat Condensé, CEA-Saclay, F-91191, France

Transistors have continuously reduced in size and increased in switching speed since their invention in 1947. The exponential pace of transistor evolution has led to a revolution in information acquisition, processing and communication technologies. And reigning over most digital applications is a single device structure — the field-effect transistor (FET). But as device dimensions approach the nanometre scale, quantum effects become increasingly important for device operation, and conceptually new transistor structures may need to be adopted. A notable example of such a structure is the single-electron transistor, or SET<sup>1–4</sup>. Although it is unlikely that SETs will replace FETs in conventional electronics, they should prove useful in ultra-low-noise analog applications. Moreover, because it is not affected by the same technological limitations as the FET, the SET can approach closely the quantum limit of sensitivity. It might also be a useful read-out device for a solid-state quantum computer.

It is now possible to put a billion transistors on a single chip operating with a clock period of a billionth of a second. Most probably, the trend in reducing dimensions and times will continue in the next decade. But as the number and density of gates and memory elements increase, the energy of signals also has to be reduced to keep the power dissipation sufficiently low.

Surprisingly, even though the size of a typical transistor in a microcomputer chip is now just a few hundred nanometers, its functioning remains essentially classical: quantum mechanics only enters in the explanation of the values of the physical parameters of materials, like the band-gap of a semiconductor. Otherwise, the discreteness of matter and the wave-like properties of electrons can be largely ignored in the understanding of the behaviour of electrical signals in today's integrated circuits.

But as devices get smaller, faster and more densely packed, quantum effects will have increasingly to be taken into account. Even well before we reach the ultimate limit where transistors are reduced to the size of an atom or a molecule, we encounter four limits. Quantum phenomena become significant when (1) signal energy, (2) signal charge, (3) device dimension, and (4) device size tolerance approach, respectively, the energy of one photon, the charge of one electron, the electron wavelength, and the size of one atom.

Much research has been devoted to assess if quantum effects arising from these conditions will force the adoption of new physical principles or if they can simply be tamed by better control of the chip structure at the atomic level. To our knowledge, there is no general consensus on the answer to this question.

Another research direction has been to exploit quantum effects arising in devices of nanometer scale to implement a function that cannot be performed by present devices. In some applications, which operate at limits (1) or (2) or both, it is not only inevitable but also desirable. In astronomy, for instance, it is important to extract as much information as possible from a single photon<sup>5</sup>. Recent advances in quantum information theory<sup>6</sup> indicate that scalable switching elements that behave fully as quantum systems would not

simply make calculations with minimal energy, they could in addition perform tasks that would be impossible with conventional computers. In a quantum computer, usual bits are replaced by quantum bits or 'qubits' which can be 'entangled' with each other, thereby carrying a new type of information that is useful in solving highly parallel tasks. New types of devices are needed to read-out such qubits, that is, to amplify their associated single-quantum signals.

In the realm of atomic physics and quantum optics, the detection of individual microscopic particles travelling in vacuum, such as photons and electrons, is now performed routinely with almost unity efficiency by instruments derived from the photomultiplier. However, the measurement of electrical signals resulting from the motion of a single electron in a circuit involves an amplifier having not only a good energy sensitivity, but also electrical characteristics that are adapted to this circuit.

A particularly simple and spectacular example of such a device is the single-electron transistor (SET)<sup>1–3</sup>, which exploits the quantum phenomenon of tunnelling to control and measure the movement of single electrons inside a solid-state circuit. SETs are extremely precise solid-state electrometers<sup>4,7</sup>, already out-performing state-of-the-art conventional transistors<sup>8</sup> by three orders of magnitude. Their charge sensitivity has been shown to be as low as a few  $10^{-5} e/\sqrt{\text{Hz}}$ , which means that a charge variation of  $10^{-5} e$  can be detected in a measurement time of 1 s (the precision improves as the square root of the measurement time). This result is only an order of magnitude away from the theoretical limit of  $10^{-6} e/\sqrt{\text{Hz}}$ . SETs have applications in metrology<sup>9</sup> and single-photon detection<sup>10,11</sup>. Furthermore, it has been realized in the past few years that SETs can perform a measurement on a single quantum two-state system (qubit)<sup>12,13</sup>, perturbing its quantum evolution in a minimal way. That is, the SET is a charge amplifier operating in the vicinity of the quantum limit. It would be a practical read-out device for several solid-state implementations of qubits<sup>14</sup>. In this article we review these latest developments.

## Conventional transistors

Before discussing the performance of SETs, it is useful to recall the operating principle of the most common transistor,

the metal-oxide semiconductor field-effect transistor (MOSFET). Figure 1 depicts schematically the layout of the device and its operating principle (we restrict ourselves here to the nMOSFET, in which the majority charge carriers are electrons). Two conducting electrodes, called the source and drain, are connected by a channel made of a material in which the number of conduction electrons can be varied, in practice a semiconductor (Fig. 1a). A voltage is applied to the 'gate', a third conducting electrode that is separated from the channel by a thin insulating layer. When the gate–source voltage is zero, there are no conduction electrons in the channel as the effective potential they would experience there is larger than in the leads (Fig. 1b). The channel is therefore in an insulating state. But when the gate voltage is increased with respect to the source, the potential experienced by the electrons in the channel decreases and they populate the channel just under the gate (Fig. 1c). The channel becomes conducting. The larger the gate voltage, the larger will be the channel electron population that can participate in the current. Eventually, all the electron states in the energy window set by the source–drain voltage can propagate through the channel and the current no longer depends on the gate voltage. This saturation regime is depicted in Fig. 1d.

This field effect provides an amplification mechanism since an increase in gate voltage, bringing a modest current to the gate electrode, can switch on a larger current through the channel (Fig. 2). The source–drain current is determined by the conductance of the channel, which in turn depends on two factors: the density of its conduction electrons and their mobility. The electron density is controlled directly by the gate voltage. The electron mobility is set by the collisions of electrons with static irregularities of the crystal as well as with its dynamic deformations due to thermal agitation. When thermal agitation is the predominant factor, electron mobility is, to a large extent, independent of the gate voltage. However, at low temperatures, mobility can also increase when the density increases, reinforcing the influence of the gate voltage on the source–drain current.

Note that so far we have made no reference to the wave-like properties of electrons nor to the fact that the channel is made from individual atoms. The only quantum property that has had a role in our explanation is the Pauli principle, which dictates that each possible state for an electron in the channel can be occupied at most by only one electron. This means that only a certain number of electrons can accumulate in the channel, setting a limit on the current flow.

However, the quantum properties of electrons and atoms will be increasingly important as FETs are made smaller. For example, the wave nature of electrons will influence the way they travel through the channel. When the transverse dimension of the channel becomes comparable to the wavelength of electrons (around 100 nm), electron propagation becomes more sensitive to the atomic disorder in the device, which is inherent in the present fabrication process. The disorder makes the channel remain insulating even when the density of electrons is increased. Effects of this kind, which result from reaching the limit to device dimension (limit (3) above), pose a major problem if the reduction of size is not accompanied by an improvement in the atomic structure of the fabricated devices.

If, however, the atomic structure of the FET could be made defect-free, a recent analysis<sup>15</sup> shows it would continue to function in the regime where the electron propagation in the channel is wave-like. It would thus 'break' limit (3) and could be further scaled down until a channel length of about 8 nm is reached, a stage at which limit (4) seems to severely affect the performance of the FET.

In an ideal situation, we might want electrons to be scattered only by the gate-dependent potential, with other scattering mechanisms always being detrimental to amplification. But the confinement of electrons in the channel by tunnel barriers, in the source–drain direction, can also lead to a new kind of amplification principle. This is the basis of the SET. As we shall see, this new principle circumvents the problem of the FET that the gate capacitance, which is an important factor in determining charge sensitivity, is tied to the size of the

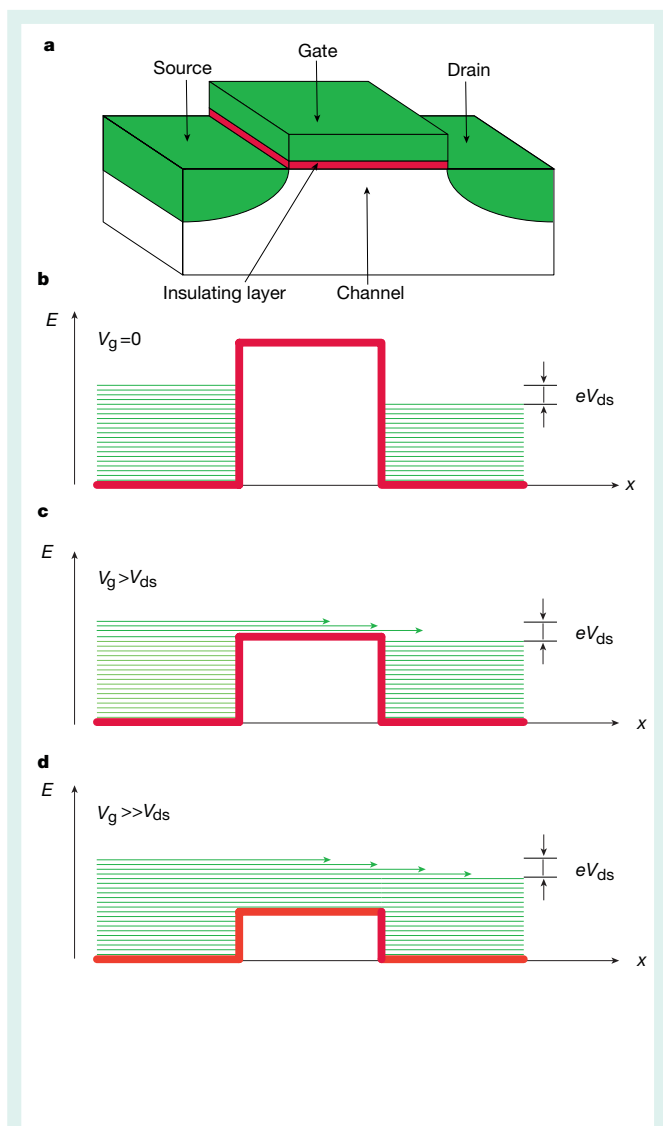


**Figure 1** Principle of a metal-oxide semiconductor field-effect transistor (MOSFET). **a**, The device consists of two conducting electrodes (source and drain) connected by a semiconducting channel. The channel is influenced electrostatically by the gate, a conducting electrode separated from the channel by thin insulating layer. **b**, When the voltage applied between the gate and the source is zero, the Fermi energy of the source and drain lies in the gap of the semiconductor. Here, we sketch the potential (red curve) seen by conduction electrons when they travel from source to drain along a line in the channel just under the gate. There are no filled electron states (green lines) in the channel, which as a result remains insulating. **c**, When the gate voltage is increased, the potential seen by conduction electrons is lowered. There are now filled states in the channel at the Fermi energy of the source and drain. The device conducts. **d**, When the gate voltage is increased further, the current finally saturates when all the states in the bias window are filled.

channel. Until the technology for reliably fabricating FETs with channels of nanometre-scale dimensions has been developed, the SET is the best device in terms of charge sensitivity.

### Operating principle of SETs

Unlike the FET, whose principle does not require the motion of electrons to be quantum-mechanical, the SET is based on an intrinsically quantum phenomenon: the tunnel effect through a metal–insulator–metal junction. When two metallic electrodes are separated by an insulating barrier whose thickness is only  $\sim 1$  nm, electrons at the Fermi energy can traverse the insulator even though their energy is too

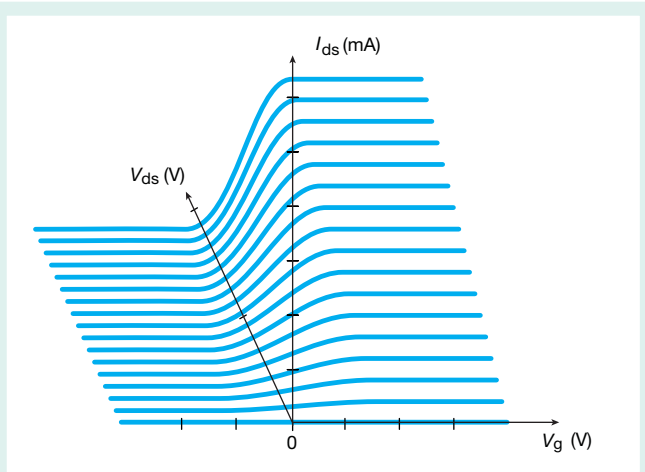


**Figure 2** Variation of the source–drain current in a MOSFET as a function of the gate voltage. When the gate voltage is increased from zero, the source–drain current is turned on. This device can be used both in digital electronics and as an amplifier for analog signals.

low to overcome, in a classical motion, the large potential barrier of the insulating region. The tunnel effect manifests itself by a finite resistance  $R_T$  of the insulating barrier. This resistance depends both on the transmission coefficient  $\mathcal{T}$  of the barrier to electron waves (which is an exponentially decreasing function of its thickness) and on the number  $M$  of independent electron wave modes impinging on the barrier (this number is equal to the area of the junction divided by the square of the electron wavelength). The SET uses a key property of the tunnel effect in a many-electron system: for barriers such that  $\mathcal{T}M \ll 1$ , the charge  $Q$  transferred through the barrier becomes quantized with  $Q = Ne$ , where  $N$  is an integer<sup>16</sup>. In other words, for  $N$  not to be subject to quantum fluctuations, the resistance of the junction must be large compared with the resistance quantum  $R_T \gg h/e^2 = R_K = 25.8\text{ k}\Omega$  (refs 17,18).

The SET consists of two such tunnel junctions placed in series (Fig. 3a,b). An ‘island’ is thus formed between the two junctions. A gate electrode is coupled electrostatically to the island. The SET can thus be described as a FET in which the semiconducting channel has been replaced by a metallic island sandwiched between two tunnel barriers. The island has a total capacitance  $C_S$ , which is the sum of the gate and junction capacitances  $C_S = C_g + C_{J1} + C_{J2}$ .

If the dimensions of the island are sufficiently small, the charging energy  $E_C = e^2/(2C_S)$  of one extra electron in the island will become larger than the energy of thermal fluctuations:  $E_C \gg k_B T$ , where  $k_B$  is the Boltzmann constant and  $T$  is temperature. In practice, for devices fabricated by standard electron-beam lithography,  $C_S$  is of the order of a femtofarad and the charging energy is of order 1 K, necessitating temperatures below 300 mK to satisfy the above charging energy criterion. Over the past few years, however, experiments have shown that with advanced fabrication methods, room temperature operation is possible<sup>19–21</sup>.

Because electrons interact strongly via the Coulomb interaction when they pass through the island, the analysis of the SET differs fundamentally from that of the FET. In the FET, electrons go from source to drain independently, and in such numbers that one can consider that the potential seen by one is an average which does not depend on the configuration adopted by all of the others. Electrical transport results from a simple addition of the motion of each electron. In the SET, by contrast, transport results from transitions between collective charge states of the system. These charge states are described by the two numbers  $N_1$  and  $N_2$  of electrons having traversed the junctions (Fig. 3b).

The behaviour of the device is governed by the global electrostatic

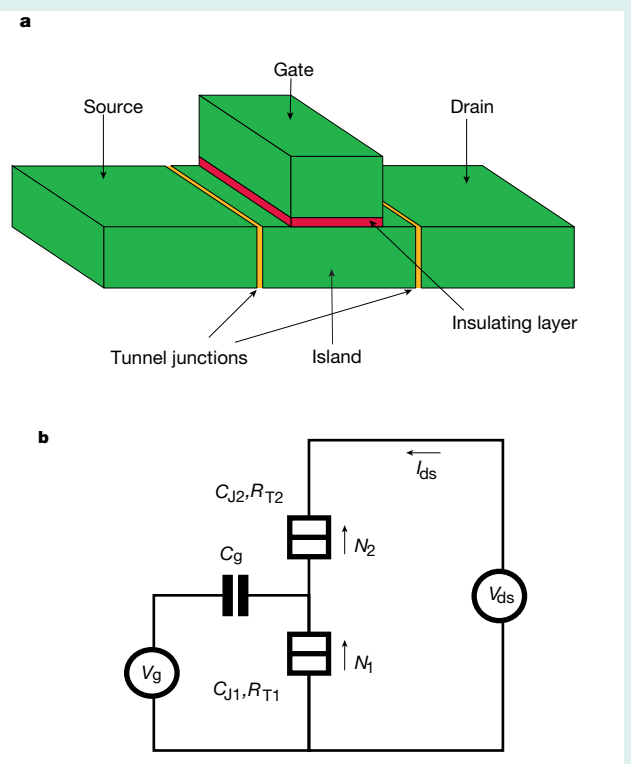


**Figure 3** The single-electron tunnelling transistor (SET). **a**, Simplified three-dimensional structure of the SET. The channel of the FET is replaced here by a sandwich consisting of a nanoscale metal electrode (island), which is connected to the drain and the source by tunnel junctions. As in the FET, a gate electrode influences the island electrostatically. **b**, Circuit diagram of the SET. The square box symbol represents a tunnel junction, and integers  $N_1$  and  $N_2$  denote the numbers of electrons having tunneled through the two junctions. Each junction is characterized by its capacitance and its tunnel resistance.

energy<sup>16</sup>  $E_{cl} = E_C[N_2 - N_1 - (C_g V_g/e) - (C_2 V_{ds}/e) + q_0]^2 - eN_2 V_{ds}$ , which includes the energy stored in the junction and gate capacitances, as well as the work done by the voltage sources. Here,  $V_g$  and  $V_{ds}$  are the voltages applied between gate and source, and drain and source, respectively. The so-called offset gate charge  $q_0$  is a phenomenological quantity describing the fact that electric fields in the capacitances of the system are non-zero even when the island is neutral and when no voltage is applied. It takes a randomly different, non-integer value for each device and cool-down. It also fluctuates slowly in time with a  $1/f$  spectral density<sup>22</sup>. We will discuss its effect in more detail below. But as far as the amplification mechanism of the SET is concerned, we can treat it as a constant.

According to the so-called ‘global rules’, also known as ‘orthodox theory’, tunnel events will take place independently on each junction at a rate governed by the global energy, provided that the junction resistances satisfy  $R_{T1}, R_{T2} \gg R_K$  and that the voltage sources  $V_g$  and  $V_{ds}$  have negligible internal impedance, on the scale of the resistance quantum, around the Coulomb frequency  $E_C/\hbar$  (ref. 17).

In this regime, each tunnel event creates one electron–hole pair, the electron and the hole being on opposite sides of the junction. The succession of tunnel events constitutes a Poisson process. More specifically, a tunnel event will take place on junction  $i$  with a rate given by  $T_i = [1/(R_{T_i} e^2)] [\Delta E_i / (1 - \exp(-\Delta E_i/k_B T))]$  where  $\Delta E_i = E_{cl}\{N_i^{\text{before}}, N_j\} - E_{cl}\{N_i^{\text{after}}, N_j\}$ .

At zero temperature, tunnel events take place only if they are energetically allowed, that is,  $\Delta E_i > 0$ . For a drain–source voltage below the Coulomb gap voltage  $e/C_S$ , the current therefore depends critically on the value of the gate voltage. If the gate voltage is such that

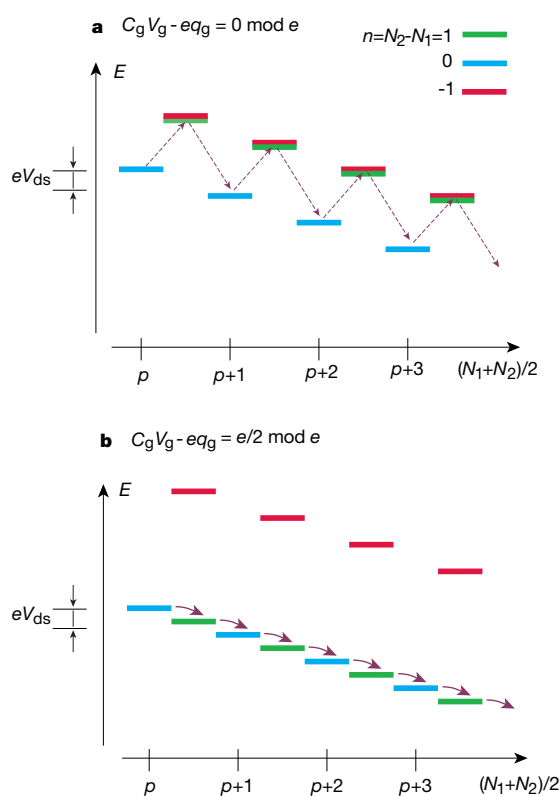


**Figure 4** Charge levels of the SET. **a**, Charge levels in the full Coulomb blockade; **b**, charge levels in the lifted Coulomb blockade case. The integers  $N_1$  and  $N_2$  denote the numbers of electrons having tunnelled through the two junctions (see Fig. 3). In **a**, the only possible conduction process is co-tunnelling, that is, a weak second-order process involving the tunnelling of two electrons on two different junctions and a virtual charge state (dashed purple arrows). In **b**, the main conduction process is a cascade of tunnel events involving the two junctions sequentially (full purple arrows).

$C_g V_g = q_0 e \bmod e$ , the island has a well defined number of electrons. Tunnel events cannot take place on the junctions because the global energy would increase (Fig. 4a) and the current is zero. This is the phenomenon of Coulomb blockade. But if the gate voltage is such that there is a charge equivalent to one half electron on the gate capacitance,  $C_g V_g = (q_0 + \frac{1}{2}) e \bmod e$ , tunnel events are energetically allowed (Fig. 4b). A cascade of transitions between charge states occurs, and current flows between source and drain.

Note that in practice the current cannot be turned off completely in the Coulomb-blockaded state. Higher-order processes in which several tunnel events occur simultaneously (co-tunnelling processes), and whose relative importance scale as powers of  $R_K/R_T$ , will induce a small leakage current not described by the orthodox theory. However, as long as  $R_K \gg R_T$ , the SET behaves as a charge amplifier as the presence or absence of a fraction of an electron on the gate capacitance can control an easily measurable current (the order of magnitude is around  $10^9 e/s$  in practical cases) (Fig. 5). This gain is not the only factor determining the sensitivity of the device. One must take into account the shot noise in the source–drain current, which is attributable to the quantum randomness of the time intervals between tunnel events (we work in a regime where thermal fluctuations can be neglected). This quantum randomness, corresponding to electrons having to ‘choose’ between the two sides of the barrier, is the process that ultimately limits the sensitivity of the device. As we will show below, the noise characteristics of the SET can be calculated exactly in a simple regime, which is rich enough to yield semi-quantitative understanding of the quantum limit of sensitivity.

Returning to the offset gate charge, it is believed that its value is determined in part by differences between the work functions of the metal of the island and that of the other electrodes. Even minute variations in the work functions are sufficient to cause  $q_0$  to fluctuate by numbers much greater than unity, which is the case observed in practice. Another potential source of fluctuation in offset charge is charge motion in the substrate or even in the tunnel barrier oxide. The absence of control over offset charges severely hinders any application of SETs to digital electronics, where the gate thresholds must be rigorously fixed and uniform. However, SETs can still be used as sensitive amplifiers in the audio-frequency (a.f.) or radio-frequency (r.f.) domains, as a simple additional feedback circuit can compensate for the fluctuations in offset charge that occur mainly at lower frequencies.

### Noise characteristics of an amplifier

Before we examine how quantum shot noise affects the ultimate performances of SETs, it is useful to discuss the noise properties of a general amplifier.

A linear amplifier can be described phenomenologically as a ‘black box’ with two input leads and two output leads. We can represent the inside of the black box by effective elementary components which accurately describe how it appears to the outside circuitry. If we limit ourselves to the simpler case where the amplifier has no feedback (that is, input current is independent of output voltage), we arrive at the schematics of Fig. 6 (feedback introduces complications that are not crucial in our discussion). Three elements describe the transformation of the signal by the amplifier: an ideal voltage amplifier with infinite input impedance, zero output impedance and a voltage gain  $G(\omega)$ , and the input and output impedances,  $Z_{in}(\omega)$  and  $Z_{out}(\omega)$ . In these parameters, the argument  $\omega$  denotes the signal angular frequency.

In addition, the random fluctuations due to the amplifier are described by two noise sources with very different roles. The voltage noise source  $V_N$  describes the output noise, that is, the noise added by the amplifier to the output signal, referred to the input. The current noise  $I_N$ , on the other hand, describes the back-action of the amplifier on the circuit at the input. The voltage and current noise are assumed to be gaussian, and are characterized by the spectral densities  $S_V(\omega)$  and  $S_I(\omega)$ , which are the Fourier transforms of the autocorrelation functions of  $V_N$  and  $I_N$ , respectively. We neglect here the correlations  $S_{VI}(\omega)$ , which are not essential for our discussion. These spectral densities, together with the input impedance, determine the ultimate resolving power of the amplifier for small signals.

It is useful, in the discussions of this resolving power, to introduce several combinations of these quantities. The first one is the charge sensitivity  $\delta Q(\omega) = \sqrt{S_V(\omega)/|\omega Z_{in}(\omega)|}$ , which we have already discussed. The second quantity is the energy sensitivity  $\epsilon(\omega) = \delta Q^2(\omega)/2C_{in}$  where  $C_{in} = \text{Re}\{1/[i\omega Z_{in}(\omega)]\}$ . Assuming that the amplifier is driven by a voltage source with strictly zero internal impedance (and hence always in the classical regime, as the zero-point voltage fluctuations are proportional to the real part of the impedance), this quantity tells us the smallest amount of energy  $\delta E = \epsilon/\tau$  fed by the source into the input circuit of the amplifier which will give an output signal that is distinguishable from zero when we accumulate it during a time  $\tau$ . Even though  $\epsilon$  has the dimension of an action and is conveniently measured in units of  $\hbar$ , quantum mechanics does not impose any restriction on the ratio  $\epsilon/\hbar$ , which can in principle tend to zero<sup>23</sup>. Nevertheless, in systems studied so far, a value of  $\epsilon/\hbar$  of order unity usually means that the contribution of thermal fluctuations to the noise of the amplifier have been suppressed down below those of quantum fluctuations.

Although the energy sensitivity seems initially to be a very powerful concept, it neglects the back-action of the amplifier and is insufficient to determine how well the amplifier performs when we use it to measure a quantum signal coming from a system with a finite source impedance  $Z_s$ . The current noise, which induces back-action voltage fluctuations across the source impedance, and hence on the

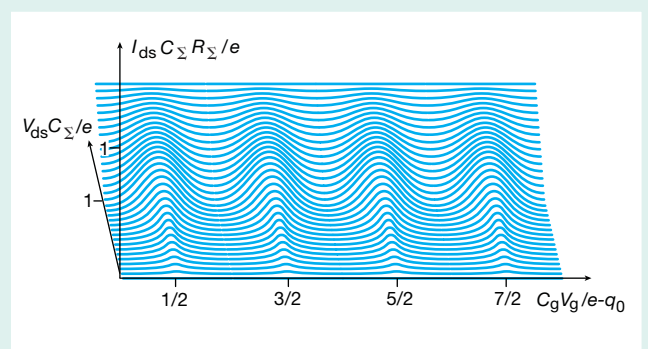


**Figure 5** Variation at  $T = 0$  of the source–drain current in a SET as a function of the voltage between drain and source and the voltage between gate and source. We have assumed that the two junctions have identical parameters. The sum of the junction tunnel resistances  $R_{\Sigma}$  is twice the resistance quantum  $h/e^2$  and a small amount of co-tunnelling rounds the peaks associated with the lifting of the Coulomb blockade (gate charge corresponding to half-integers multiplied by the charge quantum). The sensitivity of the SET is based on the rapid variation of the source–drain current as the gate charge varies by a fraction of one electron.

signal going into the amplifier, must be considered together with the voltage noise.

We therefore introduce the noise impedance  $Z_N = \sqrt{S_V/S_I}$  and the noise energy  $E_N = \sqrt{S_V S_I}$ . They have the following meaning: supposing that  $1/Z_{in}(\omega) = 0$ , the amplifier will add a minimal amount of noise to the signal coming from the source when  $Z_S = Z_N$  (noise matching). This minimal noise has a power per unit bandwidth given by  $E_N$  (this quantity has the dimension of an energy, hence the name noise energy). Quantum mechanics places a strict restriction on the noise energy. No amplifier can have an  $E_N$  smaller than  $\hbar\omega/2$ , half a photon energy at the signal frequency  $\omega$  (refs 23–25). This fundamental limitation is a form of Heisenberg’s uncertainty principle (see Table 1). It is worth mentioning that in the classical regime, that is, the regime where the contribution of quantum fluctuations to the noise of the amplifier is negligible, the noise temperature  $T_N = E_N/k_B$  is often used in place of the noise energy. The meaning of  $T_N$  corresponds to a well-defined procedure: imagine one connects a resistor with value  $Z_N$  at the input of the amplifier. The temperature to which one must heat the resistor to double the noise measured at the output of the amplifier is precisely  $T_N$ .

If we now apply these concepts to FET amplifiers, we find that the best performance in the r.f. domain 0.1–10 GHz is obtained with heterostructure FETs cooled to 4 K (ref. 26). At 500 MHz, their noise temperature is around 2 K (the corresponding thermal energy is equivalent to the energy of 40 photons at 1 GHz), their noise impedance is about 50  $\Omega$  and their energy sensitivity is of the order  $10^2 \hbar$ . They are thus far from the quantum limit (at higher frequencies the minimum noise energy improves and can be equivalent to only ten photons). As a charge-sensing device, their best performance is around  $10^{-2} e/\sqrt{\text{Hz}}$  (ref. 8).

Although theoretically the heterostructure FET could reach the quantum limit of sensitivity in the form of a ballistic, two-dimensional electron gas quantum-point contact<sup>27</sup>, it is difficult in

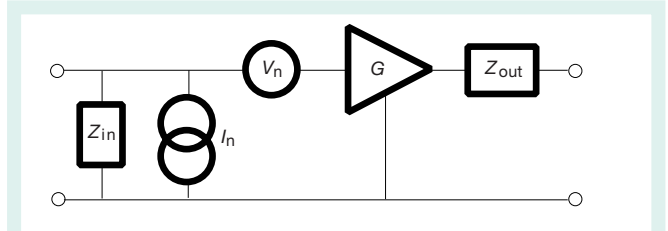


**Figure 6** Effective circuit elements describing the properties of a linear voltage amplifier with no feedback. The triangle represents an ideal noiseless voltage amplifier with infinite input impedance and zero output impedance. Its gain is denoted by  $G$ . The boxes marked  $Z_{in}$  and  $Z_{out}$  correspond to the input and output impedances, respectively. The noise sources  $V_n$  and  $I_n$  represent the voltage noise (noise added by the amplifier at the output, but referred to the input) and the current noise (back-action noise of the amplifier sent to the circuit feeding the input). These elements are eventually dependent on the signal frequency  $\omega$

this device to achieve effective electrostatic coupling of the gate electrode to the channel without affecting its mobility and inducing parasitic input capacitance. In the SET, by contrast, there is more flexibility in the design of the gate capacitance. The fabrication of the latter is to a large extent disconnected from that of the tunnel barriers, whose quality is analogous to the mobility of the channel in the FET. We will now examine how the operating principle of the SET brings us close to the quantum limit.

### Ultimate sensitivity of SETs

In the framework of the orthodox theory, the tunnel events constitute a generalized Poisson process with correlations. It is possible to calculate analytically the noise characteristics of the SET at temperatures such that  $k_B T \ll eV_{ds}$  (refs 7, 28). The following expressions are obtained for the voltage and current noise, in the simple case where the two junctions have identical parameters:

$$S_V(\omega) = \frac{(1 - \alpha^2)(1 + \alpha^2)}{8\alpha^2} eV_{ds} R_{\Sigma} \left( \frac{C_{\Sigma}}{C_g} \right)^2$$

$$S_I(\omega) = \frac{(1 - \alpha^2)}{4} \frac{eV_{ds}}{R_{\Sigma}} \left( \frac{C_g}{C_{\Sigma}} \right)^2 \left( \frac{e\omega R_{\Sigma}}{V_{ds}} \right)^2$$

In what follows, we neglect the influence of the correlation

$$S_{VI}(\omega) = \frac{(1 - \alpha^2)}{8} eV_{ds} \left( \frac{i\omega e R_{\Sigma}}{V_{ds}} \right)$$

between voltage and current noise, whose effect would be to reduce the noise energy if an appropriate complex source impedance could be presented to the SET.

In these noise expressions the Coulomb blockade parameter  $\alpha = (2C_g V_g - e)/C_{\Sigma} V_{ds}$ , which is limited here to the range  $0 < \alpha < 1 - \text{Max}(R_K/\pi R_{\Sigma}, eV_{ds}/k_B T)$ , fixes the relative values of the gate and

**Table 1 Constraints on sensitivity and back-action imposed by quantum mechanics**

System	Sensitivity	Back-action	Limiting relation	Limited quantity
Heisenberg microscope	$\Delta x$	$\Delta p$	$\Delta x \Delta p \geq \hbar/2$	Action
Electronic amplifier	$S_V$	$S_I$	$(S_V S_I)^{1/2} \geq \hbar\omega/2$	Noise energy
Qubit read-out	$T_m$	$\Gamma_{\phi}$	$T_m \Gamma_{\phi} \geq 1/2$	Information

Table 1 shows different forms of Heisenberg’s uncertainty relation linking the sensitivity of a measurement of a given physical quantity and the simultaneous back-action on the conjugate quantity. The precision with which the position of an object would be measured with a photon is related to the momentum transferred to this object by the radiation pressure of the photon (row 1). Similarly, the voltage sensitivity with which an amplifier measures the circuit at its input is related to the back-action current noise that this amplifier produces in the circuit (row 2). Finally, the time needed to acquire the value of a qubit is related to the rate of dephasing of the qubit induced by the back-action of the read-out (row 3). Quantities characterizing sensitivity and back-action, respectively, are given in columns 2 and 4.

drain–source voltage. For  $1 - R_K/(\pi R_\Sigma) < \alpha$ , co-tunnelling processes dominate over the single tunnelling processes we consider here, and for  $1 - eV_{ds}/k_B T < \alpha$  the influence of thermal fluctuations would have to be taken into account in the above expressions. The resistance  $R_\Sigma = R_{T1} + R_{T2}$  is the sum of the two junction resistances. The above expressions are valid for source–drain voltages below the Coulomb gap  $V_{ds} C_\Sigma/e < 1$  and at frequencies  $\omega$  that are low on the tunnel rate scale  $(eR_\Sigma/V_{ds})^{-1}$ . We have taken the mean offset charge to be zero because it appears only as a shift in  $V_g$ , but the typical value of the expected  $1/f$  offset charge fluctuations make our expressions valid only above the crossover to the intrinsic device shot noise at a few  $10^5$  Hz. Note that at this level of approximation the input impedance is simply a capacitance resulting from the series combination of the gate and the sum  $C_J = C_{J1} + C_{J2}$  of the two junction capacitances:  $Z_{in} = C_\Sigma/[i\omega C_g(C_{J1} + C_{J2})]$ . A dissipative part in the input impedance appears only at higher orders in the dimensionless signal frequency  $(e\omega R_\Sigma/V_{ds})^{-1}$ .

It is straightforward to go from these expressions to the charge sensitivity, energy sensitivity, noise energy and noise impedance:

$$\delta Q(\omega) = \frac{C_J}{\alpha} \sqrt{\frac{(1-\alpha^4)}{8} \left(\frac{R_\Sigma}{R_K}\right) \left(\frac{\hbar V_{ds}}{e}\right)}$$

$$\epsilon(\omega) = \frac{\pi \hbar (1-\alpha^4)}{8\alpha^2} \left(\frac{R_\Sigma}{R_K}\right) \left(\frac{V_{ds}}{e/C_\Sigma}\right) \left(\frac{C_J}{C_g}\right)$$

$$E_N(\omega) = \frac{\pi(1-\alpha^2)}{2\alpha} \sqrt{\frac{(1+\alpha^2)}{2} \frac{R_\Sigma}{R_K} \hbar \omega}$$

$$Z_N(\omega) = \sqrt{\frac{1+\alpha^2}{8\alpha^2} \left(\frac{C_\Sigma}{C_g}\right)^2 \frac{V_{ds}}{e\omega}}$$

We can find a conservative upper bound for the optimal value of the quantities that characterize the sensitivity of the SET by minimizing the above expressions over the range of parameter values that correspond to our hypotheses. We therefore take  $\alpha = 1 - 2R_K/3R_\Sigma$  and  $R_\Sigma = 2R_K$ , values at which co-tunnelling remains marginal. We also take the source–drain voltage  $V_{ds} = e/(2C_\Sigma)$  to be able to neglect thermal fluctuations in practical situations. In addition, we take  $C_J = 1$  fF as a compromise between reaching attainable temperatures, keeping the heating of the island by the drain–source current at a reasonable level and achieving an acceptable output signal (in contrast with the previous parameter choices, this last value is dictated essentially by the current technology issues and not by the validity of our expressions). We arrive at the optimal values

$$\delta Q_{opt} \approx 1.7 \times 10^{-6} e/\sqrt{\text{Hz}}$$

$$\epsilon_{opt} \approx 0.7 \hbar (C_J/C_g)$$

$$E_{N,opt} \approx 2.2 \hbar \omega$$

$$[G \times E_N]_{opt} = 0.14 e V_{ds} \approx 75 \text{ mK} \times k_B$$

We have left the internal coupling ratio ( $C_J/C_g$ ) of the SET in the right-hand side of the expression for  $\epsilon_{opt}$  as this parameter can easily be modified by changing the lithography of the device. This ratio determines how much of the energy fed by the gate voltage into the SET is used to charge the island, which is the active element, rather than the gate capacitance.

The value for  $E_{N,opt}$  shows that the SET operates in the vicinity of the quantum limit. The product  $[G \times E_N]_{opt}$  gives the SET output noise which would ideally be higher than the added noise of the following amplifier, that is, a cryogenic heterostructure FET. Today, this FET is the limiting factor in the system noise, and the best experimental upper bound so far for the energy sensitivity is  $\epsilon \approx 40 \hbar (C_J/C_g)$

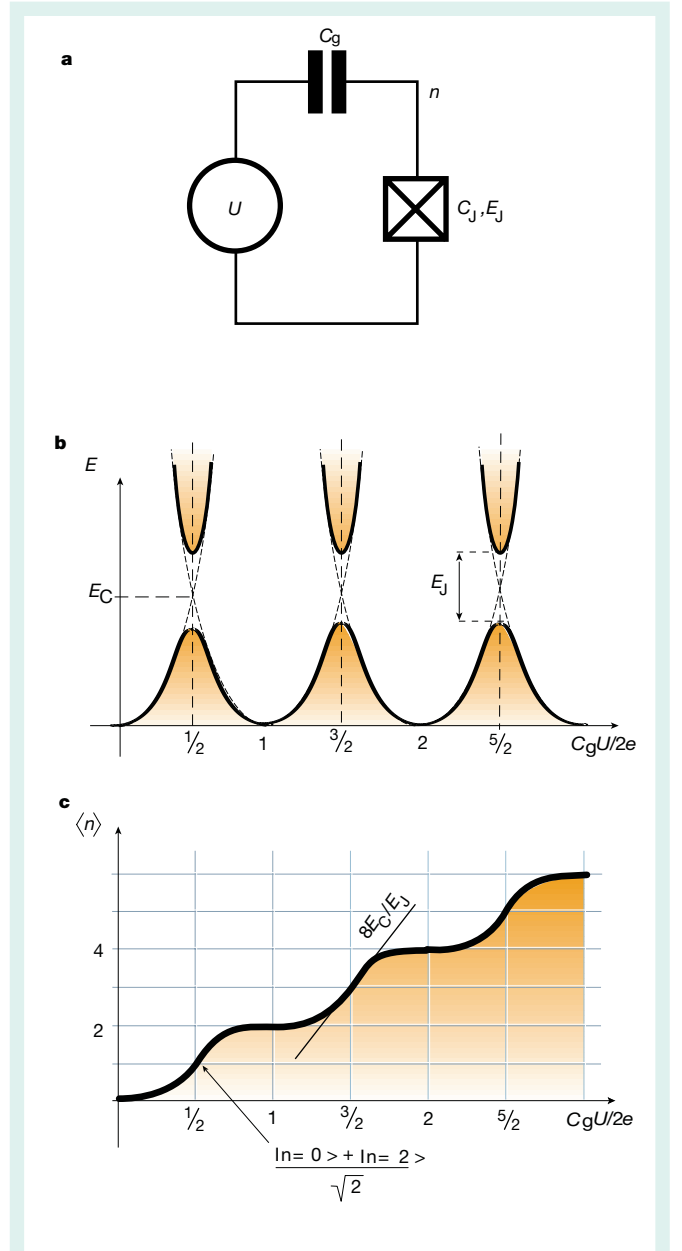


**Figure 7** The single-Cooper-pair box. **a**, Circuit diagram of the single-Cooper-pair box. This simple system consists of one superconducting tunnel junction (box with cross) in series with a voltage source  $U$  and a gate capacitance  $C_g$ . When the charging energy of the island is less than the superconducting gap, all electrons are paired and the number  $n$  of excess electrons is even. Cooper pairs can tunnel reversibly through the tunnel junction. Charge states differing by one Cooper pair are coupled by the Josephson energy  $E_J$ . **b**, Energy of the two lower quantum states of the Cooper-pair box (full line) as a function of  $U$ . The dashed lines represent the electrostatic energy of the box including the work done by the voltage source. At the avoided crossings, the two charge states are mixed and constitute a solid-state implementation of a qubit. **c**, Quantum mechanical average of the number of electrons in the ground state of the box, as a function of  $U$ .

in the r.f. domain<sup>4</sup>. The improvement of the combination of the SET with a FET, or with a superconducting quantum interference device (SQUID) amplifier (see below), as well as the verification of the above predictions for the noise, is a topic for future research.

### Other quantum-limited, solid-state r.f. amplifiers

According to the above analysis, the SET approaches but does not quite reach the quantum limit. The back-action noise due to the

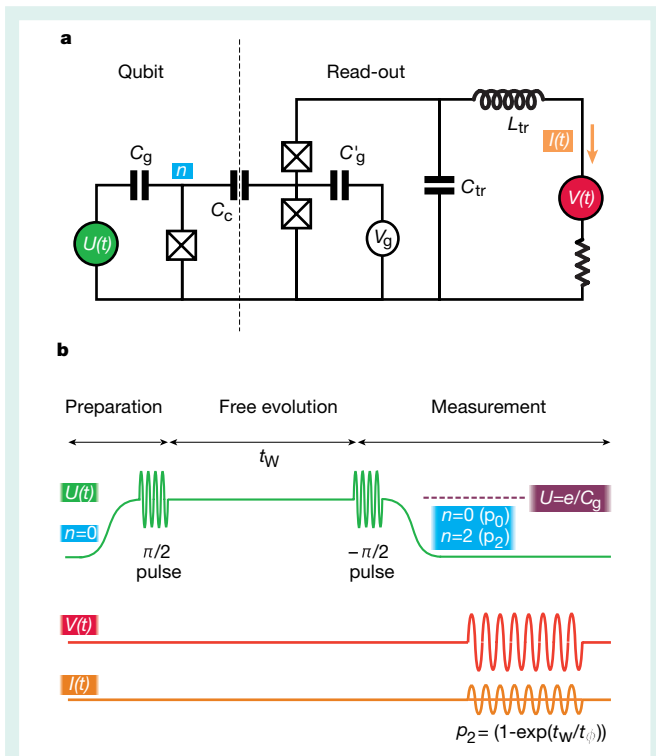


**Figure 8** Measuring the state of a quantum system. **a**, Schematic circuit showing how a qubit implemented by a Cooper-pair box could be read-out by an r.f.-SET. **b**, Time evolution of signals in the circuit of **a**. While the read-out r.f.-SET is turned off, a first pulse prepares the qubit in a quantum superposition of ground and excited state at the crossing point  $C_g U = e$ . After a waiting period, a second pulse is applied which, in absence of decoherence, would make the qubit return to the ground state. Finally, after these manipulations, the read-out transistor is switched on while the box gate charge is moved away from  $C_g U = e$ . If decoherence occurs, the qubit will be left in the  $n = 2$  charge state with a non-zero probability  $p_2$ . Given its sensitivity and low back-action noise, the r.f.-SET should be able to detect this event with a signal-to-noise ratio better than unity.  $C_g$  and  $L_{tr}$  refer respectively to the capacitance and inductance of the impedance transformer. The times  $t_w$  and  $t_\phi$  are the waiting time between the two pulses and the intrinsic decoherence time of the box, respectively.

randomness of tunnel events is dominated by phase-scrambling processes inside the island. But in the co-tunnelling regime, back-action noise is dominated by fluctuations of the island voltage associated with the measurement of the gate voltage itself and should therefore be more efficient. More work, experimental and theoretical, is needed to quantify this conjecture.

The superconducting SET can measure the charge on the gate with fully coherent carriers, the Cooper pairs. Zorin has analysed theoretically a version of this device shunted by a resistor and found that the noise energy could in this case exactly reach the quantum limit<sup>29</sup>. However, the mode of operation seems to involve a more precise tuning of the device parameters than for the SET.

So far we have considered voltage amplifiers, that is, amplifiers with an input impedance that is large compared with the resistance quantum  $R_K$ . For several years already, SQUID devices have played the role of the SET in the realm of low-impedance amplifiers. There is in fact a duality relationship between the d.c.-SQUID and the SET<sup>1</sup>. Whereas the SET is based on charge quantization of a metallic island surrounded by an insulator, the d.c.-SQUID is based on the quantization of flux in a superconducting loop. The sub-electron sensitivity of the SET has its analogue in the sub-flux quantum sensitivity of the SQUID. Although it has been known for many years that a SQUID could operate at the quantum limit, this has been achieved only recently in the r.f. domain. Andre *et al.* have shown that a

SQUID with a microstrip input line could achieve  $k_B T_N \approx 5\hbar\omega$  at 438 MHz (ref. 30).

Finally, we should mention a special class of linear amplifiers: the mixers based on photon-assisted tunnelling in superconductor–insulator–superconductor (SIS) junctions. They convert a signal at several hundred GHz into a signal at several GHz. Even though the absolute power of the output signal is weaker than the power of the input signal, these devices have a large ‘photon number’ gain. Furthermore, their noise closely approaches the quantum limit:  $E_N = 0.6\hbar\omega$  (ref. 31). Closely related to SIS mixers are Josephson parametric amplifiers, which have been operated at the quantum limit<sup>32</sup>. However, these devices do not have the advantage of the SET and the SQUID to amplify at the same time both a.f. and r.f. signals, a useful feature for tuning and trouble-shooting.

### Measuring the state of a two-level system

In the past few years there has been much interest in the possibility of realizing a quantum computer<sup>6</sup>. Although the more advanced experiments in this field are taking place in quantum optics systems<sup>33,34</sup>, several implementations of quantum bits and quantum gates in solid-state systems have been proposed<sup>35–38</sup>. We focus here on a charge qubit which is now well understood experimentally<sup>12,13</sup> and theoretically<sup>39,40</sup>: the Cooper-pair box (Fig. 7). It consists of a superconducting island with Coulomb energy  $E_C$  connected to a superconducting charge reservoir by means of a Josephson tunnel junction with Josephson coupling energy  $E_J$ . The island is influenced electrostatically through a gate capacitor  $C_g$  connected to voltage source (Fig. 7a). If the conditions  $k_B T \ll E_J \ll E_C < \Delta$  are realized, where  $\Delta$  is the energy gap of the superconductor, then the island will have only an even number  $n$  of excess electrons. This only degree of freedom will be a good quantum number, except at the avoided crossings of the charge levels (Fig. 7b,c). A recent experiment has shown that such a solid-state qubit was able to display several Rabi oscillations when stimulated by a microwave pulse<sup>13</sup>. However, the measurement scheme in this experiment involved a probe tunnel junction which observed the qubit continuously, but weakly. Such a continuous observation dephases the qubit and prevents a measurement of its intrinsic decoherence time. It is therefore desirable to read-out the qubit only at the end of the coherent manipulation and evolution period (Fig. 8). An obvious candidate for the read-out is the SET. In a version with r.f. bias<sup>4</sup>, the transistor can be turned on and off very quickly, the turn-on time being set by the damping time of the tank circuit. This latter is of the order of several tens of nanoseconds, a time supposedly shorter than the intrinsic decoherence time of the box, estimated to be longer than 1  $\mu$ s. The question therefore arises as to whether the SET is sufficiently sensitive to detect the state of the box with a signal-to-noise ratio allowing the study of decoherence mechanisms.

### Measurement time and dephasing rate

An important concept is the measurement time  $T_m$  of the read-out SET<sup>14</sup>, which is defined as the time needed for discriminating between the two charge states of the box differing by a Cooper pair, assumed to be good eigenstates, with a signal-to-noise ratio of 1. Island box charge is a good quantum number when  $E_J/E_{cl} \ll 1$ , where the electrostatic energy  $E_{cl} = 2e^2(1 - C_g U/e)/C_{tot}$  of the box is controlled by the voltage  $U$  (here  $C_g$  and  $C_{tot}$  refer to the box gate capacitance and total island capacitance). In practice, the charge measurement is made just after  $U$  is varied away from the crossing point (Fig. 8b). The circuit of Fig. 8a shows that  $T_m$  is closely related to the voltage noise of the SET, with  $T_m = 4S_V/(2e/C_{tot})^2$ . We thus find that  $T_m = (\delta Q/e)^2(C_{tot}/C_{in})^2$ , where  $C_{in}/C_{tot}$  is the charge-coupling coefficient.

It is interesting to note that the back-action current noise dephases the charge states relative to one another only if charge is a

good quantum number. The general expression for the dephasing rate is

$$\Gamma_\phi = \left(\frac{e}{\hbar}\right)^2 \frac{E_{cl}^2}{E_J^2 + E_{cl}^2} S_V^{\text{box}}(\omega=0)$$

where  $S_V^{\text{box}}(\omega) = S_I(\omega)/C_{\text{tot}}\omega^2$  is the fluctuation spectral density of the box island voltage induced by the SET current noise. In the regime  $E_J/E_{cl} \ll 1$ , we find that the product  $T_m \Gamma_\phi = 2[E_N(\omega)/\hbar\omega]_{\omega=0}^2$  involves only the noise energy and is of order unity. Once again, this is another close approach to the quantum limit as the minimum value for  $T_m \Gamma_\phi$  is  $\frac{1}{2}$  (Table 1).

So in principle it seems that the SET could acquire charge with any given large signal-to-noise ratio by measuring the box for a long enough time. However, any coupling between charge states will induce transitions and will corrupt the measurement. The transition rate between charge states due to the current noise is given by

$$\Gamma_1 = \left(\frac{e}{\hbar}\right)^2 \frac{E_J^2}{E_J^2 + E_{cl}^2} S_V^{\text{box}}(\omega=\Omega)$$

where  $\Omega = \sqrt{E_J^2 + E_{cl}^2}/\hbar$  is the transition frequency between charge states.

We thus find that the signal-to-noise ratio including the effect of transitions between charge states is

$$S/N = (\Gamma_1 T_m)^{-1/2} = \frac{1}{(E_N/\hbar\omega)_{\omega=0}} \left(\frac{2E_J^2}{E_J^2 + E_{cl}^2}\right)^{-1/2}$$

In practice, a signal-to-noise ratio significantly greater than 1 seems possible with an optimized r.f.-SET in a single charge measurement, even when taking into account the 50% reduction in sensitivity of the SET in the r.f.-bias mode<sup>41</sup>.

### Towards single-photon sensitivity in the r.f. domain

To summarize, the SET transistor is a charge amplifying device whose sensitivity in the r.f. domain is limited in principle only by a well understood process, quantum shot noise. This property displays a marked contrast with a FET. It should be possible in the near future to show experimentally that the noise energy of the SET approaches the quantum limit within a factor of order unity. Although the SET will not be 100% efficient in acquiring charge information with only the minimal back-action noise required by quantum mechanics, it should still be able to read-out a charge qubit in a single-shot measurement. In more sophisticated devices using Cooper-pair tunnelling or co-tunnelling processes, the quantum limit could be approached even more closely. Furthermore, by transposing in the r.f. domain the manipulations of the quantum signal that are now performed routinely in experiments in cavity quantum electrodynamics<sup>42</sup>, one could use these ultimate amplifiers for measuring signals consisting of a single photon, without even destroying the photon. □

1. Averin, D. V. & Likharev, K. K. Coulomb blockade of tunneling and coherent oscillations in small tunnel junctions. *J. Low Temp. Phys.* **62**, 345–372 (1986).
2. Fulton, T. A. & Dolan, G. J. Observation of single-electron charging effects in small tunnel junctions. *Phys. Rev. Lett.* **59**, 109–112 (1987).
3. Meirav U., Kastner, M. A. & Wind, S. J. Single-electron charging and periodic conductance resonances in GaAs nanostructures. *Phys. Rev. Lett.* **65**, 771–774 (1990).
4. Schoelkopf, R. J., Wahlgren, P., Kozhevnikov, A. A., Delsing, P. & Prober, D. The radio-frequency single-

5. electron transistor (RF-SET): a fast and ultrasensitive electrometer. *Science* **280**, 1238–1242 (1998).
6. Mather, J. C. Super photon counters. *Nature* **401**, 654–655 (1999).
7. Steane, A. Quantum computation. *Rep. Prog. Phys.* **61**, 117 (1998).
8. Korotkov, A. N., Averin, D., Likharev, K. K. & Vasenko, S. A. in *Single-Electron Tunneling and Mesoscopic Physics* (eds Koch, H. & Lubbjg, H.) 45–59 (Springer, Berlin, 1992).
9. Mar, D. J., Westervelt R. & Hopkins, P. F. Cryogenic field-effect transistor with single electronic charge sensitivity. *Appl. Phys. Lett.* **64**, 631–633 (1994).
10. Keller, M. W., Eichenberger, A., Martinis, J. M. & Zimmerman, N. M. A capacitance standard based on counting electrons. *Science* **285**, 1706–1709 (1999).
11. Schoelkopf, R. J., Moseley, S. H., Stahle, C. M., Wahlgreen, P. & Delsing, P. A concept for a submillimeter-wave single-photon counter? *IEEE Trans. Appl. Supercond.* **9**, 2935–2938 (1999).
12. Komiya, S., Astafiev, O., Antonov, V., Kutsuwa, T. & Hirai, H. A single-photon detector in the far-infrared range. *Nature* **403**, 405–407 (2000).
13. Bouchiat, V., Vion, D., Joyez, P., Esteve, D. & Devoret, M. H. Quantum coherence with a single Cooper pair. *Phys. Scr.* **T76**, 165–170 (1998).
14. Nakamura, Y., Pashkin, Yu. A. & Tsai, J. S. Coherent control of macroscopic quantum states in a single-Cooper-pair box. *Nature* **398**, 786–788 (1999).
15. Shnirman, A. & Schoen, G. Quantum measurements performed with a single-electron transistor. *Phys. Rev. B* **57**, 15400–15407 (1997).
16. Naveh, Y. & Likharev, K. K. Modeling of 10-nm-scale ballistic MOSFETs. *IEEE Electron Devices Lett.* **21**, 242–244 (2000).
17. Devoret, M. H. & Grabert, H. in *Single Charge Tunneling* (eds Grabert, H. & Devoret, M. H.) 1–19 (Plenum, New York, 1992).
18. Grabert, H. Charge fluctuations in the single-electron box: perturbation expansion in the tunneling conductance. *Phys. Rev.* **50**, 17364–17377 (1994).
19. Schoeller, H. & Schoen, G. Mesoscopic quantum transport: resonant tunneling in the presence of a strong Coulomb interaction. *Phys. Rev. B* **50**, 18436–18442 (1994).
20. Shirakashi, J., Matsumoto, K., Miura, N. & Konagai, N. Single-electron charging effects in Nb/Nb oxide-based single-electron transistors at room temperature. *Appl. Phys. Lett.* **72**, 1893–1895 (1998).
21. Zhuang, L., Guo, L. & Chou, S. Y. Silicon single-electron quantum-dot transistor switch operating at room temperature. *Appl. Phys. Lett.* **72**, 1205–1207 (1998).
22. Pashkin, Yu. A., Nakamura, Y. & Tsai, J. S. Room-temperature Al single-electron transistor made by electron-beam lithography. *Appl. Phys. Lett.* **76**, 2256–2258 (2000).
23. Wolf, H. et al. Investigation of the offset charge noise in single electron tunneling devices. *IEEE Trans. Instrum. Measurement* **46**, 303–306 (1997).
24. Caves, C. M., Thorne, K. S., Drever, W. P., Sandberg, V. D. & Zimmermann, N. On the measurement of a weak classical force coupled to a quantum-mechanical oscillator. I. Issues of principle. *Rev. Mod. Phys.* **52**, 341–392 (1980).
25. Caves, C. M. Quantum limits on noise in linear amplifiers. *Phys. Rev. D* **26**, 1817–1839 (1982).
26. Braginsky, V. B. & Khalili, F. Ya. *Quantum Measurement* (Cambridge Univ. Press, 1992).
27. Pospieszalski, M. W. & Wollack, E. J. in *Proceedings of 2nd ESA Workshop on Millimetre Wave Technology and Applications (WPP-149)* 221–226 (ESA, Paris, 1998).
28. Gurvitz, S. A. Measurements with a noninvasive detector and dephasing mechanism. *Phys. Rev. B* **56**, 15215–15223 (1997).
29. Korotkov, A. N. Preprint cond-mat/0003225 at <http://xxx.lanl.gov> (2000).
30. Zorin, A. B. Quantum-limited electrometer based on single Cooper pair tunneling. *Phys. Rev. Lett.* **76**, 4408–4411 (1996).
31. André, M.-O., Mück, M., Clarke, J., Gail, J. & Heiden, C. Radio-frequency amplifier with tenth-kelvin noise temperature based on microstrip direct current superconducting quantum interference device. *Appl. Phys. Lett.* **75**, 698–700 (1999).
32. Mears, C. A. et al. Quantum-limited heterodyne detection of millimeter waves using superconducting tantalum tunnel junctions. *Appl. Phys. Lett.* **57**, 2487–2489 (1990).
33. Movshovich, R. et al. Observation of zero-point noise squeezing via a Josephson parametric amplifier. *Phys. Rev. Lett.* **65**, 1419–1422 (1990).
34. Turchette, Q. A., Hood, C. J., Lange, W., Mabuchi, H. & Kimble, H. J. Measurement of conditional phase shifts for quantum logic. *Phys. Rev. Lett.* **75**, 4710–4713 (1995).
35. Monroe, C. et al. Resolved-sideband Raman cooling of a bound atom to the 3D zero-point energy. *Phys. Rev. Lett.* **75**, 4011–4014 (1995).
36. Bocko, M. F., Herr, A. M. & Feldman, M. F. Prospects for quantum coherent computation using superconducting electronics. *IEEE Trans. Appl. Supercond.* **7**, 3638–3641 (1997).
37. Kane, B. E. A silicon-based nuclear spin quantum computer. *Nature* **393**, 133–137 (1998).
38. Loss, D. & DiVincenzo, D. P. Quantum computation with quantum dots. *Phys. Rev. A* **57**, 120–126 (1998).
39. Mooij, J. E. et al. Josephson persistent-current qubit. *Science* **285**, 1036–1039 (1999).
40. Averin, D. V. Adiabatic quantum computation with Cooper pairs. *Solid State Commun.* **105**, 657–659 (1998).
41. Makhlin, Yu., Schoen, G. & Shnirman, A. Josephson-junction qubits with controlled couplings. *Nature* **398**, 786–789 (1999).
42. Korotkov, A. N. & Paalanen, M. A. Charge sensitivity of radio frequency single-electron transistor. *Appl. Phys. Lett.* **74**, 4052–4054 (1999).
43. Noguees, C. et al. Seeing a single photon without destroying it. *Nature* **400**, 239–242 (1999).

### Acknowledgements

This work was supported in part by the National Security Agency (NSA), the Advanced Research and Development Activity (ARDA) and the Army Research Office (ARO). One of us (M.H.D) acknowledges support from Commissariat à l’Energie Atomique (CEA). We thank D. Averin, J. Clarke, P. Delsing, D. Esteve, A. Korotkov, K. Likharev, H. Mooij, D. Prober, G. Schoen and E. Wollack for helpful discussions and communications of results prior to publication.

# Measurement of the excited-state lifetime of a microelectronic circuit

K. W. Lehnert,<sup>1,\*</sup> K. Bladh,<sup>2</sup> L. F. Spietz,<sup>1</sup> D. Gunnarson,<sup>2</sup>  
D. I. Schuster,<sup>1</sup> Per Delsing,<sup>2</sup> and R. J. Schoelkopf<sup>1,†</sup>

<sup>1</sup>*Department of Applied Physics and Physics,  
Yale University, New Haven, CT 06511 USA*

<sup>2</sup>*Microtechnology Center at Chalmers MC2,  
Department of Microelectronics and Nanoscience,*

*Chalmers University of Technology and Göteborg University, SE-412 96, Göteborg, Sweden*

(Dated: November 18, 2002)

## Abstract

We demonstrate that a continuously measured microelectronic circuit, the Cooper-pair box measured by a radio-frequency single-electron transistor (RF-SET), approximates a quantum two-level system. We extract the Hamiltonian of the circuit through resonant spectroscopy and measure the excited-state lifetime. The lifetime is more than  $10^5$  times longer than the inverse transition frequency of the two-level system, even though the measurement is active. This lifetime is also comparable to an estimate of the known upper limit, set by spontaneous emission, for this circuit.

PACS numbers: 74.40+k, 85.25Na, 85.35Gv

Recently, microelectronic circuits have been coaxed into behaving as quantum two-level systems (TLS) [1–5]. The TLS behavior of circuits is revolutionary because it demonstrates the quantum behavior of a macroscopic degree of freedom composed of many microscopic degrees of freedom. Quantum coherence was believed to be fragile in electrical circuits both because it required the suppression of the dynamics of the microscopic elements in a condensed matter system, and because the quantum oscillations of an electric or magnetic degree of freedom would efficiently radiate energy into the electromagnetic environment. Discussed in terms of the Bloch equations [6], familiar from nuclear magnetic resonance, a TLS in a coherent superposition of states has characteristic times  $T_2$  to become an incoherent mixture and  $T_1$  to relax back to its ground state.

In this paper, we observe that a microelectronic circuit, the Cooper-pair box, may be measured continuously while still behaving approximately as a two-level system. The box is integrated with a measurement apparatus, the RF-SET, which we operate as weak, continuous measurement of the box’s state. Under these conditions we are able to determine the parameters that appear in the box’s Hamiltonian, make a worst case estimate  $T_2^*$  of the decoherence time  $T_2$ , and measure the excited-state lifetime  $T_1$  of the two-level system. We determine the parameters in the Hamiltonian through a kind of spectroscopy where we observe a resonant change in the box’s state when its transition frequency matches a multiple of the frequency of an applied oscillatory excitation. From the width in frequency of these resonances we can find  $T_2^*$  [7]. We stimulate the box into its excited state and measure  $T_1$  directly by exploiting the large measurement bandwidth of the RF-SET to resolve in time the circuit’s decay to its ground state. Most remarkably, the value of  $T_1$  that we find while *continuously measuring* the state of the box is comparable to estimates of the excited-state lifetime limited by the quantum fluctuations of the electromagnetic environment. This demonstrates that the Cooper-pair box, when embedded in a circuit for control and measurement, remains well decoupled from other sources of dissipation. Based on the observed noise in the readout and the lifetime we conclude that RF-SET is a promising qubit readout because a ‘single-shot’ measurement, where the box is observed in its excited state before it has relaxed into its ground state, is possible.

The Cooper-pair box is a microelectronic circuit composed of an isolated superconducting island, attached to a superconducting lead through a thin insulating layer across which Cooper-pairs can tunnel. An additional lead, called the gate lead, lies near the island and

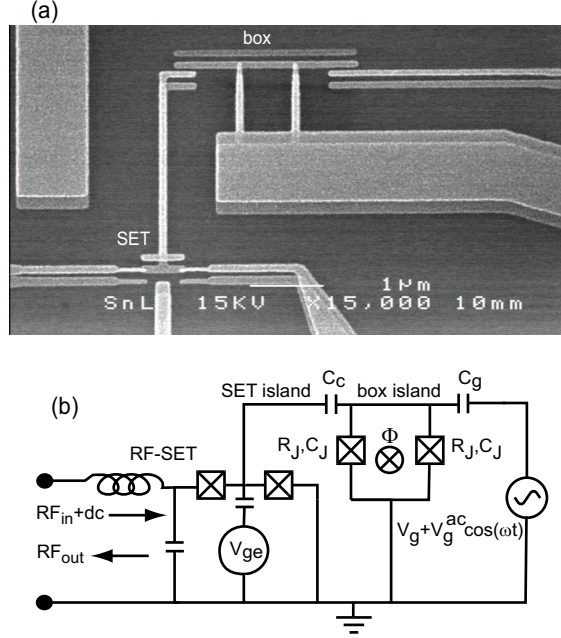


FIG. 1: (a) An SEM micrograph of the Cooper-pair box and SET electrometer. The device is made from an evaporated aluminum film (light gray regions) on an insulating SiO<sub>2</sub> substrate (dark gray regions) by the technique of double angle evaporation [8], which gives the double image. The aluminum has BCS gap  $\Delta/k_B = 2.4$  K. (b) A circuit diagram of the box and RF-SET electrometer showing: the voltage  $V_g$  and magnetic flux  $\Phi$  which control the box's Hamiltonian, the quantities  $V_g^{ac}$  and  $\omega$  which set the amplitude and frequency of the microwave excitation, the voltage  $V_{ge}$  and the dc and 500 MHz oscillatory ( $RF_{in}$ ) bias which determine the electrometer's operating point, and the capacitance  $C_C$  that couples charge between box and electrometer. The charge on the box is inferred from variation in the amount of applied RF power that is reflected ( $RF_{out}$ ) from the SET electrometer, which is a sensitive function of SET's conductance [9]. The tunnel junctions (crosses in boxes) are characterized by a junction resistance  $R_J$  and capacitance  $C_J$ , which control the box's Hamiltonian through  $C_\Sigma = C_C + 2C_J + C_g$  and  $R_\Sigma = R_J/2$  (see text).

changes the electrostatic potential of the island with the application of a voltage  $V_g$  to the gate lead through the gate capacitance  $C_g$  [Fig. 1(a)]. The island's total capacitance  $C_\Sigma$  is small enough that the addition of a single Cooper-pair to the island requires a large electrostatic energy, leading to suppressed fluctuations of charge on the island. Because the island and the lead are superconducting, all of the electrons form Cooper-pairs and participate in the macroscopic quantum ground state of the island. The only degree of

freedom is the number of pairs  $n$  on the island. Because of the large charging energy, we need only consider two states, a state  $|0\rangle$  with no excess Cooper-pairs ( $n = 0$ ), and a state  $|1\rangle$  with one excess Cooper-pair ( $n = 1$ ), as reckoned from electrical neutrality. The Hamiltonian of the Cooper-pair box circuit is

$$\mathbf{H} = -2E_c(1 - 2n_g)\boldsymbol{\sigma}_z - \frac{E_J}{2}\boldsymbol{\sigma}_x \quad (1)$$

where  $\boldsymbol{\sigma}_z$  and  $\boldsymbol{\sigma}_x$  are the Pauli spin matrices and  $n_g$  is total polarization charge applied to the gate electrode,  $n_g = C_g V_g / 2e - n_{off}$ , in units of a Cooper-pair's charge [10, 11]. The offset charge  $n_{off}$  accounts for the uncontrolled potential arising from charges nearby the box island. The charging energy,  $E_c = e^2 / 2C_\Sigma$ , is the electrostatic energy required to add one electron to the island and the Josephson energy,  $E_J^{max} = h\Delta / 8e^2 R_\Sigma$ , is the effective tunnelling matrix element for Cooper-pairs across a junction with resistance  $R_\Sigma$  in a superconductor with BCS gap  $\Delta$ . The junction is in fact a composite of two parallel junctions connected to form a loop with  $1 (\mu\text{m})^2$  area (Fig. 1). The effective Josephson energy  $E_J$  of the pair of junctions is then tuneable with magnetic flux  $\Phi$  through this loop, as  $E_J = E_J^{max} \cos(\pi\Phi/\Phi_0)$ , where  $\Phi_0$  is the quantum of flux ( $h/2e$ ). Equation 1 is the Hamiltonian of a quasi-spin 1/2 particle in a fictitious magnetic field that can be decomposed into two orthogonal fields. The  $z$  component of this fictitious field which accounts for the box's electrostatic energy,  $E_{el}(V_g) = 2E_c(1 - 2n_g)$ , is tuned with  $V_g$  and the  $x$  component, which accounts for the Josephson energy  $E_J(\Phi) = E_J^{max} \cos(\pi\Phi/\Phi_0)$ , is tuned with  $\Phi$  [11]. The box is an artificial two-level system and both of the terms in its Hamiltonian are tuneable *in situ*.

In the box, states of definite numbers of Cooper pairs on the island are states of definite charge. In order to measure the charge of the Cooper-pair box, we fabricate the box next to a radio-frequency single-electron transistor (RF-SET)[8, 9], an exquisitely sensitive electrometer, so that the addition of a Cooper-pair to the box's island causes a small fraction ( $C_C/C_\Sigma=3.7\%$ ) of the Cooper-pair's charge to appear as polarization charge on the capacitor  $C_C$  that couples the box and the RF-SET (Fig. 1). The electrometer used here had a sensitivity of  $4 \times 10^{-5} e/\sqrt{\text{Hz}}$  and 10 MHz of measurement bandwidth. Because the RF-SET measures charge, its action can be described as projecting the state of the box into a state of definite Cooper-pair number. In the formal terms of Eq. 1, it measures  $Q_{box} = (1 + \langle\boldsymbol{\sigma}_z\rangle)e$  where  $Q_{box}$  is further averaged over the measurement time.

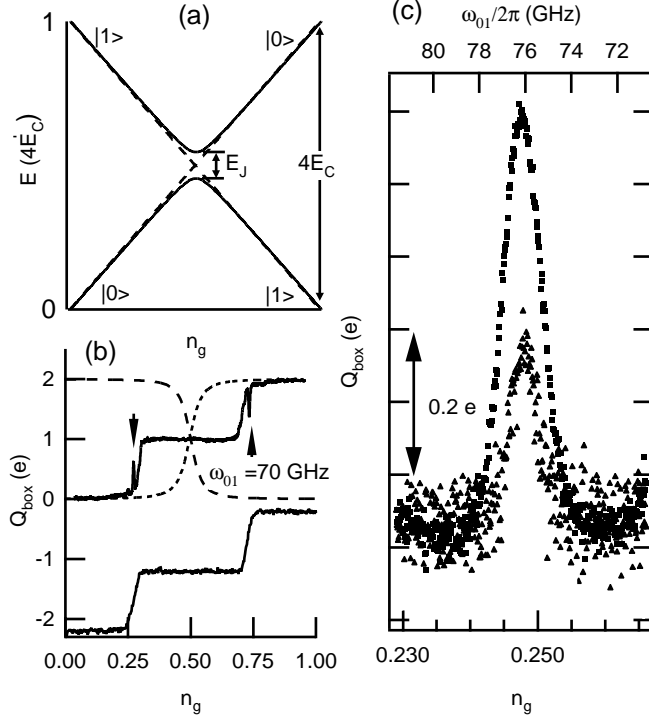


FIG. 2: (a) The ground and excited state energies versus  $n_g$  for Eq. 1, with  $4E_C = 12E_J$  (solid line) and  $E_J = 0$  (dashed lines). Energy eigenstates asymptotically approach charge states ( $|1\rangle$  and  $|0\rangle$ ) far from  $n_g = 0.5$ . (b)  $Q_{box}$  vs.  $n_g$ , calculated for the ground state (dotted line), excited state (dashed line), and measured (solid line) with 35 GHz microwaves applied to the box gate. The arrows indicate resonant peaks. Also shown is  $Q_{box}$  measured with no microwaves applied (solid line), with the y-axis shifted down by  $2.2 e$ . (c) Two resonant peaks in  $Q_{box}$  vs.  $n_g$  on the bottom axis and vs.  $\omega_{01}$  on the top axis, with  $\omega = 38$  GHz and where the larger value of  $V_g^{ac}$  (squares) is twice the smaller value (triangles).

We perform spectroscopy by applying a continuous microwave stimulus to the gate of the Cooper-pair box, and sweeping  $n_g$  to tune the parameters of the TLS and find the resonance condition (Fig. 2). A measurement of  $Q_{box}$  vs.  $n_g$  shows that the box does not remain in its ground state over a range  $0.3 < n_g < 0.7$ . This behavior is caused by backaction [12, 13] generated by currents flowing through RF-SET [14]. We proceed by studying the box in the range of  $n_g$  where it does remain in its ground state.

When a 35 GHz microwave signal is applied to the gate, we observe clear evidence that the box is a coherent two-level system. Resonant peaks appear [Fig. 2(b)] in  $Q_{box}$  that are

sharp and symmetrically spaced about  $n_g = 0.5$ . The two features, a peak for  $n_g < 0.5$  and a dip for  $n_g > 0.5$ , both correspond to the change in  $Q_{box}$  when the box spends some time in the excited state. Because  $Q_{box}$  is an average of thousands of repeated measurements, the peak height indicates the probability of finding the box in its excited state [Fig 2(c)].

The resonant peaks permit a spectroscopic determination of  $E_C$  and  $E_J^{max}$ . By tuning  $n_g$  and  $\Phi$  while exciting the box with a fixed microwave frequency, we find good agreement between the locations of resonant peaks and the difference  $E_{01}(n_g, \Phi) = \hbar\omega_{01}$  between ground-state and excited-state energy expected from Eq. 1. An independent measurement of  $E_C$  [15] demonstrates that these peaks occur when the irradiating frequency  $\omega$  is half  $\omega_{01}$ , indicating that these peaks correspond to a two-photon transition [16]. At lower frequencies and for single-photon transitions, the peaks would appear at an  $n_g$  for which the box does not stay in the ground state while being measured and are therefore not visible. We find a single value for  $E_C$  and for  $E_J^{max}$  that account for the location of the resonant peaks at applied frequencies between 32 and 38 GHz giving resonant peaks for  $\omega_{01}$  between 64 and 76 GHz [Fig. 3(a)]. We are able to extract the parameters of the Hamiltonian,  $4E_C/h = 149.1 \pm 0.4$  GHz and  $E_J^{max}/h = 13.0 \pm 0.2$  GHz, which imply  $C_\Sigma = 518$  aF and  $R_\Sigma = 12.1$  k $\Omega$ . Through spectroscopy we have measured the parameters of an electrical circuit that could not have been measured with transport [Fig. 1(b)]. Because these measurements were made at a temperature  $T < 40$  mK, they are in the limit  $k_B T \ll E_J < E_C$ .

Consistent with the behavior of a TLS, the peaks disappear for  $\Phi = \Phi_0/2$  when  $E_J$  approaches zero. This demonstrates that  $E_J$  provides the coupling between the charge states [Fig. 3(b)]. An oscillating gate voltage with amplitude  $V_g^{ac}$  adds a term to the Hamiltonian in Eq. 1 which is  $(C_g V_g^{ac}/2e) \cos(\omega t) \sigma_z$ , and is collinear with ground state of the quasi-spin described by Eq. 1 when  $E_J = 0$ . The microwave excitation therefore applies no torque which could excite the quasi-spin from its ground state [6].

The width of the resonant peaks we observe provides a worst-case estimate of the decoherence time of the two-level system. We express the width of a resonance  $\delta n_g$  as a width in frequency  $\delta\omega_{01} = (1/\hbar)(dE_{01}/dn_g)\delta n_g$ . In the absence of inhomogenous broadening, the half-width at half maximum inferred for zero power is the decoherence rate  $1/T_2$  of a TLS [6]. From  $\delta\omega_{01}$  measured at the lowest value of  $V_g^{ac}$  applied, we estimate a time  $T_2^*$  of about 325 ps [7]. The resonant peaks have a Gaussian shape, and  $n_{off}$  drifts an amount comparable to  $\delta n_g$  during the two minutes required to complete a measurement. Both observations

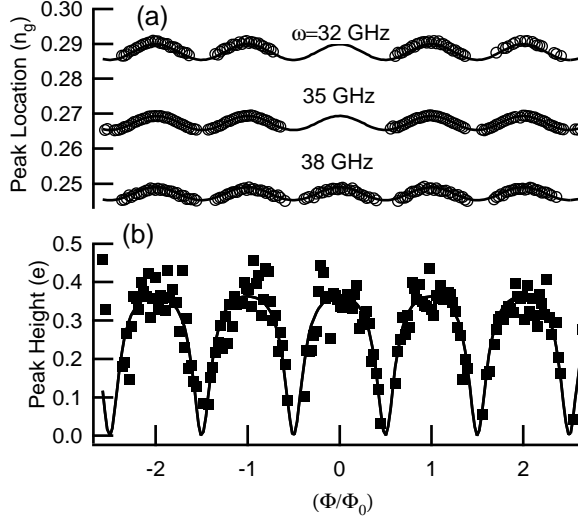


FIG. 3: Resonant spectroscopy of the box versus the two control parameters of the Hamiltonian,  $V_g$  and  $\Phi$ . (a) The locations of resonant peaks (circles) in  $n_g$  and  $\Phi$ , for  $\omega = 32, 35,$  and  $38$  GHz and fits (lines), using Eq. 1 for  $\omega_{01} = 2\omega = 64, 70$  and  $76$  GHz to find single value of  $E_C$  and of  $E_J^{max}$ . The systematic uncertainty in  $n_g$  is represented by the size of the open circle symbols. (b) The height, in electrons, of a  $76$  GHz resonant peak as a function of  $\Phi$  (squares) and a guide to the eye (line).

imply that the width of the peaks expresses not the intrinsic loss of phase coherence due to coupling the TLS to the environment, but rather the degree to which an ensemble of measurements are not identical, due to the well-known  $1/f$  noise of single-electron devices [17]. This  $T_2^*$  is a worst-case estimate because it is extracted while the system is measured continuously by the RF-SET and because it represents an ensemble average of many single measurements that require about two minutes to complete. Nevertheless,  $T_2^*$  is about 150 times longer than  $1/\omega_{01}$  [Fig. 2(c)] and is similar to the times found in [18], another Cooper-pair box implementation, as well as [5] a SQUID circuit. Reference [4] demonstrates that this inhomogeneous broadening may be overcome by operating the Cooper-box at  $n_g = 0.5$  where  $E_{01}$  is to first-order insensitive to fluctuations in  $n_{off}$ .

In order to measure the excited-state lifetime  $T_1$ , we excite the box and then measure the time required to relax back to the ground state. A  $38$  GHz signal is continuously applied to the gate and the box gate is tuned to  $n_g = 0.248$  and  $E_J = E_J^{max}$  so that the microwaves resonantly couple the ground and excited state through a two-photon transition. Abruptly,

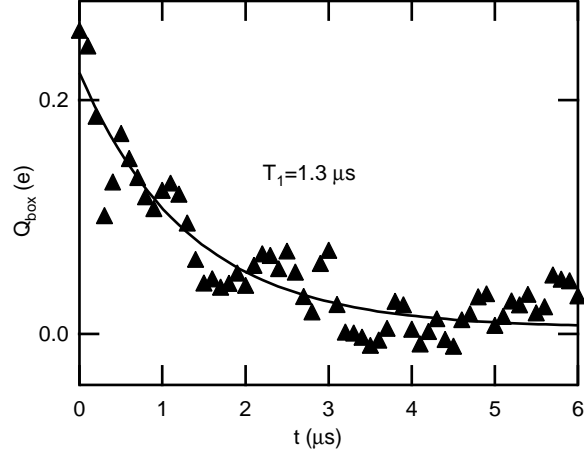


FIG. 4: A determination of the excited-state lifetime of the box.  $Q_{box}$  vs. time  $t$ , (triangles), relative to  $t = 0$ , when  $n_g$  is shifted from  $= 0.248$  to  $0.171$  in  $30$  ns, with  $38$  GHz microwaves applied. The shift in  $n_g$  brings the box out of resonance with the microwave excitation. An exponential fit to the data implies  $T_1 = 1.3 \mu\text{s}$  (line).

$n_g$  is then shifted to  $n_g = 0.171$  in  $30$  ns, slowly enough to be adiabatic but much faster than  $T_1$ . The microwave excitation then no longer resonantly couples the ground and excited state, and the probability of being in the excited state decays in a time  $T_1$ . By averaging many of the transient responses to this stimulus, we find  $T_1 = 1.3 \mu\text{s}$  (Fig. 4). A similar  $T_1$  was found in [4] for a Cooper-pair box with much smaller  $E_C$  and operated at  $n_g = 0.5$ . The lifetime is a quantity which is insensitive to slow drifts in  $n_{off}$  and demonstrates that the TLS, which oscillates  $T_1 \times \omega_{01} = 6 \times 10^5$  times before relaxing into its ground state, is well decoupled from all other sources of dissipation.

We can compare this long lifetime with the spontaneous emission rate expected from the quantum fluctuations of a generic electromagnetic environment. Calculating the spontaneous emission rate using Fermi's golden rule gives

$$\frac{1}{T_1} = \left( \frac{C_g^T}{C_\Sigma} \right)^2 \left( \frac{e}{\hbar} \right)^2 \sin^2(\theta) S_V(\nu_{01} = \omega_{01}/2\pi) \quad (2)$$

where  $S_V(\nu) = 2h\nu(\text{Re}(Z_0))$  is the voltage spectral density of the quantum fluctuations of an environment with an impedance  $Z_0$  at frequency  $\nu$  and  $\sin \theta = E_J/\hbar\omega_{01}$  [11]. The quantity  $C_g^T$  is the total capacitance of the box to nearby metal traces, including intentional coupling to the gate lead and other unintended capacitive coupling (Fig. 1). We calculate  $T_1$  for a  $50 \Omega$

environment to be between 0.25 and 1  $\mu\text{s}$ , extracting  $C_g^T = 45 \pm 15$  aF from an electrostatic simulation of the chip layout [11, 12]. We do not claim to have demonstrated that the lifetime is limited by spontaneous emission; however, if there are additional relaxation processes, either due to the electrometer or fluctuations of some microscopic degree of freedom in the box, their influence is at most comparable to that of spontaneous emission into a typical ( $Z_0 \approx 50 \Omega$ ) electromagnetic environment.

In these experiments, we demonstrate that a Cooper-pair box is a coherent two-level system with a long excited-state lifetime. With spectroscopy, we determine the box's Hamiltonian and estimate the rate of spontaneous emission of the box into a typical environment. We measure an excited-state lifetime of box that is remarkable for two reasons. First, it shows that a quantum-coherent microelectronic circuit can have a  $T_1$  that approaches the limit set by spontaneous emission of a photon into the electromagnetic environment. Second, it is observed by resolving, on sub-microsecond time scales, the decay of the excited-state charge signal while the two-level system is continuously measured. Given the observed electrometer sensitivity of  $4 \times 10^{-5} e/\sqrt{\text{Hz}}$ , the excited-state lifetime is long enough that a single measurement can discriminate between the box in its excited state and the box in its ground state. In a coherent superposition of states the box oscillates  $6 \times 10^5$  times before decaying to the ground state, demonstrating that the circuit is a promising qubit implementation if, as in [4], the sources of inhomogeneous broadening can be overcome.

This work was supported in part by the National Security Agency (NSA) and Advanced Research and Development Activity (ARDA) under Army Research Office (ARO) contract number DAAD19-99-1-0346. This work was also supported by the David and Lucile Packard Foundation and the Wallenberg Foundation. The authors wish to acknowledge M. Devoret, S. Girvin and A. Clerk for useful discussions.

---

\* email: [konrad.lehnert@yale.edu](mailto:konrad.lehnert@yale.edu)

† Group website. [www.eng.yale.edu/rslab](http://www.eng.yale.edu/rslab)

- [1] Y. Nakamura, Y. A. Pashkin, and J. S. Tsai, *Nature* **398**, 786 (1999).
- [2] Y. Nakamura, C. D. Chen, and J. S. Tsai, *Phys. Rev. Lett.* **79**, 2328 (1997).
- [3] J. R. Friedman, V. Patel, W. Chen, S. K. Tolpygo, and J. E. Lukens, *Nature* **406**, 40 (2000).

- [4] D. Vion, A. Aassime, A. Cottet, P. Joyez, H. Pothier, C. Urbina, D. Esteve, and M. H. Devoret, *Science* **296**, 886 (2002).
- [5] C. H. van der Wal, A. C. J. ter Haar, F. K. Wilhelm, R. N. Schouten, C. J. P. M. Harmans, T. P. Orlando, S. Lloyd, and J. E. Mooij, *Science* **290**, 773 (2000).
- [6] A. Abragam, *The Principles of Nuclear Magnetism: The International Series of Monographs on Physics 32* (Oxford University Press, 1983).
- [7] We refer to the inverse linewidth as  $T_2^*$  because our measurements share some features of liquid-state NMR in a spatially inhomogenous magnetic field [6].
- [8] T. A. Fulton and G. J. Dolan, *Phys. Rev. Lett.* **59**, 109 (1987).
- [9] R. J. Schoelkopf, P. Wahlgren, A. A. Kozhevnikov, P. Delsing, , and D. Prober, *Science* **280**, 1238 (1998).
- [10] V. Bouchiat, D. Vion, P. Joyez, D. Esteve, and M. Devoret, *Physica Scripta* **T76**, 165 (1998).
- [11] Y. Makhlin, G. Schön, and A. Shnirman, *Rev. Mod. Phys.* **73**, 357 (2001).
- [12] M. H. Devoret and R. J. Schoelkopf, *Nature* **406**, 1039 (2000).
- [13] A. A. Clerk, S. M. Girvin, A. K. Nguyen, , and A. D. Stone, *Phys. Rev. Lett.* **89**, 176804 (2002).
- [14] The 1 electron step around  $n_g = 0.5$  arises from non-equilibrium quasiparticle excitations on the box island, generated by currents flowing in the RF-SET electrometer. The RF-SET's bias is selected as a compromise between minimizing the width of this feature and maximizing the RF-SET's sensitivity. See Ref. [10] and references therein.
- [15] We determine  $E_c$  by measuring the thermal broadening of the transistions between charge states when the box is driven into its normal state. This method is used in Ref. [10].
- [16] C. Cohen-Tannoudji, B. Diu, and F. Laloë, *Quantum Mechanics* (John Wiley and Sons, 1977), vol. 2, chap. B13, pp. 1336–8.
- [17] N. M. Zimmerman, J. L. Cobb, and A. F. Clark, *Phys. Rev. B* **56**, 7675 (1997).
- [18] Y. Nakamura, Y. A. Pashkin, T. Yamamoto, and J. S. Tsai, *Phys. Rev. Lett.* **88**, 047901 (2002).

# QUBITS AS SPECTROMETERS OF QUANTUM NOISE

R.J. SCHOELKOPF, A.A. CLERK, S.M. GIRVIN, K.W. LEHN-  
ERT and M.H. DEVORET

*Departments of Applied Physics and Physics  
Yale University, PO Box 208284, New Haven, CT 06520-8284*

## 1. Introduction

Electrical engineers and physicists are naturally very interested in the noise of circuits, amplifiers and detectors. This noise has many origins, some of which are completely unavoidable. For example, a dissipative element (a resistor) at finite temperature inevitably generates Johnson noise. Engineers long ago developed spectrum analyzers to measure the intensity of this noise. Roughly speaking, these spectrum analyzers consist of a resonant circuit to select a particular frequency of interest, followed by an amplifier and square law detector (e.g. a diode rectifier) which measures the mean square amplitude of the signal at that frequency.

With the advent of very high frequency electronics operating at low temperatures, we have entered a new regime  $\hbar\omega > k_B T$ , where quantum mechanics plays an important role and one has to begin to think about *quantum noise* and quantum-limited amplifiers and detectors. This topic is well-studied in the quantum optics community and is also commonplace in the radio astronomy community. It has recently become of importance in connection with quantum computation and the construction of mesoscopic electrical circuits which act like artificial atoms with quantized energy levels. It is also important for understanding the quantum measurement process in mesoscopic systems.

In a classical picture, the intensity of Johnson noise from a resistor vanishes linearly with temperature because thermal fluctuations of the charge carriers cease at zero temperature. One knows from quantum mechanics, however, that there are quantum fluctuations even at zero temperature, due to zero-point motion. Zero-point motion is a notion from quantum mechanics that is frequently misunderstood. One might wonder, for example, whether it is physically possible to use a spectrum analyzer to detect the zero-point motion. The answer is quite definitely yes, if we use a quantum

system! Consider for example a hydrogen atom in the 2p excited state lying  $3/4$  of a Rydberg above the 1s ground state. We know that this state is unstable and has a lifetime of only about 1 ns before it decays to the ground state and emits an ultraviolet photon. This spontaneous decay is a natural consequence of the zero-point motion of the electromagnetic fields in the vacuum surrounding the atom. In fact, the rate of spontaneous decay gives a simple way in which to *measure* this zero point motion of the vacuum. Placing the atom in a resonant cavity can modify the strength of the noise at the transition frequency, and this effect can be measured via a change in the decay rate.

At finite temperature, the vacuum will contain blackbody photons which will increase the rate of decay due to stimulated emission and also cause transitions in the reverse direction,  $1s \rightarrow 2p$ , by photon absorption. With these ideas in mind, it is now possible to see how to build a quantum spectrum analyzer.

The remainder of this article is organized as follows. First we describe the general concept of a two-level system as a quantum spectrum analyzer. We next review the Caldeira-Leggett formalism for the modelling of a dissipative circuit element, such as a resistor, and its associated quantum noise. Then, a brief discussion of the single Cooper-pair box, a circuit which behaves as a two-level system or qubit, is given. We then discuss the effects of a dissipative electromagnetic environment on the box, and treat the case of a simple linear, but *nonequilibrium* environment, consisting of a classical tunnel junction which produces shot noise under bias. Finally, we describe a theoretical technique for calculating the properties of a Cooper-pair box coupled to a measurement system, which will be a *nonlinear, nonequilibrium* device, such as a single-electron transistor. Equivalently, this allows one to calculate the full *quantum noise spectrum* of the measurement device. Results of this calculation for the case of a normal SET are presented.

## 2. Two-level systems as spectrum analyzers

Consider a quantum system (atom or electrical circuit) which has its two lowest energy levels  $\epsilon_0$  and  $\epsilon_1$  separated by energy  $E_{01} = \hbar\omega_{01}$ . We suppose for simplicity that all the other levels are far away in energy and can be ignored. The states of any two-level system can be mapped onto the states of a fictitious spin-1/2 particle since such a spin also has only two states in its Hilbert space. With spin up representing the ground state ( $|g\rangle$ ) and spin down representing the excited state ( $|e\rangle$ ), the Hamiltonian is (taking the zero of energy to be the center of gravity of the two levels)

$$H_0 = -\frac{\hbar\omega_{01}}{2}\sigma_z. \quad (1)$$

In keeping with the discussion above, our goal is to see how the rate of ‘spin-flip’ transitions induced by an external noise source can be used to analyze the spectrum of that noise. Suppose for example that there is a noise source with amplitude  $f(t)$  which can cause transitions via the perturbation<sup>1</sup>

$$V = Af(t)\sigma_x, \quad (2)$$

where  $A$  is a coupling constant. The variable  $f(t)$  represents the noise source. We can temporarily pretend that  $f$  is a classical variable, although its quantum operator properties will be forced upon us very soon. For now, only our two-level spectrum analyzer will be treated quantum mechanically.

We assume that the coupling  $A$  is under our control and can be made small enough that the noise can be treated in lowest order perturbation theory. We take the state of the two-level system to be

$$|\psi(t)\rangle = \begin{pmatrix} \alpha_g(t) \\ \alpha_e(t) \end{pmatrix}. \quad (3)$$

In the interaction representation, first-order time-dependent perturbation theory gives

$$|\psi_1(t)\rangle = |\psi(0)\rangle - \frac{i}{\hbar} \int_0^t d\tau \hat{V}(\tau)|\psi(0)\rangle. \quad (4)$$

If we initially prepare the two-level system in its ground state then the amplitude to find it in the excited state at time  $t$  is

$$\alpha_e = -\frac{iA}{\hbar} \int_0^t d\tau \langle e|\hat{\sigma}_x(\tau)|g\rangle f(\tau) + O(A^2), \quad (5)$$

$$= -\frac{iA}{\hbar} \int_0^t d\tau e^{i\omega_{01}\tau} f(\tau) + O(A^2). \quad (6)$$

We can now compute the probability

$$p_e(t) \equiv |\alpha_e|^2 = \frac{A^2}{\hbar^2} \int_0^t \int_0^t d\tau_1 d\tau_2 e^{-i\omega_{01}(\tau_1-\tau_2)} f(\tau_1)f(\tau_2) + O(A^3) \quad (7)$$

We are actually only interested on the average time evolution of the system

$$\bar{p}_e(t) = \frac{A^2}{\hbar^2} \int_0^t \int_0^t d\tau_1 d\tau_2 e^{-i\omega_{01}(\tau_1-\tau_2)} \langle f(\tau_1)f(\tau_2) \rangle + O(A^3) \quad (8)$$

---

<sup>1</sup> The most general perturbation would also couple to  $\sigma_y$  but we assume that (as is often, though not always, the case) a spin coordinate system can be chosen so that the perturbation only couples to  $\sigma_x$ . Noise coupled to  $\sigma_z$  commutes with the Hamiltonian but is nevertheless important in dephasing coherent superpositions of the two states. We will not discuss such processes here.

We can now perform a change of variables in the integrals,  $\tau = \tau_1 - \tau_2$  and  $T = (\tau_1 + \tau_2)/2$ , and we get

$$\bar{p}_e(t) = \frac{A^2}{\hbar^2} \int_0^t dT \int_{-B(T)}^{B(T)} d\tau e^{-i\omega_{01}\tau} \langle f(T + \tau/2)f(T - \tau/2) \rangle + O(A^3) \quad (9)$$

where

$$\begin{aligned} B(T) &= T \text{ if } T < t/2 \\ &= t - T \text{ if } T > t/2. \end{aligned}$$

Let us now suppose that the noise correlation function is stationary (time translation invariant) and has a finite but small autocorrelation time  $\tau_f$ . Then for  $t \gg \tau_f$  we can set the bound  $B(T)$  to infinity in the last integral and write

$$\bar{p}_e(t) = \frac{A^2}{\hbar^2} \int_0^t dT \int_{-\infty}^{\infty} d\tau e^{-i\omega_{01}\tau} \langle f(\tau)f(0) \rangle + O(A^3) \quad (10)$$

The integral over  $\tau$  is effectively a sum of a very large number  $N \sim t/\tau_f$  of random terms<sup>2</sup> and hence the value undergoes a random walk as a function of time. Introducing the noise spectral density

$$S_f(\omega) = \int_{-\infty}^{+\infty} d\tau e^{i\omega\tau} \langle f(\tau)f(0) \rangle, \quad (11)$$

we find that the probability to be in the excited state increases *linearly* with time,<sup>3</sup>

$$\bar{p}_e(t) = t \frac{A^2}{\hbar^2} S_f(-\omega_{01}) \quad (12)$$

The time derivative of the probability gives the transition rate

$$\Gamma_{\uparrow} = \frac{A^2}{\hbar^2} S_f(-\omega_{01}) \quad (13)$$

Note that we are taking in this last expression the spectral density on the negative frequency side. If  $f$  were a strictly classical source  $\langle f(\tau)f(0) \rangle$  would

<sup>2</sup> The size of these random terms depends on the variance of  $f$  and on the value of  $\omega_{01}\tau_f$ . For  $\omega_{01}\tau_f \gg 1$  the size will be strongly reduced by the rapid phase oscillations of the exponential in the integrand.

<sup>3</sup> Note that for very long times, where there is a significant depletion of the probability of being in the initial state, first-order perturbation theory becomes invalid. However, for sufficiently small  $A$ , there is a wide range of times  $\tau_f \ll t \ll 1/\Gamma$  for which Eq. 12 is valid. Eqs. 13 and 14 then yield well-defined rates which can be used in a master equation to describe the full dynamics including long times.

be real and  $S_f(-\omega_{01}) = S_f(+\omega_{01})$ . However, because as we discuss below  $f$  is actually an operator acting on the environmental degrees of freedom,  $[f(\tau), f(0)] \neq 0$  and  $S_f(-\omega_{01}) \neq S_f(+\omega_{01})$ .

Another possible experiment is to prepare the two-level system in its excited state and look at the rate of decay into the ground state. The algebra is identical to that above except that the sign of the frequency is reversed:

$$\Gamma_{\downarrow} = \frac{A^2}{\hbar^2} S_f(+\omega_{01}). \quad (14)$$

We now see that our two-level system does indeed act as a quantum spectrum analyzer for the noise. Operationally, we prepare the system either in its ground state or in its excited state, weakly couple it to the noise source, and after an appropriate interval of time (satisfying the above inequalities) simply measure whether the system is now in its excited state or ground state. Repeating this protocol over and over again, we can find the probability of making a transition, and thereby infer the rate and hence the noise spectral density at positive and negative frequencies. Note that in contrast with a classical spectrum analyzer, we can separate the noise spectral density at positive and negative frequencies from each other since we can separately measure the downward and upward transition rates. Negative frequency noise transfers energy *from the noise source to the spectrometer*. That is, it represents energy emitted by the noise source. Positive frequency noise transfers energy *from the spectrometer to the noise source*.<sup>4</sup> In order to exhibit frequency resolution,  $\Delta\omega$ , adequate to distinguish these two cases, it is crucial that the two-level quantum spectrometer have sufficient phase coherence so that the linewidth of the transitions satisfies the condition  $\omega_{01}/\Delta\omega \geq \max[k_B T/\hbar\omega_{01}, 1]$ .

In thermodynamic equilibrium, the transition rates must obey detailed balance  $\Gamma_{\downarrow}/\Gamma_{\uparrow} = e^{\beta\hbar\omega_{01}}$  in order to give the correct equilibrium occupancies of the two states of the spectrometer. This implies that the spectral densities obey

$$S_f(+\omega_{01}) = e^{\beta\hbar\omega_{01}} S_f(-\omega_{01}). \quad (15)$$

Without the crucial distinction between positive and negative frequencies, and the resulting difference in rates, one always finds that our two level

---

<sup>4</sup> Unfortunately, there are several conventions in existence for describing the noise spectral density. It is common in engineering contexts to use the phrase ‘spectral density’ to mean  $S_f(+\omega) + S_f(-\omega)$ . This is convenient in classical problems where the two are equal. In quantum contexts, one sometimes sees the asymmetric part of the noise  $S_f(+\omega) - S_f(-\omega)$  referred to as the ‘quantum noise.’ We feel it is simpler and clearer to simply discuss the spectral density for positive and negative frequencies *separately*, since they have simple physical interpretations and directly relate to measurable quantities. This convention is especially useful in non-equilibrium situations where there is no simple relation between the spectral densities at positive and negative frequencies.

systems are completely unpolarized. If, however, the noise source is an amplifier or detector biased to be out of equilibrium, no general relation holds.

We now rigorously treat the quantity  $f(\tau)$  as quantum operator in the Hilbert space of the noise source. The previous derivation is unchanged, and Eqs. (13,14) are still valid provided that we interpret the angular brackets in Eq. (8) as representing the quantum statistical expectation value for the operator correlation (in the absence of the coupling to the spectrometer)

$$S_f(\omega) = \int_{-\infty}^{+\infty} d\tau e^{i\omega\tau} \sum_{\alpha,\gamma} \rho_{\alpha\alpha} \langle \alpha | f(\tau) | \gamma \rangle \langle \gamma | f(0) | \alpha \rangle \quad (16)$$

where for simplicity we have assumed that (in the absence of the coupling to the spectrometer) the density matrix is diagonal in the energy eigenbasis and time-independent (but not necessarily given by the equilibrium expression). This yields the standard quantum mechanical expression for the spectral density

$$S_f(\omega) = \int_{-\infty}^{+\infty} d\tau e^{i\omega\tau} \sum_{\alpha,\gamma} \rho_{\alpha\alpha} e^{\frac{i}{\hbar}(\epsilon_\alpha - \epsilon_\gamma)t} |\langle \alpha | f | \gamma \rangle|^2 \quad (17)$$

$$= 2\pi\hbar \sum_{\alpha,\gamma} \rho_{\alpha\alpha} |\langle \alpha | f | \gamma \rangle|^2 \delta(\epsilon_\gamma - \epsilon_\alpha - \hbar\omega). \quad (18)$$

Substitution of this into Eqs. (13,14) we derive the familiar Fermi Golden Rule expressions for the two transition rates.

In standard courses, one is not normally taught that the transition rate of a discrete state into a continuum as described by Fermi's Golden Rule can (and indeed should!) be viewed as resulting from the continuum acting as a quantum noise source. The above derivation hopefully provides a motivation for this interpretation.

One standard model for the continuum is an infinite collection of harmonic oscillators. The electromagnetic continuum in the hydrogen atom case mentioned above is a prototypical example. The vacuum electric field noise coupling to the hydrogen atom has an extremely short autocorrelation time because the range of mode frequencies  $\omega_\alpha$  (over which the dipole matrix element coupling the atom to the mode electric field  $\vec{E}_\alpha$  is significant) is extremely large, ranging from many times smaller than the transition frequency to many times larger. Thus the autocorrelation time of the vacuum electric field noise is considerably less than  $10^{-15}$ s, whereas the decay time of the hydrogen 2p state is about  $10^{-9}$ s. Hence the inequalities needed for the validity of our expressions are very easily satisfied.

Of course in the final expression for the transition rate, energy conservation means that only the spectral density at the transition frequency

enters. However, in order for the expression to be valid (and in order for the transition rate to be time independent), it is essential that there be a wide range of available photon frequencies so that the vacuum noise has an autocorrelation time much shorter than the inverse of the transition rate.

### 3. Quantum Noise from a Resistor

Instead of an atom in free space, we might consider a quantum bit capacitively coupled to a transmission line. The transmission line is characterized by an inductance per unit length  $\ell$  and capacitance per unit length  $c$ . A semi-infinite transmission line presents a frequency-independent impedance  $Z = R_0 = \sqrt{\ell/c}$  at its end and hence acts like an ideal resistor. The dissipation is caused by the fact that currents injected at one end launch waves which travel off to infinity and do not return. Very conveniently, however, the system is simply a large collection of harmonic oscillators (the normal modes) and hence can be readily quantized. This representation of a physical resistor is essentially the one used by Caldeira and Leggett [1] in their seminal studies of the effects of dissipation on tunneling. The only difference between this model and the vacuum fluctuations in free space discussed above is that the relativistic bosons travel in one dimension and do not carry a polarization label. This changes the density of states as a function of frequency, but has no other essential effect.

The Lagrangian for the system is

$$\mathcal{L} = \int_0^\infty dx \frac{\ell}{2} j^2 - \frac{1}{2c} q^2, \quad (19)$$

where  $j(x, t)$  is the local current density and  $q(x, t)$  is the local charge density. Charge conservation connects these two quantities via the constraint

$$\partial_x j(x, t) + \partial_t q(x, t) = 0. \quad (20)$$

We can solve this constraint by defining a new variable

$$\theta(x, t) \equiv \int_0^x dx' q(x', t) \quad (21)$$

in terms of which the current density is  $j(x, t) = -\partial_t \theta(x, t)$  and the charge density is  $q(x, t) = \partial_x \theta(x, t)$ . For any well-behaved function  $\theta(x, t)$ , the continuity equation is automatically satisfied so there are no dynamical constraints on the  $\theta$  field. In terms of this field the Lagrangian becomes

$$\mathcal{L} = \int_0^\infty dx \frac{\ell}{2} (\partial_t \theta)^2 - \frac{1}{2c} (\partial_x \theta)^2 \quad (22)$$

The Euler-Lagrange equation for this Lagrangian is simply the wave equation  $v^2 \partial_x^2 \theta - \partial_t^2 \theta = 0$  where the mode velocity is  $v = 1/\sqrt{\ell c}$ .

From Eq. (21) we can deduce that the proper boundary conditions (in the absence of any coupling to the qubit) for the  $\theta$  field are  $\theta(0, t) = \theta(L, t) = 0$ . (We have temporarily made the transmission line have a finite length  $L$ .) The normal mode expansion that satisfies these boundary conditions is

$$\theta(x, t) = \sqrt{\frac{2}{L}} \sum_{n=1}^{\infty} \varphi_n(t) \sin \frac{k_n \pi x}{L}, \quad (23)$$

where  $\varphi_n$  is the normal coordinate and  $k_n \equiv \frac{\pi n}{L}$ . Substitution of this form into the Lagrangian and carrying out the spatial integration yields a set of independent harmonic oscillators representing the normal modes.

$$\mathcal{L} = \sum_{n=1}^{\infty} \frac{\ell}{2} (\dot{\varphi}_n)^2 - \frac{1}{2c} k_n^2 \varphi_n^2. \quad (24)$$

From this we can find the momentum  $p_n$  canonically conjugate to  $\varphi_n$  and quantize the system to obtain an expression for the voltage at the end of the transmission line in terms of the mode creation and destruction operators

$$V = \sqrt{\frac{2}{L}} \frac{1}{c} \partial_x \theta(0, t) = \frac{1}{c} \sum_{n=1}^{\infty} k_n \sqrt{\frac{\hbar}{2\ell\Omega_n}} (a_n^\dagger + a_n). \quad (25)$$

The spectral density of voltage fluctuations is then found to be

$$S_V(\omega) = 2\pi \frac{2}{L} \sum_{n=1}^{\infty} \frac{\hbar\Omega_n}{2c} \{n_\gamma(\hbar\Omega_n)\delta(\omega + \Omega_n) + [n_\gamma(\hbar\Omega_n) + 1]\delta(\omega - \Omega_n)\}, \quad (26)$$

where  $n_\gamma(\hbar\omega)$  is the Bose occupancy factor for a photon with energy  $\hbar\omega$ . Taking the limit  $L \rightarrow \infty$  and converting the summation to an integral yields

$$S_V(\omega) = 2R_0 \hbar |\omega| \{n_\gamma(\hbar|\omega|)\Theta(-\omega) + [n_\gamma(\hbar\omega) + 1]\Theta(\omega)\}, \quad (27)$$

where  $\Theta$  is the step function. We see immediately that at zero temperature there is no noise at negative frequencies because energy can not be extracted from zero-point motion. However there remains noise at positive frequencies indicating that the vacuum is capable of absorbing energy from the qubit.

A more compact expression for this ‘two-sided’ spectral density of a resistor is

$$S_V(\omega) = \frac{2R_0 \hbar \omega}{1 - e^{-\hbar\omega/k_B T}}, \quad (28)$$

which reduces to the more familiar expressions in various limits. For example, in the classical limit  $k_B T \gg \hbar\omega$  the spectral density is equal to the

Johnson noise result<sup>5</sup>

$$S_V(\omega) = 2R_0k_B T, \quad (29)$$

which is frequency independent, and in the quantum limit it reduces to

$$S_V(\omega) = 2R_0\hbar\omega\Theta(\omega). \quad (30)$$

Again, the step function tells us that the resistor can only absorb energy, not emit it, at zero temperature.

If we use the engineering convention and add the noise at positive and negative frequencies we obtain

$$S_V(\omega) + S_V(-\omega) = 2R_0\hbar\omega \coth \frac{\hbar\omega}{2k_B T} \quad (31)$$

for the symmetric part of the noise, which appears in the quantum fluctuation-dissipation theorem[2]. The antisymmetric part of the noise is simply

$$S_V(\omega) - S_V(-\omega) = 2R_0\hbar\omega. \quad (32)$$

This quantum treatment can also be applied to any arbitrary dissipative network[3]. If we have a more complex circuit containing capacitors and inductors, then in all of the above expressions,  $R_0$  should be replaced by  $\text{Re}Z(\omega)$  where  $Z(\omega)$  is the complex impedance presented to the qubit.

#### 4. The Single Cooper-Pair Box: a Two-Level Quantum Circuit

The Cooper-pair box (CPB) is a simple circuit [4], consisting of a small superconducting “island”, connected to a large reservoir via a single small-capacitance Josephson junction, depicted as a box with a cross (Fig. 1). The island is charge biased by applying a voltage ( $V_g$ ) to a nearby lead, called the gate, which has a small capacitance to the island,  $C_g$ . The junction is characterized by its capacitance,  $C_j$ , and its tunnel resistance,  $R_j$ . At temperatures well below the transition temperature of the superconductor ( $T_C \sim 1.5$  K for the usual Al/AlOx/Al junctions), none of the many ( $\sim 10^9$ ) quasiparticle states on the island should be thermally occupied, and the number of Cooper-pairs on the island is the only relevant degree of freedom.

We may then write the Hamiltonian for the box in terms of the states of different numbers of pairs on the island, which are eigenstates of the number operator,  $\hat{n}|n\rangle = n|n\rangle$ . The box Hamiltonian consists of an electrostatic term, plus a Josephson term describing the coupling of the island to the

---

<sup>5</sup> Note again that in the engineering convention this would be  $S_V(\omega) = 4R_0k_B T$ .

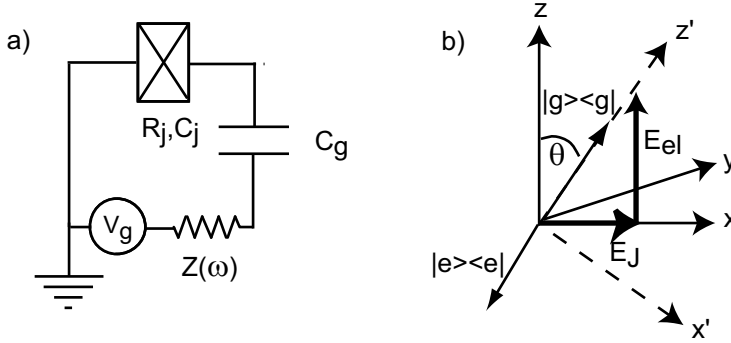


Figure 1. a) Circuit diagram of Cooper-pair box. b) Pseudo-spin representation of the energies of Cooper-pair box. The density matrix for the two pure eigenstates lie along the total effective field, collinear with the  $z'$  axis.

lead,

$$H = H_{electrostatic} + H_{Josephson} \quad (33)$$

$$= 4E_C \sum_n (n - n_g)^2 |n\rangle\langle n| - \frac{E_J}{2} \sum_n (|n+1\rangle\langle n| + h.c.) \quad (34)$$

The energy scale for the electrostatic interaction is given by the charging energy,  $E_C = e^2/2C_\Sigma$ , where  $C_\Sigma = C_j + C_g$  is the total island capacitance, while the Josephson energy,  $E_J$ , is set by the tunnel resistance and the gap of the superconductor,

$$E_J = \frac{h\Delta}{8e^2R_j} = \frac{\Delta}{8} \frac{R_K}{R_j}. \quad (35)$$

The electrostatic term is easily modulated by changing the voltage on the gate; the quantity  $n_g = C_g V_g/2e$  that appears in the Hamiltonian corresponds to the total polarization charge (in units of Cooper pairs) injected into the island by the voltage source.

This Hamiltonian leads to particularly simple behavior in the charge regime, when the electrostatic energy dominates over the Josephson coupling,  $4E_C \gg E_J$ . In this case we can restrict the discussion to only two charge states,  $|n=0\rangle$  and  $|n=1\rangle$ . For convenience we can reference the energies of the two states to their midpoint,  $E_{mid} = 4E_C(1-2n_g)^2$ , so that the Hamiltonian now becomes

$$H = \frac{1}{2} \begin{pmatrix} -E_{el} & -E_J \\ -E_J & E_{el} \end{pmatrix} \quad (36)$$

where  $E_{el}$  is the electrostatic energy that is now *linear* in the gate charge,  $E_{el} = 4E_C(1-2n_g)$ . It is also now apparent that the Hamiltonian is identical

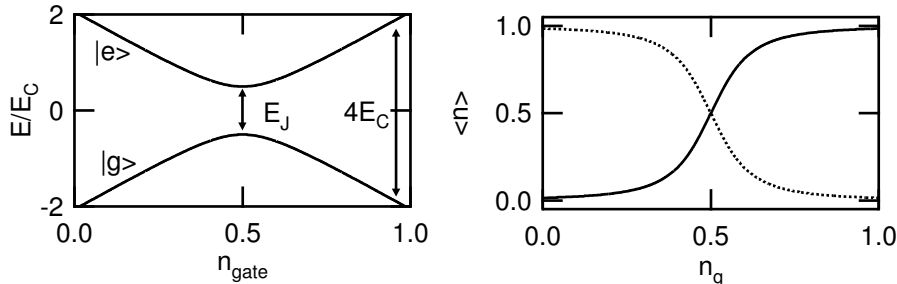


Figure 2. Energies (left) of ground and excited states of a Cooper-pair box with  $E_C = E_J$  vs. dimensionless gate charge,  $n_g = C_g V_g / 2e$ . The expectation value of a charge measurement,  $\langle n \rangle$ , (right) for the ground (solid line) and excited (dotted line) states vs.  $n_g$ .

to that of a fictitious spin-1/2 particle,

$$H = -\frac{E_{el}}{2}\sigma_z - \frac{E_J}{2}\sigma_x, \quad (37)$$

under the influence of two pseudo-magnetic fields,  $B_z = E_{el}$  and  $B_x = E_J$ , as depicted in Fig. 1. In other words, the box is a qubit or two-level system<sup>6</sup>. The state of the system is in general a linear combination of the states  $|n=0\rangle$  and  $|n=1\rangle$ . The state can be depicted using the density matrix, which corresponds to a point on the Bloch sphere, where the north pole (+z-direction) corresponds to  $|n=0\rangle$ . The ground and excited states of the system will be aligned and anti-aligned with the total fictitious field, i.e. in the  $\pm z'$  directions.

It is also apparent from this discussion that the states of the box can be easily manipulated by changing the gate voltage. The energies of the ground and excited states, as a function of  $n_g$ , are displayed in Figure 2. The energy difference between the ground and excited bands varies from  $4E_C$  at  $n_g = 0, 1$ , to a minimum at the charge degeneracy point,  $n_g = 1/2$ . At this point, the Josephson coupling leads to an avoided crossing, and the splitting is  $E_J$ .

Also plotted is the expectation value of the number operator,  $\langle \hat{n} \rangle$ , which is proportional to the total charge on the island. In the geometrical

<sup>6</sup> Of course, this is an approximation, as there are other charge states ( $|n=2\rangle$ , etc.) which are possible, but require much higher energy. Even outside the charge regime (i.e. when  $E_J \geq 4E_C$ ) the two lowest levels of the box can be used to realize a qubit [5]. In this case, the two states do not exactly correspond with eigenstates of charge, and matrix elements are more complicated to calculate. Nonetheless, this regime can also be used as an electrical quantum spectrum analyzer.

picture of Fig. 1b, a measurement of charge ( $\hat{n}$ ) is equivalent to projecting the state on the z-axis,  $\hat{n} = \frac{1}{2}(1 - \sigma_z)$ . We see that as the gate charge is changed from 0 to 1, the ground state is initially  $|n = 0\rangle$ , and the character of the ground and excited states interchange on passing through the degeneracy point, leading to the transition between  $\langle \hat{n} \rangle = 0$  and 1, which is broadened by quantum fluctuations (the  $\sigma_x$  coupling). At the degeneracy point, the ground and excited states lie in the  $\pm x$ -directions, i.e. they are symmetric and antisymmetric combinations of the two charge states. In general, we will denote the ground and excited state of the CPB at a particular gate voltage as  $|g\rangle$  and  $|e\rangle$ , which are given in terms of the charge states by  $|g\rangle = \cos(\theta/2)|0\rangle + \sin(\theta/2)|1\rangle$  and  $|e\rangle = -\sin(\theta/2)|0\rangle + \cos(\theta/2)|1\rangle$  respectively, where  $\theta = \arctan[E_J/E_{el}]$  is a function of the gate voltage.

A nice property of the CPB in this regime is that the various matrix elements can be calculated in a straightforward way. For example, the expectation value of  $\hat{n}$  in the ground state,  $\langle g|\hat{n}|g\rangle$ , is therefore equal to  $1/2(1 - \langle g|\sigma_z|g\rangle) = \sin^2(\theta/2)$ , from which we can find the ground state charge as shown in Fig. 2. A perturbation in the gate charge, due for example to a fluctuation or change in the applied gate voltage, will lead to a proportional change in the electrostatic energy, or the z-component of the fictitious magnetic field. Such a perturbation will cause both dephasing and transitions between states.

## 5. General Discussion of CPB Coupled to a Dissipative Environment

In the previous section we described the Hamiltonian and the eigenstates for a Cooper-pair box which is “charge-biased,” i.e. controlled with a voltage applied to a gate capacitor  $C_g$ , as shown in Fig. 1. In our earlier treatment of the box, the voltage and the dimensionless gate charge,  $n_g$  were treated as fixed parameters of the Hamiltonian (c-numbers). In this case, the box’s evolution is purely deterministic and conservative. However, it is impossible, even in principle, to control such a voltage with arbitrary precision at all frequencies. In Fig. 1, the idealized source of the gate voltage is drawn in series with an impedance  $Z(\omega)$  of the gate lead. Generally, this gate lead will be connected to external wiring (a transmission line), with a typical real impedance comparable to the impedance of free space ( $\sim 50 \Omega$ ) at the microwave transition frequencies of the box. From the fluctuation-dissipation theorem we know that this impedance will introduce noise on the gate voltage, even at zero temperature.

There are several effects of the voltage noise on the box, or the coupling of our spin-1/2 circuit to the many external degrees of freedom represented by the gate impedance. First, even at zero temperature, we will find a finite excited state lifetime,  $T1$ , for the box. Second, at finite temperature, we will

find a finite polarization of our psuedo-spin, i.e. some steady-state probability to find the spin in its excited state. Finally, the gate noise introduces a random effective field felt by the spin, and a loss of phase coherence for a superposition state. It is this last effect which is most important in making high-fidelity qubits and performing quantum computations, but it is the first two which depend most explicitly on the quantum nature of the noise. We deal in this manuscript with only these first two features of the box's coupling to the electromagnetic environment, and ignore the dephasing<sup>7</sup>. Of course, the other parameter in the Hamiltonian, the Josephson energy, can in principle fluctuate, especially as in many experiments the box's junction is split into a small SQUID in order to provide external tuning of  $E_J$  with an applied flux. We concentrate here only on the voltage noise (fluctuations in the  $\sigma_z$  part of the Hamiltonian) for simplicity.

We begin with a very simple treatment of the dynamics of the two-level system under the influence of the gate voltage noise. We are interested in the ensemble-averaged behavior of our psuedo-spin, which is best described using the density matrix approach, and is detailed in Section 7 on the coupling of the box to a measuring SET. The basic effects, apart from dephasing, however, can be captured simply by examining the probabilities  $p_g$  and  $p_e$  of finding the box in its ground ( $|g\rangle$ ) or excited ( $|e\rangle$ ) states. The noise of the external environment can drive transitions from ground to excited state and vice-versa, at rates  $\Gamma_\uparrow$  and  $\Gamma_\downarrow$ , respectively. The coupled master equations for these probabilities are

$$\frac{dp_e}{dt} = p_g\Gamma_\uparrow - p_e\Gamma_\downarrow \quad (38)$$

$$\frac{dp_g}{dt} = p_e\Gamma_\downarrow - p_g\Gamma_\uparrow \quad (39)$$

Of course conservation of probability tells us that  $p_e + p_g = 1$ , so we introduce the polarization of the spin-1/2 system,  $P = p_g - p_e$ . In steady-state, the detailed balance condition is  $p_e\Gamma_\downarrow = p_g\Gamma_\uparrow$ . The two rates  $\Gamma_\uparrow$  and  $\Gamma_\downarrow$  are related by Equations 13 and 14 to the spectral densities of the noise at negative and positive frequencies. We see immediately that if the spectral density is symmetric (classical!), then the rates for transitions up and down are equal, the occupancies of the two states are exactly equal, and the polarization of the psuedo-spin is identically zero. It is the quantum, or antisymmetric, part of the noise which gives the finite polarization of the spin. Even in NMR, where the temperature is large compared to the level splitting ( $\hbar\omega_{01} \leq k_B T$ ), this effect is well-known and crucial, as the small but non-zero polarization is the subject of the field!

---

<sup>7</sup> For a nice recent treatment of dephasing in Josephson junctions, see Ref. [6].

Solving for the steady-state polarization, we find

$$P_{ss} = \frac{\Gamma_{\downarrow} - \Gamma_{\uparrow}}{\Gamma_{\downarrow} + \Gamma_{\uparrow}} = \frac{S(+\omega_{01}) - S(-\omega_{01})}{S(+\omega_{01}) + S(-\omega_{01})} \quad (40)$$

An measurement of the steady-state polarization allows one to observe the amount of asymmetry in the noise, so the two-level system is a *quantum* spectrum analyzer.

If we can create a non-equilibrium polarization,  $P = P_{ss} + \Delta P$  (a pure state is not necessary) of our two-level system, we expect it to return to the steady state value. Substituting the modified probabilities  $p_e(t) = p_{e_{ss}} - \Delta P(t)/2$  and  $p_g(t) = p_{g_{ss}} + \Delta P(t)/2$  into our master equations above, we find an equation for the deviation of the polarization

$$\frac{d(\Delta P(t))}{dt} = -\Delta P(t)(\Gamma_{\uparrow} + \Gamma_{\downarrow}). \quad (41)$$

Thus the system decays to its steady-state polarization with the relaxation rate  $\Gamma_1 = \Gamma_{\uparrow} + \Gamma_{\downarrow} = (A/\hbar)^2[S(-\omega_{01}) + S(+\omega_{01})]$  related to the *total* noise at both positive and negative frequencies. In NMR, the time  $1/\Gamma_1$  is referred to as  $T1$ . In the zero-temperature limit, there is no possibility of the qubit absorbing energy from the environment, so  $\Gamma_{\uparrow} = 0$ , and we find full polarization  $P = 1$ , and a decay of any excited state population at a rate  $\Gamma_{\downarrow} = 1/T1$  which is the spontaneous emission rate.

It is worth emphasizing that a quantum noise source is always characterized by two numbers (at any frequency), related to the positive and negative frequency spectral densities, or to the symmetric and antisymmetric parts of the noise. These two quantities have different effects on a two-level system, introducing a finite polarization and finite excited-state lifetime. Consequently, a measurement of *both* the polarization and  $T1$  of a two-level system is needed to fully characterize the quantum noise coupled to the qubit. Such measurements in electrical systems are now possible, and some of us [7] have recently performed such a characterization for the specific case of a CPB coupled to a superconducting single-electron transistor.

Our discussion in this section uses the language of NMR to describe the effects on the two-level system. There are, however, several possible protocols<sup>8</sup> for measuring the quantum noise, and several different “basis sets” or measured quantities which describe the noise process or the quantum reservoir to which the two-level system is coupled. Table 1 contains a “translation” between the specific pairs of quantities that are commonly

---

<sup>8</sup> The idea of watching the decay from the pure states  $|e\rangle$  and  $|g\rangle$  to measure  $S_V(\pm|\omega_{01}|)$  separately was described in Section 2.

TABLE I. Different ways to characterize a quantum reservoir.

Fermi Golden Rule	$\Gamma_{\uparrow}(\omega) = \frac{A^2}{\hbar^2} S_V(+ \omega )$	$\Gamma_{\downarrow}(\omega) = \frac{A^2}{\hbar^2} S_V(- \omega )$
Fluct.-Diss. Relation	$n_{\gamma}(\omega) = 2\Gamma_{\uparrow}/(\Gamma_{\downarrow} - \Gamma_{\uparrow})$	$\text{Re}[Z(\omega)] = \frac{\hbar}{A^2\omega}(\Gamma_{\downarrow} - \Gamma_{\uparrow})$
NMR	$T1 = (\Gamma_{\downarrow} + \Gamma_{\uparrow})^{-1}$	$P = (\Gamma_{\downarrow} - \Gamma_{\uparrow})/(\Gamma_{\downarrow} + \Gamma_{\uparrow})$
Quantum Optics	$B_{Einstein} = \Gamma_{\uparrow}$	$A_{Einstein} = \Gamma_{\downarrow} - \Gamma_{\uparrow}$

used in different disciplines, and their relation to the positive and negative noise spectral densities. In all cases, though, *two separate numbers* are required to specify the properties of a quantum reservoir.

## 6. The Box Coupled to an Ohmic Environment

We can now proceed to the effects of a specific dissipative coupling to the Cooper-pair box. The noise on the gate voltage will lead to a fluctuation of the gate charge parameter,  $n_g$ , and thus to a fluctuation of the electrostatic energy, i.e. the  $\sigma_z$  term in the Hamiltonian (Eq. 37). Depending on the average value of  $n_g$ , this fluctuation will consist of fluctuations which are both longitudinal ( $\parallel$  to  $\sigma'_z$ ) and transverse ( $\perp$  to  $\sigma'_z$ ). To calculate the rates of transitions between the states  $|e\rangle$  and  $|g\rangle$ , we need to find the coupling strength  $A$  of this perturbation in the  $\sigma'_x$  direction. Referring to Fig. 1, we see that  $\sigma_z = \cos(\theta)\sigma'_z - \sin(\theta)\sigma'_x$ . If we let the gate charge now be  $n_g(t) = \bar{n}_g + \delta n_g(t)$ , we may rewrite the Hamiltonian Eq. 37 in the new eigenbasis as

$$H = -\frac{E_{01}}{2\hbar}\sigma'_z + 4E_C \cos(\theta)\delta n_g(t)\sigma'_z - 4E_C \sin(\theta)\delta n_g(t)\sigma'_x. \quad (42)$$

The time-varying term in the  $\sigma'_z$  direction will effectively modulate the transition frequency,  $\omega_{01} = E_{01}/\hbar$ , and cause dephasing. In terms of the gate voltage noise,  $V(t)$ , the  $\sigma'_x$  perturbation term has the form  $AV(t)\sigma'_x = e\kappa \sin(\theta)V(t)\sigma'_x$ , where  $e$  is the electron's charge and  $\kappa = C_g/C_{\Sigma}$  is the capacitive coupling. Using Eq. 14, we find

$$\Gamma_{\downarrow} = \left(\frac{e}{\hbar}\right)^2 \kappa^2 \sin^2(\theta) S_V(+\omega_{01}). \quad (43)$$

If the environment is effectively at zero temperature ( $\hbar\omega_{01} \gg k_B T$ ), then  $S_V(+\omega_{01}) = 2\hbar\omega_{01}R$ , and the quality factor of the transition is

$$Q = \omega_{01}/\Gamma_{\downarrow} = \frac{1}{\kappa^2 \sin^2 \theta} \frac{R_K}{4\pi R}, \quad (44)$$

where  $R_K = h/e^2$  is the resistance quantum.

For a finite temperature, we have rates in both directions, and the polarization of the psuedo-spin is given by the ratio of the antisymmetric (Eq. 32) to symmetric (Eq. 31) spectral densities,  $P = \tanh(\hbar\omega_{01}/2k_B T)$ , as one expects for any two-level system at temperature  $T$ . An example of the average charge state of a Cooper-pair box at finite temperature, and of the polarization and equilibration time T1, are shown in Figure 3. As the gate voltage is varied, the transition frequency of the box changes from a maximum near  $n_g = 0$ , to a minimum  $\omega_{01} = E_J/\hbar$  at the degeneracy point  $n_g = 0.5$  and then back again. We see that the states of the box are generally most “fragile” near the avoided crossing. First, the energy splitting is a minimum here, leading to the lowest polarization of the psuedo-spin. Second, because the eigenstates  $|g\rangle$  and  $|e\rangle$  point in the  $\sigma_x$  direction, the matrix elements for the voltage fluctuations of the environment are maximal, i.e. the noise is orthogonal to the spin. This also implies that the dephasing effects are minimal at this degeneracy point, which offers great advantages for improving the decoherence times [5], but the excited state lifetimes are smallest at this point. One also sees that the lifetimes become large away from the degeneracy, where the electrostatic energy dominates over the Josephson energy, which offers advantages when measuring the charge state. In the limit that  $E_J$  could be suppressed to zero during a measurement, the matrix elements (for voltage noise) vanish, and a quantum non-demolition (QND) measurement [8] could be performed. The idea of using the qubit as a quantum spectrum analyzer is precisely the reverse, where we measure the “destruction” in the two-level system (i.e. inelastic transitions caused by the coupling of the states to the environment), in order to learn about the quantum noise spectrum of the fluctuations.

The Cooper-pair box can of course also be used to measure the more interesting spectral densities of *nonequilibrium* devices. The simplest example is to replace the gate resistance by a tunnel junction. If we arrange to bias the junction using, e.g. an inductor, a dc current  $I$  and an average dc voltage  $V$  can be maintained across the junction. Classically, the current noise of such a tunneling process is frequency independent,  $S_I = 2eI$ . The voltage noise density presented to the CPB’s gate would then be  $S_V = 2eIR_T^2$ , where  $R_T$  is the junction tunnel resistance. In fact, this “white” spectral density can only extend up to frequencies of order  $\omega = eV/\hbar$ , the maximum energy of electrons tunneling through the junction. The correct high-frequency form of the *symmetrized* noise density was calculated by Rogovin and Scalapino [9],

$$S_V(\omega) = R(\hbar\omega + eV) \coth\left[\frac{\hbar\omega + eV}{2k_B T}\right] + R(\hbar\omega - eV) \coth\left[\frac{\hbar\omega - eV}{2k_B T}\right], \quad (45)$$

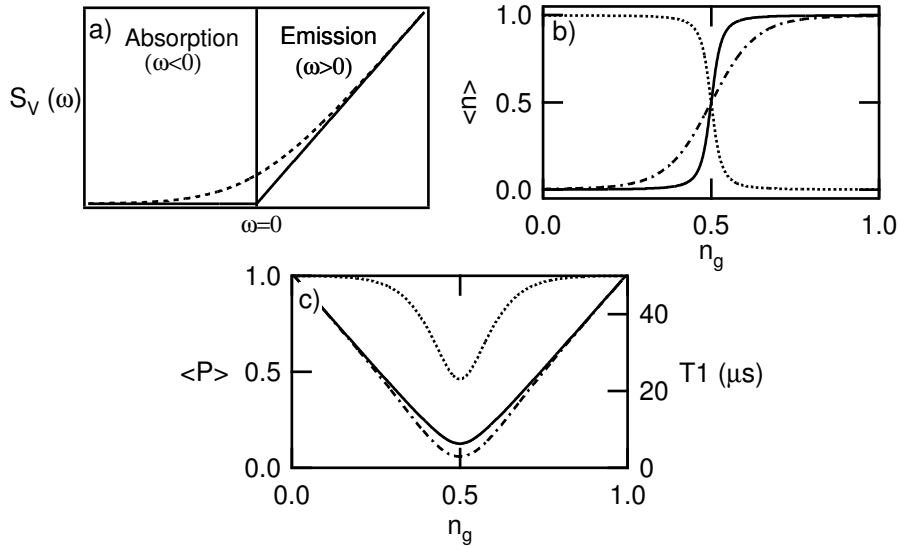


Figure 3. The box coupled to an equilibrium, Ohmic environment, i.e. a resistor. a) Two-sided noise spectral density, of the voltage,  $S_V(\omega)$ , for a resistor at  $T=0$  (solid line) and finite temperature (dashed line) b) Average charge of box with  $E_C = 1K$ ,  $E_J = 0.5K$  when coupled with strength  $\kappa = 0.01$  to a resistor with resistance  $R = 50 \Omega$  and temperature  $T = 0.5K$ . c) Polarization (dotted line) and relaxation time  $T1$  for the same parameters. Full line is the rate of spontaneous emission, i.e.  $T1$  at zero temperature.

and was *indirectly* measured in a mesoscopic conductor using a conventional spectrum analyzer [10]. This noise can also be expressed [11] in its two-sided form

$$S_V(\omega) = \frac{(\hbar\omega + eV) R_T}{1 - e^{-\frac{\hbar\omega + eV}{k_B T}}} + \frac{(\hbar\omega - eV) R_T}{1 - e^{-\frac{\hbar\omega - eV}{k_B T}}}, \quad (46)$$

and is displayed in Fig. 4. Notice that the antisymmetric part of this noise is the same as that of the ordinary resistor,  $S_V(+\omega) - S_V(-\omega) = 2\hbar\omega R_T$ , and is independent of the voltage. Also shown in Fig. 5 is the polarization and relaxation time,  $T1$ , of a CPB coupled to a shot noise environment. We see that full polarization is achieved only when  $\hbar\omega_{01} \gg eV$ . For low transition frequencies, the polarization is inversely proportional to the current through the junction. Aguado and Kouwenhoven [11] have described the use of a double quantum dot as a two-level system to probe this behavior of the shot noise.

Given our discussion so far, it is now interesting to ask what the effects of a real quantum measurement on a quantum circuit will be. A quantum measurement device will in general be neither linear, Ohmic, nor equilib-

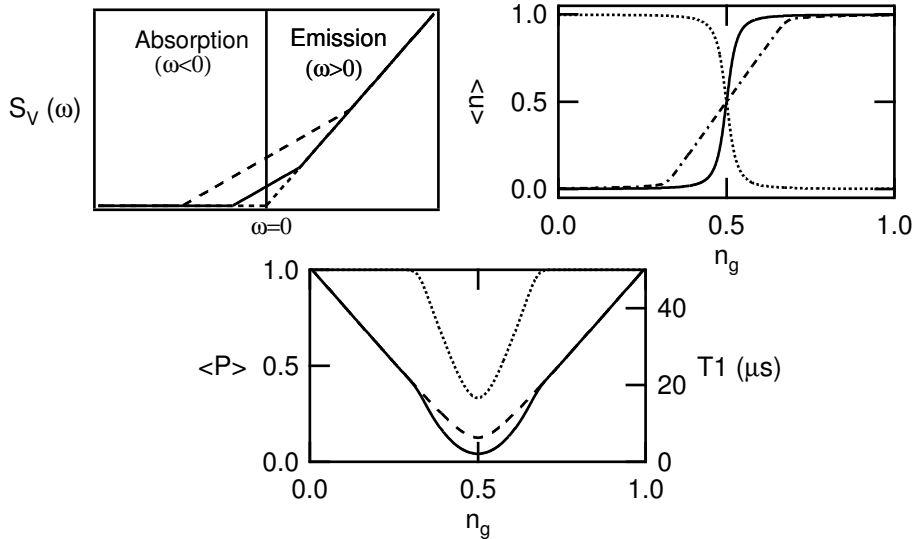


Figure 4. The box coupled to a nonequilibrium, Ohmic environment, i.e. a  $50 \Omega$  tunnel junction. a) Two-sided noise spectral density, of the voltage,  $S_V(\omega)$ , for a junction at  $T=0.02$  K, with zero voltage (dotted line), and increasing bias voltages (solid and dashed lines). b) Average charge of box with  $E_C = 1K$ ,  $E_J = 0.5K$  when coupled with strength  $\kappa = 0.01$  to a junction biased at  $eV = 1.5$  K. c) Polarization (dotted line) and relaxation time  $T1$  for the same parameters (solid) and for  $T=0$ ,  $V=0$  (dashed line).

rium. Obviously, if we hope to characterize this measurement process, and to understand what one will observed when the qubit is coupled to the noise processes of the measuring device, we will need to calculate the full quantum (two-sided!) noise spectrum of the amplifier or detector.

## 7. Single-Electron Transistor Coupled to a Two-Level System

We have seen in previous sections that a two-level system (TLS) may be used as a “spectrum analyzer” to measure quantum noise. Here, we use this technique to *theoretically* calculate quantum noise. Instead of simply studying the “noisy” system of interest in isolation, one can study a composite system consisting of the “noisy” system coupled to a TLS; by calculating the relaxation and excitation rates of the TLS, one can efficiently calculate the quantum noise of interest<sup>9</sup>. We demonstrate the usefulness of this

<sup>9</sup> Note that the spirit of our approach is similar to that employed in the theory of full counting statistics [12]. There too one attaches an auxiliary spin  $1/2$  to the scattering system of interest, and studies the dynamics of the fully coupled system to obtain the

technique by outlining a calculation of the quantum charge noise of a single electron transistor (SET). This is an important example, as when an SET is used as an electrometer, it is this noise which determines the measurement backaction.

The SET consists of a metallic island attached via tunnel junctions to source and drain reservoirs. It is described by the Hamiltonian:

$$H_{SET} = \sum_{k,\alpha=L,R,I} (\varepsilon_k - \mu_\alpha) c_{k\alpha}^\dagger c_{k\alpha} + E_C(n - \mathcal{N})^2 + H_T \quad (47)$$

$$H_T = t \sum_{k,q,\alpha=L,R} \left( F^\dagger c_{kI}^\dagger c_{q\alpha} + h.c. \right) \quad (48)$$

The first term in  $H_{SET}$  describes the kinetic energy of electrons in the leads ( $\alpha = L, R$ ) and on the island ( $\alpha = I$ ). The second term is the Coulomb charging energy which depends on  $n$ , the number of excess electrons on the island. This interaction term can be tuned by changing the voltage on a nearby gate electrode which is capacitively coupled to the island;  $\mathcal{N}$  represents the dimensionless value of this voltage. Finally,  $H_T$  describes the tunneling of electrons through the two SET tunnel junctions; the conductance of each junction (in units of  $e^2/h$ ) is given by  $g = 4\pi^2 t^2 \nu_0^2$ , with  $\nu_0$  being the density of states.  $F^\dagger$  is an auxiliary operator which increases  $n$  by one:  $[n, F^\dagger] = F^\dagger$ . For simplicity, we assume that the two junctions of the SET are completely symmetric (i.e. equal junction capacitances and dimensionless conductances).

Throughout this section, we will be interested in the regime of sequential tunneling in the SET, where transport involves energy-conserving transitions between two charge states of the SET island, say  $n = 0$  and  $n = 1$ . These transitions are described by simple rates, which can be derived via Fermi's Golden rule:

$$\Gamma_{n\pm 1,n}^\alpha = \gamma([\Delta E]_{n\pm 1,n}^\alpha) \quad (49)$$

$$\gamma(\Delta E) = \frac{g\Delta E/h}{1 - e^{-\Delta E/(k_B T)}} \quad (50)$$

$$\Delta E_{n\pm 1,n}^\alpha = \mp 2E_C \left( n \pm \frac{1}{2} - \mathcal{N} \right) \pm \left( \frac{1}{2} - \delta_{\alpha,R} \right) eV_{DS} \quad (51)$$

$\Gamma_{n\pm 1,n}^\alpha$  is the tunneling rate from the charge state  $n$  to  $n \pm 1$  through junction  $\alpha$ ;  $\Delta E$  is the energy gained in making the tunneling transition, and includes contributions both from the drain-source voltage  $V_{DS}$  and from the charging energy. Sequential tunneling is the dominant transport mechanism when the junction conductances are small (i.e.  $g/(2\pi) \ll 1$ ),

---

statistics of charge transfer in the scatterer.

and the dimensionless gate voltage  $\mathcal{N}$  is not too far away from a charge degeneracy point. Sequential tunneling is the most important regime for measurement applications, as it yields the largest SET currents.

At low temperatures, only tunnel events which follow the voltage are possible. There are thus there only two relevant rates:  $n = 0 \rightarrow 1$  transitions occur through the left junction at a rate  $\Gamma_{10}^L$ , while  $n = 1 \rightarrow 0$  occur through the right junction at a rate  $\Gamma_{01}^R$ . The average current will be given by:

$$\langle I \rangle = e\bar{\Gamma} \equiv e \frac{\Gamma_{10}^L \Gamma_{01}^R}{\Gamma_{10}^L + \Gamma_{01}^R} \quad (52)$$

We are interested in calculating  $S_Q(\omega)$ , the quantum noise associated with fluctuations of the charge on the central island of the SET. It is defined as:

$$S_Q(\omega) = \int_{-\infty}^{\infty} dt \langle n(t)n(0) \rangle e^{-i\omega t} \quad (53)$$

Note that we can equivalently think of  $S_Q$  as describing the voltage noise of the island, as  $V_{island} = en/C_\Sigma$ , where  $C_\Sigma$  is the total capacitance of the island. In two limits, the form of the island charge noise can be anticipated. For  $\omega \rightarrow 0$ , the noise will correspond to classical telegraph noise— the island charge  $n$  fluctuates between the values 0 and 1, with Poisson-distributed waiting times determined by the rates  $\Gamma_{10}^L$  and  $\Gamma_{01}^R$ . We thus expect a symmetric, Lorentzian form [13] for the noise at low frequencies:

$$S_Q(\omega) \rightarrow \frac{2\bar{\Gamma}}{\omega^2 + (\Gamma_{10}^L + \Gamma_{01}^R)^2} \quad (\omega \ll E_C) \quad (54)$$

For large frequencies  $|\omega| \gg E_C$ , we expect that correlations due to the charging energy will have no influence on the noise. The system will effectively look like two tunnel junctions in parallel, and we can use the results of Sec. 6 for the corresponding voltage noise. Noting that each junction effectively consists of a resistor and capacitor in parallel, we have at zero temperature:

$$\begin{aligned} S_Q(\omega) &= \frac{C_\Sigma^2}{e^2} \times S_V(\omega) \rightarrow \frac{C_\Sigma^2}{e^2} [2\hbar\omega \text{Re } Z_{tot} \Theta(\omega)] \quad (|\omega| \gg E_C) \\ &= 4 \left( \frac{g}{2\pi} \right) \frac{\omega}{\left( \frac{g}{2\pi} \frac{4E_C}{\hbar} \right)^2 + \omega^2} \Theta(\omega) \end{aligned} \quad (55)$$

Note that  $S_Q(\omega)$  decays as  $1/\omega$  at large frequencies, whereas Eq. (54) for classical telegraph noise decays as  $1/\omega^2$ .

Given these two limiting forms, the question now becomes one of how the SET interpolates between them. One might expect that the two results

should simply be added in quadrature, but as with combining thermal and quantum noise (see Sec. 6), this approach is too simple. A completely quantum mechanical way of calculating the noise for any frequency is needed. This was recently accomplished by Johansson *et. al* [14] using an extension of a technique developed by Schöller and Schön [15]. Here, we re-derive their results using the coupled system approach outlined above. This method is physically motivated and allows for a heuristic interpretation of the final result.

## 8. SET Coupled to a Qubit

We now consider a system where the SET is coupled to a two-level system (i.e. a qubit), with a coupling Hamiltonian which can induce transitions in the TLS. Using spin operators to describe the qubit, and assuming operation at the degeneracy point for simplicity, where the transitions are fastest<sup>10</sup>, we have:

$$H = H_{SET} - \frac{1}{2}\Omega\sigma_x + A\sigma_z n, \quad (56)$$

where  $\Omega$  is the qubit splitting frequency<sup>11</sup>, and  $A$  is the coupling strength. We can define the rates  $\Gamma_\uparrow$  and  $\Gamma_\downarrow$  which are, respectively, the rate at which the qubit is excited by the SET, and the rate at which the qubit is relaxed by the SET. For a weak coupling ( $A \rightarrow 0$ ), one has (c.f. Eq. 14,13 in Sec. 2):

$$\Gamma_{\downarrow/\uparrow} = \frac{A^2}{\hbar} S_Q(\pm\Omega) \quad (57)$$

Eq. (57) tells us that if we know the rates  $\Gamma_\uparrow$  and  $\Gamma_\downarrow$  for a weakly coupled system at an arbitrary splitting frequency  $\Omega$ , we know the quantum noise  $S_Q(\Omega)$  at all frequencies. This is the essence of the technique previously described, in which a qubit acts as a quantum spectrum analyzer of noise. Here, we mimic this approach theoretically by obtaining  $\Gamma_\uparrow$  and  $\Gamma_\downarrow$  from a *direct* analysis of the coupled system in the limit of weak coupling ( $A \rightarrow 0$ ). The object of interest is the reduced density matrix  $\rho$  which describes both the charge  $n$  of the transistor island *and* the state of the qubit. We are interested in two quantities. First, what is the stationary state of the qubit? The stationary populations of the two qubit states (which are determined

---

<sup>10</sup> This amounts to maximizing the “destruction” due to the SET’s noise, and the case where  $\theta = \pi/2$ , the qubit eigenstates are in the  $\sigma'_z = \sigma_x$  direction, and the SET’s perturbation is in the  $-\sigma'_x = \sigma_z$  direction (c.f. Eq. 42). After the noise of the SET is found, we can then recalculate the effects on the qubit at various  $n_g$  or values of  $\theta$  by including the modified matrix elements in the coupling coefficient,  $A$ .

<sup>11</sup> Henceforth we use  $\Omega$  for the transition frequency, instead of the previous notation  $\omega_{01} = E_{01}/\hbar$ , for compactness.

from the time-independent solution for  $\rho$ ) will tell us the polarization of the qubit, and the amount of asymmetry in the noise (c.f. Eq.40). Second, how quickly do the qubit populations relax to their stationary value? This relaxation will be described by a time-dependent solution of  $\rho$  characterized by a mixing rate  $\Gamma_{mix}$  which is the *sum* of  $\Gamma_{\uparrow}$  and  $\Gamma_{\downarrow}$  (c.f. Eq. 41). From these two results we can solve for the individual values of  $\Gamma_{\uparrow/\downarrow}$ .

To deal with the dynamics of  $\rho$ , we make use of the fact that sequential tunneling processes are completely described by lowest-order perturbation theory in the tunneling Hamiltonian  $H_T$ . Keeping only second order terms (there are no non-vanishing first order terms), one obtains the following standard evolution equation in the interaction picture:

$$\frac{d}{dt}\rho(t) = -\frac{1}{\hbar} \int_{-\infty}^t dt' \langle [H_T(t), [H_T(t'), \rho(t') \otimes \rho_F]] \rangle \quad (58)$$

The angular brackets denote the trace over the single-particle degrees of freedom in the SET leads and island;  $\rho_F$  is the equilibrium density matrix corresponding to the state of these degrees of freedom in the absence of tunneling.<sup>12</sup> Note that a similar density matrix analysis of a qubit coupled to a SET was recently discussed by Makhlin *et. al* [16]; unlike the present case, these authors restricted attention to a vanishingly small splitting frequency  $\Omega$ .

To make progress with Eq. (58), we make a Markov approximation, which involves replacing  $\rho(t')$  on the right-hand side with  $\rho(t)$ . This is permissible as we are interested in the *slow* dynamics of  $\rho$ . We want to find both the stationary solution of  $\rho$ , for which the Markov approximation is exact, and the mixing mode, a mode whose time dependence is  $\propto e^{-(\Gamma_{\uparrow}+\Gamma_{\downarrow})t}$ . This mode is also arbitrarily slow in the weak coupling limit  $A \rightarrow 0$  of interest. Finding the stationary mode and the mixing mode correspond to evaluating the polarization and T1 of the qubit (c.f. Eq. 40 and Eq. 41), as was shown earlier for the master equation of the *probabilities* in Section 5. Note that the Markov approximation should be made in the *Schrödinger* picture, as it is in the Schrödinger picture that  $\rho$  will be nearly stationary (i.e. all oscillations associated with the qubit splitting frequency  $\Omega$  will be damped out in the long-time limit).

Evaluation of Eq. (58) in the Markov approximation results in the appearance of rates which are generalizations of those given in Eq. (49). Now, however, these rates depend on the initial and final state of the qubit-tunneling transitions can simultaneously change both the charge state of the SET island *and* the state of the qubit. The resulting equation is most

---

<sup>12</sup> In the diagrammatic language of Ref. [15], Eq. (58) is equivalent to keeping all  $(H_T)^2$  terms in the self-energy of the Keldysh propagator governing the evolution of  $\rho$ .

easily presented if we write the reduced density matrix  $\rho$  in the basis of eigenstates at zero tunneling. For each value of island charge  $n$ , there is a different qubit Hamiltonian, and correspondingly a different a qubit ground state  $|g_n\rangle$  and excited state  $|e_n\rangle$ . When a tunneling event occurs in the SET, there is a sudden change in the qubit Hamiltonian. As the qubit ground and excited states at different values of  $n$  are *not* orthogonal, tunneling transitions in the SET are able to cause “shake-up” transitions in the qubit. In the limit  $A \rightarrow 0$ , the relevant matrix overlaps are given by:

$$\langle g_m | g_n \rangle = 1 - \frac{1}{2} \left( \frac{A(m-n)}{\Omega} \right)^2 = \langle e_m | e_n \rangle \quad (59)$$

$$\langle e_m | g_n \rangle = \frac{A(m-n)}{\Omega} \quad (60)$$

Defining the frequency dependent rate  $\Gamma_{n\pm 1, n}(\omega)$  as:

$$\Gamma_{n\pm 1, n}(\omega) \equiv \sum_{\alpha=L,R} \gamma([\Delta E]_{n\pm 1, n}^\alpha + \hbar\omega), \quad (61)$$

where  $\Delta E$  and  $\gamma(\Delta E)$  are defined in Eqs. (51) and (50), the required tunnel rates take the form:

$$\Gamma_{m, n} \equiv \Gamma_{m, n}(0) \quad \Gamma_{m, n}^\pm \equiv \Gamma_{m, n}(\pm\Omega) \quad (62)$$

The  $\Gamma^+$  rates correspond to tunneling events where the qubit is simultaneously relaxed, and thus there is an additional energy  $\Omega$  available for tunneling. For large  $\Omega$ , tunneling processes which are normally energetically forbidden can occur if they are accompanied by qubit relaxation. Similarly, the  $\Gamma^-$  rates describe tunnelling events where the qubit is simultaneously excited, with the consequence that there is less energy available for tunneling.

Returning to the evolution equation Eq. (58), note that we do not need to track elements of  $\rho$  which are off-diagonal in the island charge index  $n$ —there is no coherence between different charge states, as tunneling events necessarily create an electron-hole excitation. Further, if we focus on small qubit frequencies, we may continue to restrict attention to only  $n = 0$  and  $n = 1$  (i.e.  $\Omega$  is not large enough to “turn on” tunneling processes which are normally energetically forbidden). Thus, there are 8 relevant matrix elements of  $\rho$ —for each of the four qubit density matrix elements (i.e.  $gg$ ,  $ee$ ,  $ge$ ,  $eg$ ), there are two possible island charge states. We combine these elements into a vector  $\vec{\rho} = (\rho_{gg}, \rho_{ee}, \rho_{ge}, \rho_{eg})$ , where  $\rho_{gg} = (\langle 0, g_0 | \rho | 0, g_0 \rangle, \langle 1, g_1 | \rho | 1, g_1 \rangle)$ , etc. Organizing the resulting evolution equation in powers of the coupling  $A$ , we obtain in the Schrödinger picture:

$$\frac{d}{dt} \vec{\rho} = (\mathbf{\Lambda}_0 + \frac{A}{\Omega} \mathbf{\Lambda}_1 + \frac{A^2}{\Omega^2} \mathbf{\Lambda}_2 + \dots) \vec{\rho} \quad (63)$$

We discuss the significance of the matrices  $\mathbf{\Lambda}_j$  in what follows.

The  $8 \times 8$  matrix  $\mathbf{\Lambda}_0$  describes the evolution of the system at zero coupling:

$$\mathbf{\Lambda}_0 = \begin{pmatrix} M & 0 & 0 & 0 \\ 0 & M & 0 & 0 \\ 0 & 0 & +i\Omega + M' & 0 \\ 0 & 0 & 0 & -i\Omega + M' \end{pmatrix}, \quad (64)$$

with the  $2 \times 2$  matrices  $M$  and  $M'$  being defined by:

$$M = \begin{pmatrix} -\Gamma_{10} & \Gamma_{01} \\ \Gamma_{10} & -\Gamma_{01} \end{pmatrix} \quad M' = \frac{1}{2} \begin{pmatrix} -(\Gamma_{10}^+ + \Gamma_{10}^-) & \Gamma_{01}^+ + \Gamma_{01}^- \\ \Gamma_{10}^+ + \Gamma_{10}^- & -(\Gamma_{01}^+ + \Gamma_{01}^-) \end{pmatrix} \quad (65)$$

At zero coupling there are no transitions between different qubit states, and hence  $\mathbf{\Lambda}_0$  has a block-diagonal form. There are two independent stationary solutions of Eq. (63) at  $A = 0$  (i.e. two zero eigenvectors of  $\mathbf{\Lambda}_0$ ), which correspond to being either in the qubit ground or qubit excited state:

$$\vec{z}_g = (p_0, p_1, 0, 0, 0, 0, 0, 0), \quad \vec{z}_e = (0, 0, p_0, p_1, 0, 0, 0, 0). \quad (66)$$

$(p_0, p_1)$  are the stationary probabilities of being in the  $n = 0$  or  $n = 1$  charge states:

$$(p_0, p_1) = \left( \frac{\Gamma_{01}}{\Gamma_{01} + \Gamma_{10}}, \frac{\Gamma_{10}}{\Gamma_{01} + \Gamma_{10}} \right) \quad (67)$$

The existence of two zero-modes is directly related to the fact that at zero coupling ( $A = 0$ ), the probabilities to be in the qubit ground and excited state are individually conserved.

At non-zero coupling, the matrices  $\mathbf{\Lambda}_1$  and  $\mathbf{\Lambda}_2$  appearing in Eq. (63) generate transitions between different qubit states. The matrix  $\mathbf{\Lambda}_2$  directly couples  $\rho_{gg}$  and  $\rho_{ee}$ , while  $\mathbf{\Lambda}_1$  couples  $\rho_{gg}$  and  $\rho_{ee}$  to the off-diagonal blocks  $\rho_{ge}$  and  $\rho_{eg}$ . The effect of these matrices will be to break the degeneracy of the two zero modes of Eq. (63) existing at  $A = 0$ . After this degeneracy is broken, there will still be one zero mode  $\rho_0$ , describing the stationary state of the *coupled* system (the existence of a stationary solution is guaranteed by the conservation of probability). For weak coupling, the qubit density matrix obtained from  $\rho_0$  will be diagonal in the basis  $\{|g_{\langle n \rangle}\rangle, |e_{\langle n \rangle}\rangle\}$ , which corresponds to the average SET charge  $\langle n \rangle = p_1$ . The ratio of the occupancies of these two qubit states will yield the ratio between the relaxation rate  $\Gamma_{\downarrow}$  and the excitation rate  $\Gamma_{\uparrow}$ . In addition, there will also be a slow, time-dependent mode of Eq. (63) arising from breaking the degeneracy of the two  $A = 0$  zero modes. This time-dependent mode will describe how a linear combination of  $z_g$  and  $z_e$  relaxes to the true stationary state, and will have an eigenvalue  $\lambda = -\Gamma_{\uparrow} - \Gamma_{\downarrow}$ , i.e. the mixing rate.

Thus, we need to do degenerate second order perturbation theory in the coupling  $A$  to obtain the relaxation and excitation rates  $\Gamma_\downarrow$  and  $\Gamma_\uparrow$ . The only subtlety here is that the matrix  $M$  is not Hermitian, implying that it has distinct right and left eigenvectors. Letting  $\tilde{z}$  represent the left eigenvector of  $\mathbf{\Lambda}_0$  corresponding to the right eigenvector  $\tilde{z}$ , we define the projector matrix  $\mathbf{P}$  as:

$$\mathbf{P} = |z_g\rangle\langle\tilde{z}_g| + |z_e\rangle\langle\tilde{z}_e|, \quad (68)$$

and let  $\mathbf{P}_\perp$  denote  $1 - \mathbf{P}$ . As usual, degenerate second order perturbation theory requires diagonalizing the perturbation in the space of the degenerate eigenvectors. We are thus led to look at the matrix  $Q$ , defined as:

$$Q = \frac{A^2}{\Omega^2} \left( \mathbf{P}\mathbf{\Lambda}_2\mathbf{P} + \mathbf{P}\mathbf{\Lambda}_1\mathbf{P}_\perp [-\mathbf{\Lambda}_0]^{-1} \mathbf{P}_\perp\mathbf{\Lambda}_1\mathbf{P} \right) \quad (69)$$

From the definition of  $Q$ , we may immediately identify the rates  $\Gamma_\uparrow$  and  $\Gamma_\downarrow$ :

$$\Gamma_\uparrow = \langle\tilde{z}_e|Q|z_g\rangle \quad \Gamma_\downarrow = \langle\tilde{z}_g|Q|z_e\rangle \quad (70)$$

We thus see how the rates  $\Gamma_{\uparrow,\downarrow}$  arise in the present approach— they are related to breaking the degeneracy between two zero-modes (stationary solutions) which exist at zero coupling. Note that there are two distinct contributions to  $\Gamma_{\uparrow,\downarrow}$ , coming from the two terms in the matrix  $Q$ : a “direct” contribution involving  $\mathbf{\Lambda}_2$  and an “interference” contribution involving  $\mathbf{\Lambda}_1$  acting twice. These two terms have a different physical interpretation, as will become clear.

Let us first consider the rate  $\Gamma_\uparrow$ , which describes how noise in the SET causes ground to excited state transitions in the qubit. For this rate, our approximation of only keeping two charge states will be valid for all splitting frequencies  $\Omega$ . To evaluate the “direct” contribution to this rate, which involves the first term in the matrix  $Q$ , note that the relevant part of  $\mathbf{\Lambda}_2$  has the expected form:

$$\mathbf{\Lambda}_2|_{ee,gg} = \begin{pmatrix} 0 & \Gamma_{01}^- \\ \Gamma_{10}^- & 0 \end{pmatrix} \quad (71)$$

i.e. it consists of tunnel rates which correspond to having given up an energy  $\Omega$  to the qubit. Using Eqs. (69) and (70), we find:

$$\Gamma_\uparrow|_{direct} = \left(\frac{A}{\Omega}\right)^2 (p_0\Gamma_{10}^- + p_1\Gamma_{01}^-) = \left(\frac{A}{\Omega}\right)^2 \left(\frac{\Gamma_{01}\Gamma_{10}^- + \Gamma_{10}\Gamma_{01}^-}{\Gamma_{10} + \Gamma_{01}}\right) \quad (72)$$

The direct contribution to  $\Gamma_\uparrow$  has a very simple form: for each charge state  $n = 0, 1$ , add the rate to tunnel out of  $n$  while exciting the qubit, weighted

by both the probability to be in state  $n$ , and the overlap between ground and excited states (i.e.  $(A/\Omega)^2$ ). This is very similar to how one typically calculates the current for a SET: one adds up the current associated with each charge state (i.e. a difference of rates), weighted by the occupancy of the state. The direct contribution to  $\Gamma_\uparrow$  neglects any possible coherence between successive excitation events; as a result, it fails to recover the classical expression of Eq. (54) in the small- $\Omega$  limit.

We now consider the ‘‘interference’’ contribution to  $\Gamma_\uparrow$  coming from the second term in the expression for matrix  $Q$  (c.f. Eq. (69)). After some algebra, we obtain the following for the interference contribution to  $\Gamma_\uparrow$ :

$$\Gamma_\uparrow|_{int} = -\frac{2A^2}{\Omega^2} (p_0\Gamma_{10}^- + p_1\Gamma_{01}^-) \frac{(\Gamma_\Sigma)^2}{\Omega^2 + (\Gamma_\Sigma)^2} \quad (73)$$

where:

$$\Gamma_\Sigma \equiv \frac{\Gamma_{10}^- + \Gamma_{10}^+ + \Gamma_{01}^- + \Gamma_{01}^+}{2} \quad (74)$$

This contribution is purely negative, and is only significant (relative to the direct contribution) at low frequencies  $\Omega < \Gamma$ . We can interpret this equation as describing the interference between *two* consecutive excitation events. For example, consider the first term in Eq. (73). This describes a process where a SET initially in the charge state  $n = 0$  undergoes a tunnel event to the  $n = 1$  state, creating a superposition of qubit ground and excited states. At some later time the SET relaxes to the stationary distribution  $(p_0, p_1)$  of the charge states, again partially exciting the qubit. Letting  $\Delta t$  represent the time between these two events, we have the approximate sequence:

$$\begin{aligned} |0, g_0\rangle &\xrightarrow{\Gamma_{10}^-} |1, g_1\rangle + \alpha|1, e_1\rangle \\ &\xrightarrow{\Delta t} e^{i\Omega\Delta t/2}|1, g_1\rangle + e^{-i\Omega\Delta t/2}\alpha|1, e_1\rangle \end{aligned} \quad (75)$$

$$\xrightarrow{\Gamma_\Sigma} \left( e^{i\Omega\Delta t/2}\beta - e^{-i\Omega\Delta t/2}\alpha \right) |0, e_0\rangle + \dots \quad (76)$$

Here,  $\alpha$  is the amplitude associated with qubit excitation having occurred during the first ( $n = 0 \rightarrow 1$ ) tunnel event, while  $\beta$  is the amplitude associated with excitation occurring during the second ( $n = 1 \rightarrow 0$ ) tunneling. These amplitudes will be given by the corresponding matrix overlap elements:

$$\alpha = \langle e_1|g_0\rangle \simeq \frac{A}{\Omega} \quad \beta = \langle e_0|g_1\rangle \simeq -\frac{A}{\Omega} \quad (77)$$

In the final state after the two tunnelings (Eq. (76)), there are two terms in the amplitude of the state  $|0, e_0\rangle$ , corresponding to the fact that qubit excitation could have occurred in either the first or the second tunnel event.

To get a rate for this double excitation event, we should take the modulus squared of the final  $|0, e_0\rangle$  state amplitude, then multiply by the occupancy of the initial state ( $p_0$ ) and the rate of the first tunnel event ( $\Gamma_{10}$ ). The interference term in the resulting expression takes the form:

$$\Gamma_{\uparrow}|_{int} = (p_0\Gamma_{10}) \times 2\text{Re}(\alpha^*\beta e^{i\Omega\Delta t}) = -(p_0\Gamma_{10})\frac{2A^2}{\Omega^2}\cos(\Omega\Delta t) \quad (78)$$

The above expression is a function of the time  $\Delta t$  between the first and second tunnel events. This time is determined by the fact that the intermediate superposition state (Eq. (75)) corresponds to a non-stationary distribution of charge on the SET island, and will decay via tunneling to the stationary distribution ( $p_0, p_1$ ) at a rate  $\Gamma_{\Sigma}$ . Taking this decay to be Poissonian, and averaging over  $\Delta t$ , we obtain:

$$\Gamma_{\uparrow}|_{int} = -(p_0\Gamma_{10})\frac{2A^2}{\Omega^2}\frac{(\Gamma_{\Sigma})^2}{\Omega^2 + (\Gamma_{\Sigma})^2} \quad (79)$$

This is precisely the first term in Eq. (73); the second term can be obtained in the same way, by now considering a situation where the SET is initially in the  $n = 1$  charge state. As claimed,  $\Gamma_{\uparrow}|_{int}$  corresponds to the interference between two consecutive excitation events. The negative sign of this contribution can be directly traced to the matrix overlap elements (c.f. Eq. 77). Also, we see that the suppression of the interference term at large  $\Omega$  results from phase randomization occurring during the delay time between the two excitation events.

Returning to the total noise, we combine Eq. (73) with the direct contribution Eq. (72) to  $\Gamma_{\uparrow}$ ; comparing against Eq. (57), we obtain the final expression for  $S_Q(\Omega)$  at all *negative* frequencies:

$$S_Q(-|\Omega|) = \frac{p_0\Gamma_{10}^- + p_1\Gamma_{01}^-}{\Omega^2 + \frac{1}{4}(\Gamma_{10}^- + \Gamma_{10}^+ + \Gamma_{01}^- + \Gamma_{01}^+)^2} \quad (80)$$

Note for large  $|\Omega|$  (i.e.  $|\Omega| > \max(\Delta E_{01}^\alpha, \Delta E_{10}^\alpha) \simeq V_{DS}/2$ ),  $S_Q(-\Omega)$  will vanish identically at zero temperature. Physically, this cutoff corresponds to the largest amount of energy the SET can give up to the qubit during a single tunnel event; giving up more energy would suppress the event completely (i.e. the tunnel rates have a step-function form at zero temperature, c.f. Eq. (50)). If one included higher order processes in the tunneling (i.e. went beyond sequential tunneling), correlated tunneling events involving the full voltage drop over both junctions,  $V_{DS}$ , would move this cutoff to higher values of absolute frequency.

We now turn to the relaxation rate  $\Gamma_{\downarrow}$ , and hence the positive frequency parts of  $S_Q$ . The calculation proceeds exactly as that for  $\Gamma_{\uparrow}$ , the only

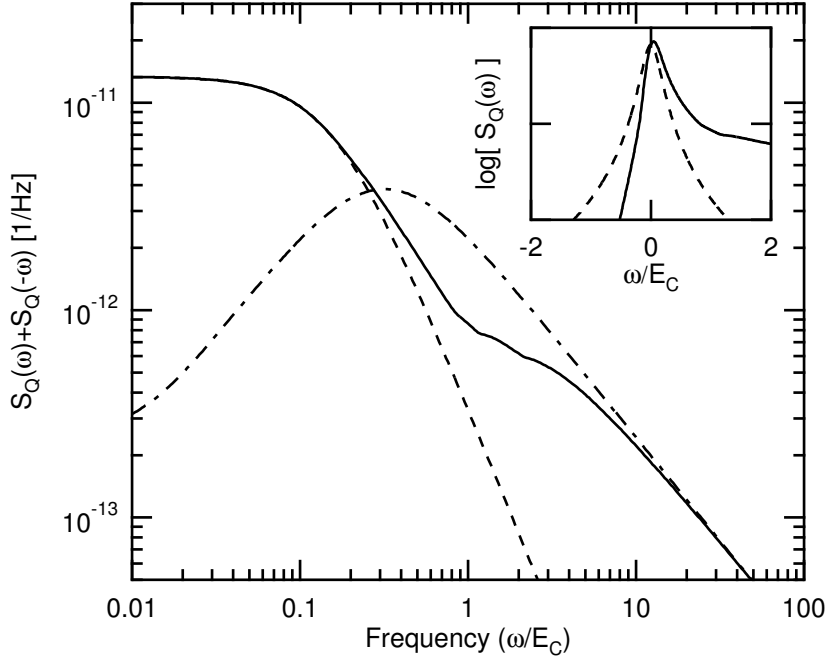


Figure 5. Symmetrized SET charge noise as a function of frequency, for typical SET parameters:  $g = 1$ ,  $E_C/k_B = 2\text{K}$ ,  $\mathcal{N} = 0.33$ ,  $eV_{DS} = E_C$ , and  $T = 20\text{mK}$ . The dashed line is the classical telegraph noise (Eq. (54)), while the dot-dashed line is the noise of two parallel tunnel junctions (Eq. (55)). Inset: full (non-symmetrized) quantum noise for identical SET parameters; the dashed line is the symmetric classical telegraph noise.

modification being that one now needs to include the charge states  $n = 2$  and  $n = -1$ , as the SET could absorb enough energy from the qubit to make transitions to these states possible. We can combine the result for  $\Gamma_{\downarrow}$  with Eq. (80) to obtain a single, compact expression for the noise at all frequencies first obtained by Johansson *et. al* [14]:<sup>13</sup>

$$S_Q(\omega) = \frac{p_0 [\Gamma_{10}(\omega) + \Gamma_{-1,0}(\omega)] + p_1 [\Gamma_{01}(\omega) + \Gamma_{21}(\omega)]}{\omega^2 + \frac{1}{4} [\Gamma_{10}(\omega) + \Gamma_{10}(-\omega) + \Gamma_{01}(\omega) + \Gamma_{01}(-\omega)]^2} \quad (81)$$

Shown in Figure 5 is the symmetrized noise  $S_Q(\omega) + S_Q(-\omega)$  for typical SET parameters. One can clearly see abrupt changes in the slope of this curve; each of these kinks corresponds to a threshold frequency at which a given tunneling process either turns on or turns off. For comparison, curves

<sup>13</sup> Eq. (81) ignores additional order  $g/(2\pi)$  terms which arise in the denominator at positive frequencies large enough to turn on tunneling to higher charge states; such terms are clearly negligible in the sequential tunneling regime due to the smallness of  $g/(2\pi)$ .

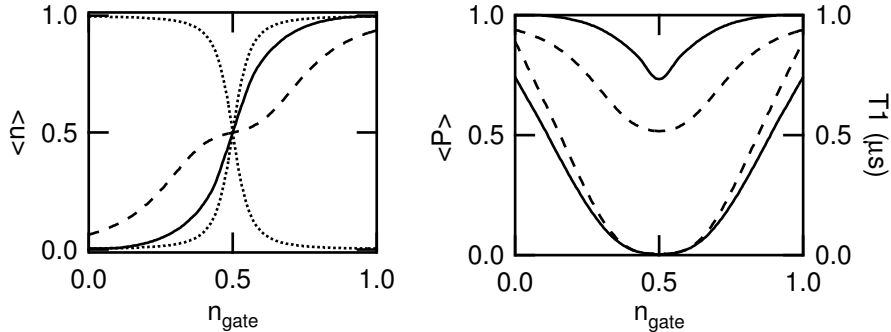


Figure 6. a) Average charge state of a Cooper pair box coupled to a SET, as a function of box gate voltage, using identical SET parameters as above. The box parameters are  $E_C/k_B = 0.5\text{K}$ ,  $E_J/k_B = 0.25\text{K}$  and the coupling constant is  $\kappa = 0.04$ . We also include relaxation effects due to a 10% coupling to a  $50\Omega$  environment. The dashed curve corresponds to assuming the SET produces classical telegraph noise, the solid curve corresponds to using the full quantum noise of the SET, and the dashed-dot curve is the box ground state. b) The relaxation time  $T_1$  for the same system, as a function of box gate voltage.

corresponding to classical telegraph noise and to the uncorrelated noise of two tunnel junctions are also shown. At low frequencies the symmetrized true noise matches the classical curve; for higher frequencies, it lies *above* the classical curve but *below* the curve corresponding to the uncorrelated case. The inset of this figure shows the both the negative and positive frequency parts of  $S_Q(\omega)$ .

It is easy to check that in the limit  $\omega \rightarrow 0$ , Eq. (81) recovers the classical telegraph expression of Eq. (54). In the high-frequency, zero temperature limit, one can also see that Eq. (81) approaches the uncorrelated result of Eq. (55) from *below*:

$$S_Q(\omega) \rightarrow \Theta(\omega) \frac{4 \left(\frac{g}{2\pi}\right) \omega \left(1 - \frac{E_C}{2\hbar\omega}\right)}{\omega^2 + \frac{g^2}{\pi^2} \omega^2} \rightarrow \Theta(\omega) \frac{2g}{\pi\omega} \quad (82)$$

Note that at high frequencies, it is only the “direct” terms which contribute to the noise— the interference contribution is not important in the limit of uncorrelated tunneling. The fact that the noise approaches the high frequency limit from below results from the tendency of charging energy induced correlations (which are present for a finite  $\omega/E_C$ ) to suppress fluctuations of  $n$ , and thus suppress the noise. Note that the interpolation between the low and high frequency limits here is very different than, e.g., interpolating between thermal noise and zero-point fluctuation noise in a tunnel junction. In the latter case, one is effectively *combining* two sources

of noise; here, one is simply turning off correlations brought on by the charging energy by increasing  $\omega$ .

Finally, shown in Figure 6 is the average charge state of a Cooper pair box coupled to a SET with identical parameters to that in Fig. 5. We have also included here the relaxation effects of the environment, modelled as in Sec. 6 as a  $50\Omega$  impedance. Note that even near the box degeneracy point, there are large deviations between the result obtained using the full quantum noise of the SET and that obtained from using only classical telegraph noise. In Fig. 6b, we show the relaxation rate  $T_1$  for the same system. Note that the differences between using the full quantum noise and the classical expression are not so evident here.

## 9. Summary

In this article, we have emphasized the need to discuss quantum noise processes using their two-sided spectral densities. Because of the quantum nature of noise, the positive and negative frequencies are generally unequal, in order to account for spontaneous emission. A two-level system was shown to be an ideal spectrum analyzer for probing the quantum nature of a noise process or reservoir. With the advent of real electrical circuits which behave as coherent two-level systems (e.g., [5],[7]), we can now build and use *quantum electrical* spectrum analyzers. We also described the use of a qubit as a *theoretical* tool, by following the evolution of the density matrix of a TLS coupled to the noise-producing system of interest. This technique appears to be quite powerful, as it can yield analytical results for the full quantum noise spectrum of a wide variety of devices, including the superconducting SET [17]. The distinction between the classical noise and the quantum noise, found in this way, leads to dramatically different predictions (c.f. Fig. 6 and Ref. [17]) for continuous measurements of qubits with an SET. The “coupled-system” calculational approach also allows predictions of the dephasing by the measurement, the performance relative to the Heisenberg uncertainty limit [13], the fidelity of single-shot measurements of the qubit states, and the effects of strong coupling to the qubit. The combined theoretical and experimental advances raise many interesting possibilities for testing our understanding of quantum measurement theory with mesoscopic devices.

## Acknowledgements

The authors acknowledge the generous support of this work by the NSA and ARDA under ARO contracts ARO-43387-PH-QC (RS,SG) and DAAD19-02-1-044 (MD), by the NSF under DMR-0196503 & DMR-0084501 (AC,SG),

the David and Lucile Packard Foundation (RS), and the W.M. Keck Foundation.

## References

1. A.O. Caldeira and A.J. Leggett, *Ann. Phys.* **149**, 374 (1983).
2. H.B. Callen and T.A. Welton, *Phys. Rev.* **83**, 34 (1951).
3. M.H. Devoret, in *Quantum Fluctuations*, S. Reynaud, E. Giacobino and J. Zinn-Justin, eds. (Elsevier, Amsterdam, 1995).
4. V. Bouchiat, D. Vion, P. Joyez, D. Esteve and M. Devoret, *Physica Scripta* **T76**, 165 (1998).
5. D. Vion, A. Aassime, A. Cottet, P. Joyez, H. Pothier, C. Urbina, D. Esteve, and M.H. Devoret, *Science* **296**, 886 (2002).
6. J.M. Martinis *et al.*, submitted to *Phys. Rev. B*, 2002.
7. K.W. Lehnert, K. Bladh, L.F. Spietz, D. Gunnarson, D.I. Schuster, P. Delsing, and R.J. Schoelkopf, submitted to *Phys. Rev. Lett.*, 2002.
8. V.B. Braginsky and F. Ya. Khalili, "Quantum Measurement," (Cambridge University Press, New York, 1992.)
9. A.J. Dahm *et al.*, *Phys. Rev. Lett.* **22**, 1416 (1969); D. Rogovin and D.J. Scalapino, *Ann. Phys.* **86**, 1 (1974).
10. R.J. Schoelkopf, P.J. Burke, A.A. Kozhevnikov, D.E. Prober, and M.J. Rooks, *Phys. Rev. Lett.* **78**, 3370 (1997).
11. R. Aguado and L.P. Kouwenhoven, *Phys. Rev. Lett.* **84**, 1986 (2000).
12. L. S. Levitov, H. Lee and G. B. Lesovik, *J. Math. Phys.* **37**, 4845 (1996).
13. M.H. Devoret and R.J. Schoelkopf, *Nature* **406**, 1039 (2000).
14. G. Johansson, Andreas Käck, and Göran Wendin, *Phys. Rev. Lett.* **88**, 046802 (2002).
15. H. Schoeller and G. Schön, *Phys. Rev.* **B**, 18436 (1994).
16. Y. Makhlin, B. Shnirman and G. Schön, *Phys. Rev. Lett.* **85**, 4578 (2000); *ibid.*, *Rev. Mod. Phys.* **73**, 357 (2001).
17. A. A. Clerk, S. M. Girvin, A. K. Nguyen and A. D. Stone, *Phys. Rev. Lett.* **89**, 176804 (2002).

**MEMORANDUM OF TRANSMITTAL**

U.S. Army Research Office  
ATTN: AMSRL-RO-RI (Hall)  
P.O. Box 12211  
Research Triangle Park, NC 27709-2211

- |  |   |
|--|---|
| <input type="checkbox"/> Reprint (Orig + 2 copies) | <input type="checkbox"/> Technical Report (Orig + 2 copies)                 |
| <input type="checkbox"/> Manuscript (1 copy)       | <input checked="" type="checkbox"/> Final Progress Report (Orig + 2 copies) |
|  | <input type="checkbox"/> Related Materials, Abstracts, Theses (1 copy)      |

CONTRACT/GRANT NUMBER: DAAD19-99-1-0346

REPORT TITLE: Final Report: Experiments in Quantum Coherence and Computation with Single Cooper-pair Electronics

is forwarded for your information.

SUBMITTED FOR PUBLICATION TO (applicable only if report is manuscript):

Sincerely,

Robert Schoelkopf